

**DEDOLOMITIZATION AND OTHER DIAGENESIS IN THE
BACKREEF SETTING OF THE PERMIAN REEF COMPLEX IN
DARK CANYON, NEW MEXICO**

Jenna Lee Donatelli

Submitted in partial fulfillment for the requirements for the Degree of Master of Science
in Geology at New Mexico Institute of Mining and Technology.

New Mexico Institute of Mining and Technology
Socorro, NM
March 2016

ABSTRACT

The presence of dedolomite has only been noted in the backreef setting of the Permian Reef Complex in one previous study. This study closely examines dedolomite in the Tansill Formation in Dark Canyon, New Mexico petrographically, elementally, and isotopically along with other diagenetic cements and replacement phases found in this environment. The focus of this project was to petrographically examine the diagenetic events in the near backreef facies (the Tansill and Yates Formations) of the Permian Reef Complex in research cores from Dark Canyon in order to better understand how dedolomitization fits into the paragenetic sequence and its implications for the diagenetic history of the reef complex. This, coupled with elemental and isotopic analyses, as well as data from previous studies, helped to gain insight into the diagenetic environments in which these events took place.

Aragonite and early calcite cements, evaporite precipitation/growth, and early dolomitization occurred at the surface during deposition of the reef and backreef facies. The higher iron content (2674.35 ppm) and finely-crystalline nature of the early stage dolomite relative to the later dolomite indicate that it is a protodolomite that formed on the surface. Later dolomitization was due to dense brines percolating through the subsurface via fractures and pore spaces. This later dolomite could have occurred during burial as opposed to in a marine setting judging by their more euhedral and clearer crystalline character based on observations from previous studies. Evaporite dissolution coupled with calcium-rich fluids were probably responsible for dedolomitization as well as the late, coarsely crystalline calcite precipitation. The dedolomite was likely a direct replacement of the euhedral dolomite with calcite, which still retains the original dolomitic rhomb morphology. Isotopic values for the dedolomite range from -5.07‰ to -4.03‰ $\delta^{18}\text{O}$ and 0.61‰ to 2.14‰ $\delta^{13}\text{C}$ (VPDB). These values differ from the bulk of previously analyzed calcite (which ranges from about -20‰ to -4‰ $\delta^{18}\text{O}$ and -14‰ to 2‰ $\delta^{13}\text{C}$ (VPDB)) and the dolomite both from this study and previous analyses (-3‰ to 6‰ $\delta^{18}\text{O}$ and -2‰ to 7‰ $\delta^{13}\text{C}$ (VPDB)). These values correspond with fracture related dolomite from previous studies.

Keywords: Permian Reef Complex; Tansill Formation; dolomitization; dedolomitization.

ACKNOWLEDGEMENTS

This project would not have been possible without Amoco Production Company and the two research cores they drilled in Dark Canyon. I would not have been able to attend NMT without the teaching assistantship offered to me by the Department of Earth and Environmental Sciences.

There are so many people I need to thank for helping me through this ordeal. First I must convey to Dana Ulmer- and Peter Scholle how much I truly appreciate all their help, microscope, and sweet puppies. To Peter Mozley and Ron Broadhead: thanks for putting up with me for so long and serving on my committee. Nelia Dunbar and Lynn Heizler, you both helped me acquire a lot of cool data without paying a cent. You have my eternal gratitude. Ingar and Patrizia Walder, you have been my saving grace. I would not have made it without the grand opportunities and you have given to me. Thanks for always pushing me in the right direction. Many thanks Pat Valentine for always knowing what is going on and saving me from more than one administrative disaster. To those of you who helped with the editing process even though this is not your field (Neil, Fred, Patrizia, Andrew), you are all amazing. Annabelle Lopez, you let me in to the core warehouse at 6 am more times than I can count. Thanks for being such a trooper! I would also like to acknowledge Penny Boston, Gary Axen, and Jolante Van Wijk for offering to step up to the plate for my sake.

Certain people have somehow managed to keep me sane for the past three years. I salute you all: Neil Currie- thanks for all the adventures! Fred Hanson- I had so much fun learning to cook so many intricate things every single day. Andrew Phillips, Kellie Kerner, and Dylan Rose-Coss- you have been so accepting of most of my weirdness, and a safe place to be me. Maggie Griffin- you taught me to breathe and slow down. This has proven to be invaluable. I must also thank my mom, who is such a sweet, supportive, and strong lady. You are an inspiration. Auntie Mare- thank you for dealing with all the finances involved in my education! Someday it will pay off and I will make you proud(er). Finally to Brian St Clair. You are my best friend in the whole world, and without you I would still be lost.

TABLE OF CONTENTS

	Page
LIST OF TABLES.....	v
LIST OF FIGURES.....	vi
INTRODUCTION.....	1
Geologic Setting and Framework.....	2
Stratigraphy.....	4
Capitan Limestone.....	5
Yates Formation.....	5
Tansill Formation.....	7
Diagenesis.....	8
Marine Cements.....	8
Evaporites.....	8
Calcitized Evaporites.....	9
Dolomites.....	9
Replacement of Cements.....	10
Late Calcite Cement.....	11
Geochemistry.....	11
Aragonite.....	11
Calcite.....	12
Calcitized Evaporites.....	13
Dolomite.....	13

Dedolomitization.....	16
METHODS.....	18
RESULTS.....	21
Marine Cementation.....	22
Aragonite.....	22
Possible High-Mg Calcite.....	27
Dolomite Cementation.....	31
Dolomite Replacement.....	33
Early/Syn depositional Dolomite.....	33
Later Dolomitization.....	36
Geochemistry of Replacive Dolomites.....	38
Calcite Replacement of Aragonite (Neomorphism).....	41
Evaporite Precipitation.....	42
Dedolomitization.....	46
Calcite Spar Precipitation and Calcitization of Evaporites.....	55
Surface Weathering.....	59
Observed Paragenetic Sequence.....	61
DISCUSSION.....	63
Dolomitization.....	63
Dedolomitization.....	67
Dedolomite and Porosity.....	70
Diagenetic Events: Summary and Relation to Burial and Uplift.....	70
CONCLUSIONS.....	73
SUGGESTIONS FOR FUTURE WORK.....	74
REFERENCES.....	75
APPENDIX A: CORE DESCRIPTION.....	85
APPENDIX B: RAW MICROPROBE DATA.....	104

LIST OF TABLES

Table	Page
Table 1: A summary of diagenetic events in the backreef facies of the Permian Reef Complex from previous work.....	8
Table 2: Average $\delta^{18}\text{O}$ and $\delta^{13}\text{C}$ of dolomites in the forereef and near-backreef facies in Dark Canyon (from Melim and Scholle, 2002).....	13
Table 3: Average isotopic compositions of dedolomites associated with different diagenetic environments analyzed by Budai et al., (1984).....	17
Table 4: Isotopically analyzed samples and their depths in the Amoco No. 2 core.....	20
Table 5: A summary of diagenetic events noted in Amoco research cores in Dark Canyon (this study).....	21
Table 6: Quantitative microprobe analysis for dolomite samples in parts per million (ppm). The light and dark labels are referring to the subtle color differences noted in high-gain mode.....	40
Table 7: Quantitative microprobe analysis for dedolomite samples in parts per million (ppm).....	53
Table 8: Data from quantitative analysis on diagenetic cements (ppm). Light and dark calcite refers to the subtle color variations in high gain mode under BSE.....	58
Table B1: Raw microprobe data (Carb10 weight %) from Amoco No. 2, 76 ft.....	104
Table B2: Raw microprobe data (Carb20 weight %) for Amoco No. 2, 76 ft.....	105
Table B3: Raw microprobe data (Carb20 weight %) for Amoco No. 2, 47 and 108 ft.....	107

LIST OF FIGURES

Figure	Page
Figure 1: A) Map showing the different segments of the Permian Reef depositional areas around the edge of the Delaware Basin. Dark Canyon is at the border of the western and northern segments of the escarpment (from Motts, 1972). The locations of the PDB-04 core and Amoco Cores in Dark Canyon are marked with stars. B) Map of the Guadalupe Mountains showing the location of Dark Canyon (marked with a star) (from Chafetz et al., 2008).....	3
Figure 2: A stratigraphic column of Amoco #2. (from unpublished Amoco Core Report by Tyrell, 1969).....	4
Figure 3: Stratigraphy of the Delaware Basin and Permian Reef, (Scholle et al. 2007)	7
Figure 4: $\delta^{13}\text{C}$ and $\delta^{18}\text{O}$ for cements in Dark Canyon. Calcite is represented by various shades of blue symbols (so that they are more visible), calcitized evaporites by purple, and dolomites are in grey.....	15
Figure 5: Location of Amoco cores No.1 and No. 2 on a topographic map near the mouth of Dark Canyon. Unpublished Amoco Core Report (1965).....	18
Figure 6: A schematic cross section through the facies present in Dark Canyon with the locations of Amoco cores No.1 and No. 2. Unpublished Amoco Core Report 1965.....	19
Figure 7: Amoco No. 1, 245 ft (DC-1 245). Formerly aragonitic botryoidal cement. Square tipped crystals, which are diagnostic of aragonite, are evident. The radial fibrous nature of the original aragonite is extremely subtle, as this cement has neomorphosed to calcite since its formation, a process in which the original radial fibrous fabric has been somewhat preserved. During neomorphism, the crystals became wider and less fibrous. There are at least three generations of aragonite visible here.....	23
Figure 8: The contact between the Tansill and Yates Formations is visible at the base of the tepee structure. This tepee is approximately 5 m (15 ft) tall. From the backreef facies in Dark Canyon (mile 0.6).....	24

- Figure 9: Dolomitized aragonite botryoids in a tepee structure. Square tipped crystals indicate that the botryoids were originally aragonite. The white cement at the tips of the botryoids is medium crystalline calcite. These calcites could either be replacive or void filling. The calcite here is thought to be replacive, as is somewhat fabric preserving. Pisoids can be seen below the botryoids. Yates Formation in Walnut Canyon (mile 0.8).....25
- Figure 10: Originally aragonitic cement forms botryoids growing on, and intergrown with, *Archaeolithoporella* sp. The brown area underneath the pencil is partly dolomitized and partly calcitized botryoidal cement that was formerly aragonite. From the reef facies in Walnut Canyon, approaching the backreef facies (mile 0.5).....26
- Figure 11: Amoco No.1, 300 ft (DC-1 300). *Archaeolithoporella* sp. encrusting formerly aragonitic botryoidal cements. The *Archaeolithoporella* sp. is also encrusted by aragonitic cement, indicating that the aragonite cement was penecontemporaneous with deposition in a marine environment.....27
- Figure 12: Amoco No.1, 56 ft (DC-1 56). Fibrous high-mg calcite cement precipitated on the edge of a void (in this case, the osculum of a sponge that has been dolomitized). This cement forms an isopachous crust on the sponge. The crystals have pointed tips, indicating that it is not aragonite.....28
- Figure 13: Amoco No. 2, 55 ft (DC-2 55). Fibrous, isopachous calcite cement lining what used to be a pore space (now filled in with coarser crystalline calcite cement). The fibrous nature of these crystals and pointed tips could indicate that this might be high magnesian calcite. Alternatively, it could be former aragonite, which is also fibrous.....29
- Figure 14: Amoco No. 1, 128 feet depth (DC-1 128). Isopachous calcite cement coats a section of a crinoid. This cement is more bladed than fibrous, which could indicate that it was originally high-Mg calcite. Alternatively, the crystals could have originally been fibrous and only became bladed after diagenesis. If this is the case, it was probably originally aragonitic and has converted to low-Mg calcite. This photomicrograph was taken in an unstained portion of the thin section.....30
- Figure 15: Early dolomite replacing a sponge. In the lower left, isopachous calcite cements line the edge of the sponge. A layer of dolomite replacing the isopachous fibrous cement overlies the first layer of marine cement. This sequence is repeated at least once; it is barely discernible outside this sponge.....32
- Figure 16: Amoco No. 2, 76 ft (DC-2 76). Finely-crystalline dolomite directly replacing an aragonitic botryoid. Square tipped crystals indicate former aragonite. The original fibrous fabric of the aragonite is well preserved.....33
- Figure 17: A backscatter electron image. Calcite displays the lightest color; dolomite is the darker grey. The black spots represent porosity. Note that the early dolomite

has much more porosity (the black spots) than the later dolomite. From DC-2 76.....	34
Figure 18: High gain BSE image of the older dolomite. Note the subtle differences in color within the circle. These represent slight chemical differences within the dolomite. These subtle chemical differences can also be seen in the younger dolomite and the calcite. They look the same as in the BSE image above. From DC-2 76.....	35
Figure 19: Amoco No.1, 56 ft (DC-1 56). Photomicrograph of possible high-Mg calcite isopachously lining a dolomitized sponge. The clean border between the sponge and the calcite suggests that the sponge was dolomitized before the calcite precipitated on top of it. The high-Mg calcite above has been replaced with low-Mg calcite. This replacement did not preserve the fibrous character of the original calcite. Alternatively, the cement isopachously lining the sponge could have been aragonite. Dolomite cement precipitated on the possible high-Mg calcite (or aragonite) cement after it was in place and before the coarsely crystalline calcite formed.....	36
Figure 20: Amoco No. 2, 76 ft (DC-2 76). This is the second type of replacive dolomite. Euhedral dolomite rhombs (upper right) replace calcite cement. In the lower left, the dolomite is less euhedral and appears to also be replacing calcite. Note the elongated, almost bladed appearance of the replacement dolomite. This could indicate that this dolomite is replacing original aragonitic cement and somewhat preserving the fibrous nature of the aragonite crystals. Alternatively, when the aragonite neomorphosed to calcite (discussed later), the crystals became wider and more bladed than fibrous. The dolomite could be replacing this neomorphosed fabric. More study is necessary to be certain.....	37
Figure 21: Amoco No. 2, 76 ft (DC-2 76). Photomicrograph of aragonitic cements that have been directly replaced by finely-crystalline dolomite (far left), marine cement that has been neomorphosed into/replaced by calcite (far right), and coarser, clearer dolomite replacing either aragonite or the later calcite. Note that the coarser dolomite appears to grow around the finer, cloudier dolomite.....	38
Figure 22: Data from the quantitative analysis of both types of dolomite in parts per million (ppm). The (Ca/Ca+Mg) range for both dolomites is very narrow, ranging from 0.622 to 0.644. Overall, the early dolomite has a higher iron content and (Ca/Ca+Mg) than the later dolomite.....	39
Figure 23: Stable isotope data for replacive dolomites (in parts per mil- ‰). Early dolomites range from -.51‰ to 1.15‰ $\delta^{18}\text{O}$ and 6.31‰ to 6.68‰ $\delta^{13}\text{C}$. Later dolomites vary from -0.2‰ to 0.52‰ $\delta^{18}\text{O}$ and from 5.76‰ to 6.89‰ $\delta^{13}\text{C}$. These values are consistent with those from previous studies (see Figure 4 and Discussion section).....	41
Figure 24: Amoco No. 2, 247 ft (DC-2 247). Aragonite that has neomorphosed into calcite. During neomorphism, the crystals became less fibrous and more wide and bladed.....	42

Figure 25: Amoco No. 2, 73 ft (DC-2 73). In cross-polarized light, it is possible to see bright spots contained within most of the coarsely crystalline calcites (red stain). These could be inclusions of evaporites. This coarse crystal of calcite is located in the osculum of a dolomitized sponge. The dolomite replacing the sponge is finely crystalline and cloudy (early). Fibrous to bladed calcite isopachously lines the osculum. This was probably originally high-Mg calcite based on the bladed character of the crystals. Coarser, clearer dolomite crystals overlie the isopachous calcite, concentrically lining the osculum of the sponge. This dolomite occurred after the calcite cement was in place. The coarse calcite crystal filling in the rest of the sponge osculum occurred the latest.....43

Figure 26: Photograph from the south side of Dark Canyon approximately 0.25 miles behind the reef. Cauliflower-shaped nodular vugs are indicative of the past presence of evaporites. These have been dissolved away and then partially or completely filled with coarsely crystalline calcite cement.....44

Figure 27: Amoco No. 2, 207 ft (DC-2 207). Floating dolomite crystals contained in the late, coarsely crystalline calcite. This could be “floating dolomite” (Scholle et al., 1992), indicative of evaporite replacement by the coarsely crystalline calcite.....45

Figure 28: Amoco No. 2, 62 ft (DC-2 62B). Dedolomite present around a void space. Most dedolomite is present as euhedral rhombs, but some is subhedral. Note the inclusion-rich cores in some of the dedolomite crystals.....47

Figure 29: Amoco No. 2, 62 ft (DC-2 62B). A medium-sized euhedral dedolomite crystal in a void-filling coarsely-crystalline calcite. The cloudy core may be remnant inclusions of dolomite (note how some of the cloudy areas do not take a stain) or other inclusions. The original dolomite crystals may have had cloudy cores and limpid rims that were later preserved during dedolomitization.....48

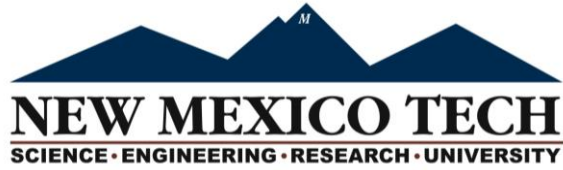
Figure 30: Amoco No. 2, 108 ft (DC-2 108B). Photomicrograph showing euhedral dedolomite rhombs and partially calcitized dolomite rhombs. The dedolomites are contained within coarsely crystalline pore-filling calcite.....49

Figure 31: Backscattered electron image of dedolomite with dolomite cores and rims. From DC-2 47A.....50

Figure 32: Amoco No. 2, 70 ft (DC-2 70). A rhomb-shaped void possibly in the midst of being filled with calcite. It is conceivable that this void was once filled with dolomite, which has since been dissolved away. It could also just be a nicely shaped void, since dolomite crystals as large as this void have not been found in the thin sections from Amoco No. 2.....51

Figure 33: Data from the quantitative microprobe analysis of dedolomites in ppm. The (Ca/Ca+Mg) ratio is much more variable than in the dolomites; it ranges from 0.96 to almost 1. Fe content varies from 0 to 157.3 ppm.....	52
Figure 34: Data from the qualitative analysis of dedolomites plotted with those of the replacive dolomites. Most of the dedolomite plots with calcite in terms of the (Ca/Ca+Mg) (approximately 0.99), except for one, which is slightly higher in Mg. That point has a (Ca/Ca+Mg) of 0.96.....	53
Figure 35: Stable isotope data from the analysis of dedolomite samples. $\delta^{18}\text{O}$ values range from -5.07‰ to -4.03‰. $\delta^{13}\text{C}$ of the dedolomites vary from 0.61‰ to 2.14‰.....	54
Figure 36: $\delta^{18}\text{O}$ and $\delta^{13}\text{C}$ values for the dedolomite samples compared with the early and late replacive dolomite samples.....	55
Figure 37: Amoco No.1, 56 ft (DC-1 56). A single coarse calcite crystal inside a void space within the osculum of a dolomitized sponge. The white is porosity. Note the cross-cutting relationship between the dolomite and the coarse crystal of calcite; the calcite grew inside the osculum of the sponge after it was dolomitized as it has grown around the dolomite crystals. Based on the clean contact between the dolomitized sponge and the high-Mg calcite growing isopachously on it, it is likely that the sponge was dolomitized before the high-Mg calcite cement precipitated. If this is the case, the early replacive dolomite was syndepositional.....	56
Figure 38: Data from the quantitative microprobe analysis of calcite. (Ca/Ca+Mg) has a very narrow range (0.993 to 0.998). Iron content varies from 0 to 393.3 ppm.....	57
Figure 39: Quantitative analysis for calcite plotted with dedolomite. The dedolomite mostly plots with the calcite in terms of (Ca/Ca+Mg), except for one outlier, which is slightly more Mg-rich. The calcites analyzed contain more iron than the dedolomites.....	59
Figure 40: Surface sample from the Tansill Formation, Dark Canyon. Coarsely-crystalline calcite with modern caliche forming in void space as pendant cements. This implies that the caliche is younger than the coarsely crystalline calcite.....	60
Figure 41: A paragenetic sequence for the rocks in Dark Canyon, based on petrographic analyses, field work, and previous studies. Aragonite and calcite cement, as well as at least one episode of dolomitization occurred early in the sequence. Evaporites were probably also relatively early, although more examination is required to know for certain. Aragonite neomorphosed to calcite probably after the early dolomitization took place. Dissolution of evaporites, dedolomitization, and the coarsely crystalline calcite cementation occurred later in the paragenetic sequence, followed by caliche precipitation at or near the surface.....	62

Figure 42: Isotope data for dolomites studied in Dark Canyon and Slaughter Canyon from previous studies and this study.....	65
Figure 43: All previous isotope data from the Yates and Tansill Formations in Dark Canyon plotted with the analyses from this study. Some data from McKittrick Canyon and Slaughter Canyon is included. The dedolomites analyzed in this study plot between the bulk of the calcite and the dolomite data, from 0.61‰ to 2.14‰ $\delta^{13}\text{C}$ and -5.07‰ to -4.03‰ $\delta^{18}\text{O}$ (VPDB).....	69
Figure 44: Burial and uplift history diagram for the Permian Reef Complex with the observed and inferred diagenetic sequence from this study. Burial and uplift data from Scholle et al. (1992).....	72
Figure A1: Amoco Core No. 2, 68-76 ft. This section of core displays most of the cements and major fabrics present in Amoco No. 2. Peloidal, dolomitized limestone, dolomitized limestone and botryoids, and calcitized botryoids.....	86
Figure A2: Amoco Core No. 2, 77 ft.....	87
Figure A3: Amoco Core No. 2, 108 ft. The dedolomite is not visible with the naked eye; it was discovered in thin section and via microprobe analysis.....	87
Figure A4: A cross section constructed from the Amoco No. 2 core.....	88



This thesis is accepted on behalf of the faculty
of the Institute by the following committee:

Peter Mozley

Academic Advisor

Dana Ulmer-Scholle

Research Advisor

Ron Broadhead

Committee Member

I release this document to New Mexico Institute of Mining and Technology

Jenna Donatelli

28 April, 2016

Student Signature

Date

INTRODUCTION

Dozens of geologic studies have been conducted in and around the Permian Basin and Permian Reef Complex of west Texas and New Mexico since the early 1900s. While the presence of dedolomite has only been noted in one previous study (Mazzullo, 1999) it has not been formerly examined petrographically, elementally, or isotopically. Dedolomitization, or the calcitization of dolomite, can increase porosity, making it an excellent reservoir for fluids such as water or hydrocarbons (Ayora et al., 1998). This study focuses on examining the diagenetic events in the near backreef facies (the Tansill and Yates Formations) of the Permian Reef Complex in Dark Canyon. The purpose of the study is to better understand how the dedolomitization fits in to the paragenetic sequence and its implications for the diagenetic history of the area. This is important for understanding fluid (water, hydrocarbons) movement through the shelf.

To accomplish this, the study utilized two research cores that were drilled by Amoco Production Company on the north side of Dark Canyon (Amoco No.1 and Amoco No. 2) in Eddy County, NM, approximately sixteen kilometers (ten miles) south of Carlsbad. Core samples are preferable over outcrop samples because they are less subject to modern alteration and surficial weathering processes, and are more representative of the overall fluid movement patterns through and effects on the rocks. Telogenetic diagenesis (uplift-related) could play a major role, though. Surficial weathering and telogenetic effects can alter the structure and composition of the rock, overprinting and eliminating depositional textures and rendering it difficult to determine a complete paragenetic sequence.

The different diagenetic cements and replacement phases and their timing were petrographically determined. Key cements and replacement phases, such as two different stages of dolomitization, dedolomite (calcitized dolomite) and coarsely crystalline calcite, were then quantitatively analyzed by electron microprobe in order to compare trace element concentrations. Comparing trace elements and isotopes of the cements and replacement phases helped gain insights into the type and environments of dolomitization and dedolomitization, and led to a better understanding of the diagenetic fluids.

There are multiple models for the formation of dedolomite. Early experiments revealed dedolomite to be a near surface process related to meteoric or CaSO_4 -rich fluids (Von Morlot, 1847; Shearman et al., 1961; Evamy, 1963; De Groot, 1967; Goldberg, 1967; Folkman, 1969). Dedolomite can also form during burial (shallow or deep) with elevated temperatures up to 200°C (Kastner, 1982). It has also been associated with fractures and replacive calcite in anhydrite nodules (Back et al., 1983; Budai et al., 1984). The dedolomite in the backreef setting Dark Canyon could be related to near surface

processes, the reaction of dolomite with CaSO₄ rich solutions, fracturing, or some combination of the three.

Geologic Setting and Framework

At the southernmost point, exposures of the Permian Reef escarpment stand approximately 300 meters (980 ft) above the surrounding plains. Moving northward, outcrop relief of the reef facies decreases to 150-meter (490 ft) hills, gradually disappearing into the subsurface south of Carlsbad, NM, just north of Dark Canyon.

The Delaware Basin margin is divided into three segments along its transect based on structural and sedimentation differences (Figure 1A). Sedimentation differences are probably an effect of tidal currents and fluid flow throughout the Delaware Basin as well as the structural configuration of the shelf. The western section is a “barrier stratigraphic reef” that parallels the basin margin. The northern segment is characterized by current-oriented mounds that are oriented perpendicular to the basin-shelf margin (Motts, 1972, 1973), and the eastern segment of the reef is completely buried. Dark Canyon is located just south of Carlsbad in the Carlsbad Embayment (Figure 1B). This area is a structural transition zone between the western and northern areas (Adams, 1965). Back-reef Tansill and Yates Formations, as well as a small section of the Capitan massive reef facies are well exposed in Dark Canyon, making it an optimal study site.

During the later part of Permian (Guadalupian) deposition, the Delaware Basin was located roughly 10° north of the equator in the southern part of the North American craton (Ross, 1978). It was subsiding due to crustal extension caused by the collision of Gondwana (South America) with Euramerica (North America) and, as a result, a basin formed and was filled by the sea (Adams, 1965). Shallow water covered the shelf that rims part of the basin. Today, many canyons cut perpendicular to the strike of the reef, exposing the different facies from forereef to basin sediments (Motts, 1972).

Aragonite seas, or seas that precipitate aragonite instead of calcite, dominated the Permian due to icehouse conditions. Icehouse Earth conditions are where CO₂ is more scarce in the atmosphere and temperatures are cooler than that of a Greenhouse Earth period (Wilkinson et al., 1985). Aragonite seas form when there is a high content of magnesium in the seawater, creating conditions in which aragonite is the primary carbonate precipitated directly from seawater. In contrast, calcite is the more stable seawater precipitate when ocean compositions are relatively low in magnesium (calcite seas, greenhouse conditions). Sea level and temperature may also affect the ocean compositions; deeper waters and cooler ocean temperatures are linked to aragonite seas (Wilkinson et al., 1985).

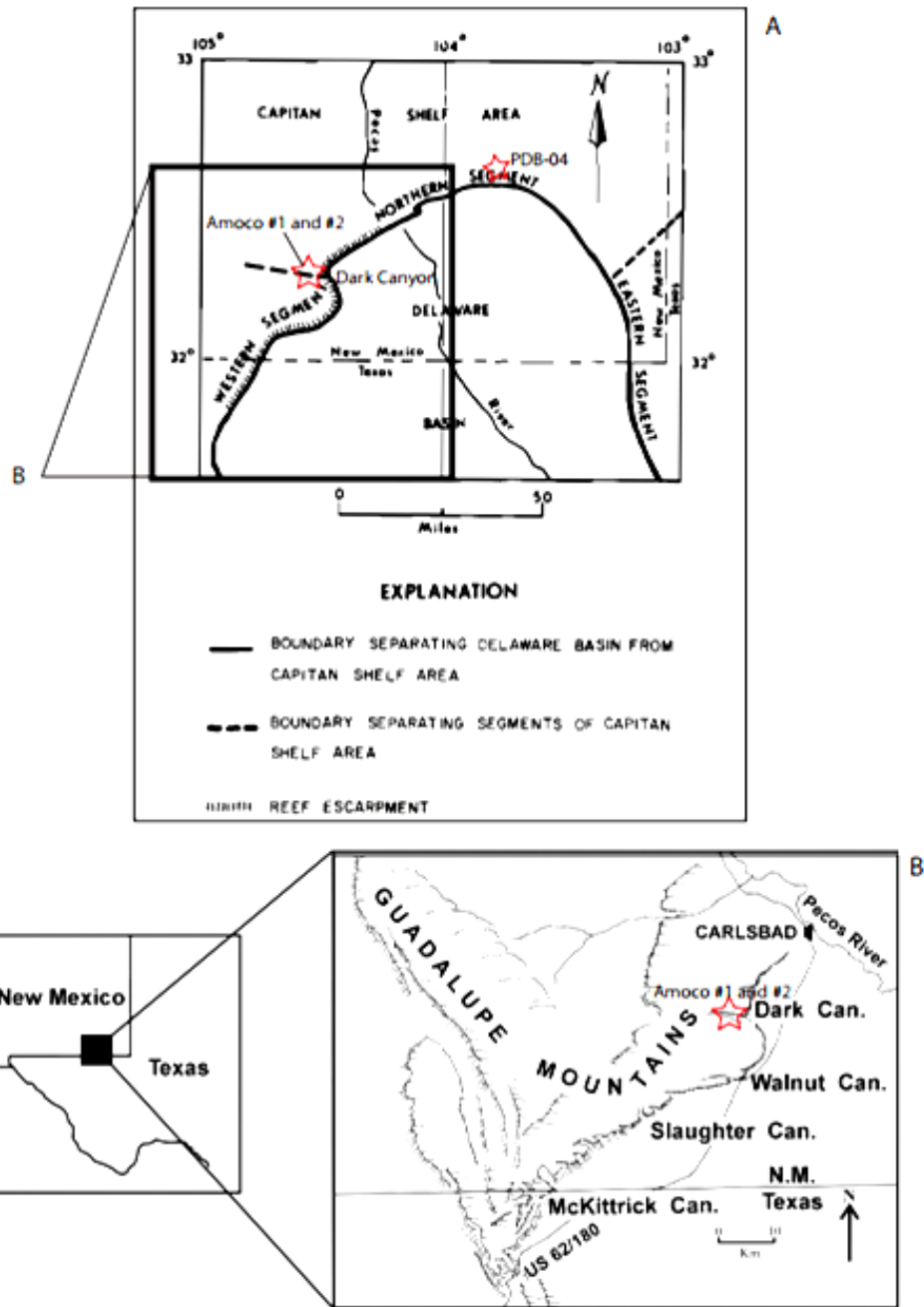


Figure 1: A) Map showing the different segments of the Permian Reef depositional areas around the edge of the Delaware Basin. Dark Canyon is at the border of the western and northern segments of the escarpment (from Motts, 1972). The locations of the PDB-04 core and Amoco Cores in Dark Canyon are marked with stars. B) Map of the Guadalupe Mountains showing the location of Dark Canyon (marked with a star) (from Chafetz et al., 2008).

Stratigraphy

This study focuses on the deposits of the Tansill and Yates Formations. Both of these formations make up most of the two research cores that Amoco Production Company drilled in Dark Canyon (Amoco No.1 and No. 2). A stratigraphic column of the Amoco No. 2 core is shown in Figure 2. Figure 3 is a stratigraphic section that illustrates the formations in the Delaware Basin and the Permian Reef Complex in cross section.

AMOCO NO. 2 DARK CANYON

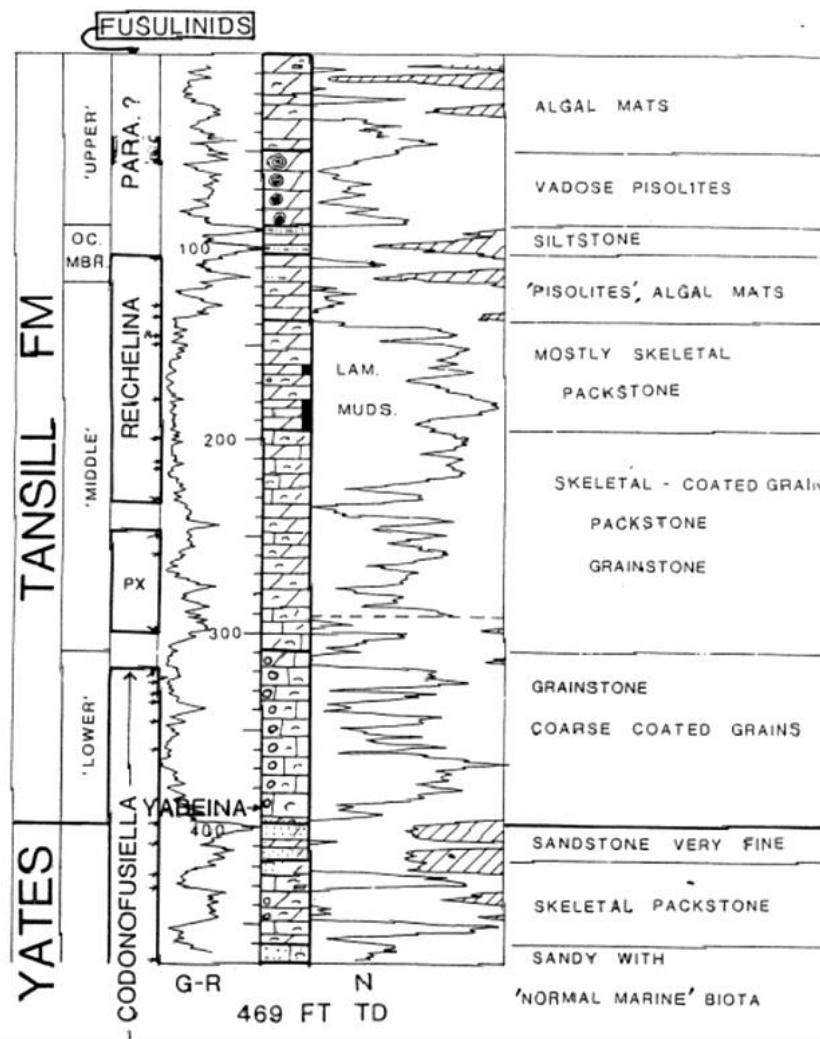


Figure 2: A stratigraphic column of Amoco No. 2 (from unpublished Amoco Core Report by Tyrell, 1969).

Capitan Limestone

The Capitan Limestone (Guadalupian) crops out as massive 300-meter (980-ft) cliffs at the southern end of the Guadalupe Mountains. Moving northward, the relief decreases to low hills as the reef disappears into the subsurface as it is buried by the Castile Formation (King, 1942). During the later Permian and Early Ochoan, fluid exchange between the Delaware Basin and the open sea was restricted causing evaporative brines to form and deposit evaporites over everything in the basin (King, 1947). The Capitan Limestone consists dominantly of limestone that is irregularly interbedded and replaced with dolomite. Dolomitization across the Permian Reef Complex varied locally and is vertically and laterally related to the edge of the shelf (Figure 2; King, 1942). Beds range from four to thirty meters (fifteen to one hundred ft) in thickness where present. Their thicknesses can vary laterally (Kendall, 1969). Most sections of the Capitan reef are massive (King, 1942).

The reef is made up of a variety of organisms that include various types of reef-building organisms common during the Permian such as sponges and bryozoans, *Archeolithoporella* sp., *Tubiphytes* sp., phylloid algae and other green algae, crinoids, rugose corals, brachiopods, and gastropods (Newell et al., 1953; Babcock, 1974, 1977; Yurewicz, 1976, Babcock and Yurewicz, 1989; Kirkland et al., 1993; Wood et al., 1994, 1996, 1999; Senowbari-Daryan and Rigby, 1996). These are not the types of organisms observed in reef building communities today; the environmental conditions, such as cementation rate, carbonate sources and water chemistry, in the Permian Delaware Basin were probably very different than those in modern reef settings (Wood, 1999).

The Capitan Limestone was deposited at the same time as the Yates and Tansill Formations. As such, the Yates and Tansill Formations represent the backreef facies that grade laterally into the reef (Figure 3). The algal and skeletal packstones and grainstones of the near backreef interfinger with the more massive, reefy limestone of the Capitan (King, 1942).

Basinward progradation of the reef was very rapid in the late Permian- too rapid for the shelf slope to support it. As a result, large sections of the reef would break off and roll down toward the basin, forming talus slopes. These talus slopes dip approximately 30° basinward (Boyd, 1958). In some areas, the reef would fracture, as opposed to breaking off completely. These fractures and faults are parallel to the platform-margin trend in the Capitan Limestone (King, 1948).

Yates Formation

Restricted to the shelf north of the Delaware Basin, the Yates Formation (Guadalupian) ranges from 30 to 125 meters (100 to 405 ft) thick on the shelf and thins further backreef (Figures 2, 3; Garber et al., 1989). Unit thickness can vary laterally. The Upper Yates Formation is characterized by sandstones and siltstones that are interbedded with limestones and dolomites (Garber et al., 1989).

The sandstone and siltstone units are laterally continuous over thousands of square miles and range from one to three meters (3 to 10 ft) thick. These sandstones have been described as well-sorted sub-arkose to quartz arenites (Candelaria, 1989) with frosted grains ranging from rounded to well rounded. These sandstones are indicative of subaerial exposure and have been interpreted to be wind-blown (King, 1942).

The carbonates that make up the Yates Formation are limestone and dolomitized limestone (King, 1942). Dolomite ranges from grey to buff colored and is mostly fine grained and limestones are medium to coarsely crystalline interbedded algal and skeletal packstones and grainstones (Boyd, 1958). Features such as pisoids and oolites vary locally. Fenestral fabrics are common throughout the formation. In the upper carbonate members of the Yates Formation, there are repetitive sequences of pisolites and fenestral fabrics. These cyclic deposits are associated with tepee structures, which are characteristic of the shelf margin and backreef pisolite shoals (Borer and Harris, 1989)

Tepee structures are interpreted to be parts of linear, low-lying island complexes. These island complexes are typically found approximately 1.6 km (1 mi) west (landward) of the reef in the Permian Reef Complex (Mazzullo et al., 1989) and range from 2 to 5 meters in height (Assertero and Kendall, 1977). Tepee structures located in the backreef facies of the Guadalupe Mountains are possibly peritidal in origin. The peritidal zone ranges from above the level of the highest tide to below the level of the lowest tide. Tepees form as the carbonate crust of the shelf expands incrementally and is immediately filled with cements and sediment. This expansion could be caused by the upwelling of water underneath an island, thermal expansion, and/ or changes in the elevation of the water table (Kendall and Warren, 1987). The force of upwelling could have pushed sediments up, forming fractures (Handford, 1984). Water sources for cement are both meteoric and marine based on a modern analogue in the Coorong region in southern Australia (Kendall and Warren, 1987).

Evaporites were noted deeper in Yates Formation of the PDB-04 core, but not in Dark Canyon (Garber et al. 1989). Evidence of prior evaporites based on petrographic and field observations (such as well-preserved gypsum in Capitan-equivalent shelf deposits in outcrop and cauliflower-shaped nodular vugs) is documented in Dark Canyon (Ulmer-Scholle et al., 1993).

The presence of fossils, such as dasycladaceans, fusulinids, and gastropods, throughout the carbonate units in the Yates Formation indicate a warm, shallow, marine depositional environment, such as a lagoon. Deposition of the Yates Formation is interpreted to have occurred during a rise in sea level after a low-stand represented by the Ramsey Sandstone Member in the Bell Canyon Formation (Figure 3) (Candelaria, 1989). Fluctuations in sea level occurred during deposition, as evidenced by the sandstones and local pisolites (Motts, 1972). The Yates Formation is separated from the Tansill Formation due to its characteristic sandstones (King, 1942).

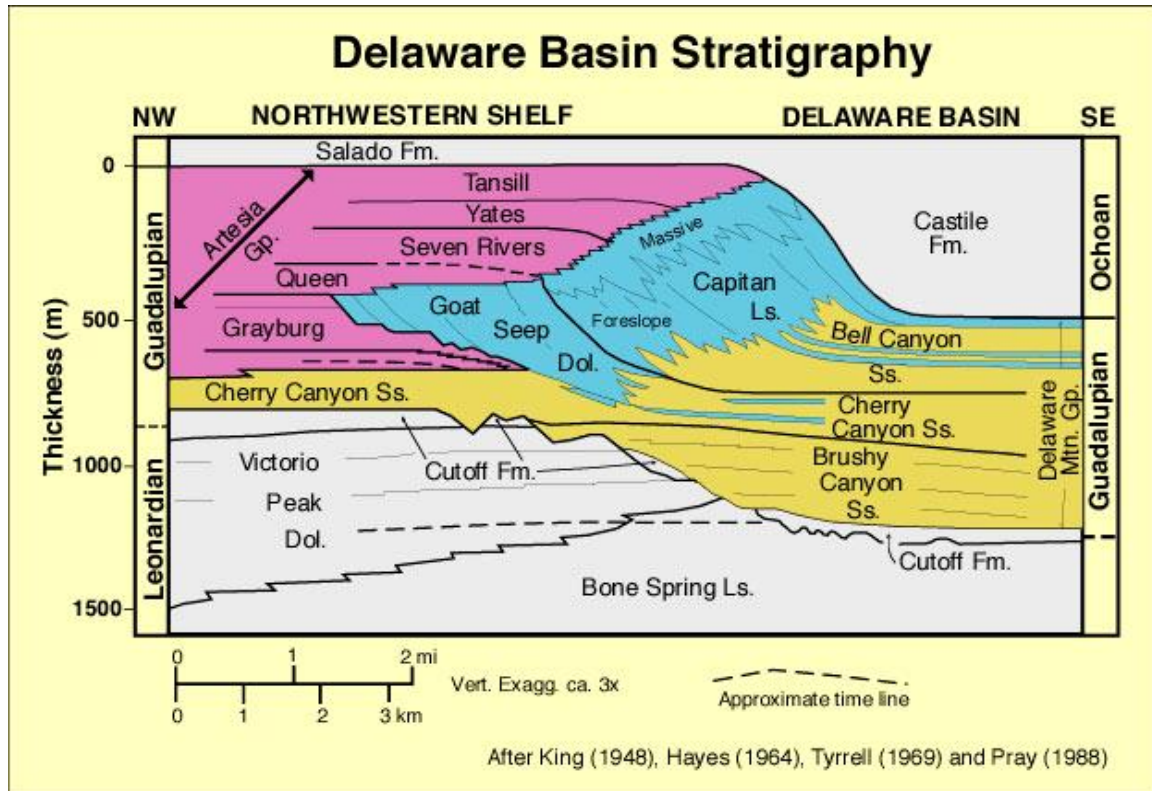


Figure 3: Stratigraphy of the Delaware Basin and Permian Reef, (Scholle et al., 2007).

Tansill Formation

The Tansill Formation (Guadalupean) lies stratigraphically above the Yates Formation (Figures 2, 3). In Dark Canyon, the Tansill Formation ranges in thickness from 30 to 100 meters (100 to 325 ft) and, like the Yates Formation, is thickest near the reef. Regionally, it averages 30 to 45 meters (100 to 150 ft) thick (Garber et al., 1989). This formation is correlated with the last episode of reef building along the shelf edge of the Delaware Basin and is the youngest backreef platform facies in the Capitan reef (King, 1942; Mazzullo et al., 1989).

In general, the Tansill Formation consists of bedded limestones and dolomites and grades laterally into the Capitan Reef. This formation does not have several zones of meters-thick beds of sandstone as the Yates Formation does; it therefore a separate unit. The top of the middle Tansill Formation is marked by the Ocotillo Silt Member, which is an excellent marker bed and the only continuous clastic part of the Tansill Formation (Candelaria, 1989). Tepee structures are also present (Kendall and Warren, 1987; Chafetz et al., 2008) as well as patch reefs (Borer and Harris, 1989). Within the tepee structures, peritidal precipitated dolomites, dolomitized peritidal limestones, grainstones and fenestral limestone are observed. The shelf crest facies in the Tansill Formation, found within the backreef facies, consists of peritidal dolomites with pisolites, tepees and some sandstones, deposited in an intertidal flat environment (Mazzullo et al., 1989). The Lower Tansill Formation represents a transgression of sea level back onto the platform (Candelaria, 1989).

Diagenesis

The diagenesis of the backreef setting of the Permian Reef complex has been studied for decades (Adams and Rhodes, 1960; Cys, 1971; Motts, 1972; Mazzullo and Cys, 1977; Cys, 1979; Crysedale, 1986; Garber et al., 1989; Scholle et al., 1992; Ulmer-Scholle et al., 1993; Melim and Scholle, 2002; Frost et al., 2012; Budd et al., 2013; Bishop et al., 2014). Table 1 is a summary of the previously examined diagenetic events.

Table 1: A summary of diagenetic events in the backreef facies of the Permian Reef Complex from previous work.

Diagenetic Event	Cement	Appearance
Marine cement	Aragonite Calcite	Square tipped crystals (aragonite) Radial fibrous, isopachous (aragonite and calcite)
Evaporites	Gypsum Anhydrite	Beds Lenses Nodules
Calcitized Evaporites	Calcite	Blocky spar
Dolomite	Dolomite	Finely to medium crystalline
Replacement of Marine Cement	Calcite Dolomite	Fabric preserving-fabric destroying
Late Calcite	Calcite	Coarsely crystalline, blocky

Marine Cements

Aragonitic cements tend to encrust allochems with isopachous needle fringes (very elongate crystals are oriented perpendicular to the substrate). They also form fan druses and botryoids. In well-preserved botryoids, square tipped crystals are visible in thin section. These cements have eliminated most of the original porosity and permeability within these facies. Aragonite found in the reef and back-reef facies are indicative of precipitation from marine waters (King, 1942; Cys, 1979; Chafetz et al., 2008).

Radial fibrous calcite cement is also thought to be syndepositional and is typically found associated with *Archaeolithoporella* sp. encrustations, inside preserved skeletal chambers of gastropods and mollusks, and in framework voids. It is also associated with sponges. The radial fibrous calcite cement can be isopachous fringes on and in allochems, but, it can also be crusts on algae, fan druses, or botryoidal in habit (Mazzullo and Cys, 1977).

Evaporites

Evaporites found in the Yates and Tansill Formations of the PDB-04 core precipitated as anhydrite, lenticular anhydrite as pseudomorphs after gypsum, and anhydrite nodules (Garber et al., 1989). The evaporites are thought to have formed in a

sabkha or evaporitic lagoon environment on the shelf based on the cauliflower-like shapes of the nodules. These grew in voids after aragonite had precipitated out of the seawater and are considered secondary (Duff Kerr, Jr. and Thomson, 1963; Kinsman, 1969). They are interbedded with limestones and siliciclastic material on the shelf. Evaporites also appear as secondary minerals in the reef facies, precipitated in voids or replaced existing material (Garber et al., 1989).

The fluids that the evaporites precipitated from were probably also dolomitizing fluids (Adams and Rhodes, 1960). When evaporites, such as gypsum, are precipitated, kinetic barriers that inhibit dolomitization are lowered. Rocks associated with these evaporites are mostly dolomitized. This is consistent with both the tidal flat/sabkha and seepage reflux models for dolomitization (Adams and Rhodes, 1960; Shinn 1983).

Calcitized Evaporites

The Yates and Tansill Formations had widespread evaporite deposits in the form of beds, nodules, individual crystals and crystal fragments that have been replaced by blocky calcite spar (Crysdale, 1986; Scholle et al., 1992; Ulmer-Scholle et al., 1993). These calcitized evaporites are contained within finely-crystalline dolomite. The evaporites were either leached partially or entirely away, forming void space, or pseudomorphically replaced by calcite. Inclusions of evaporites are rarely found in the calcitized evaporites. Evaporites replaced by silica are much less common than those replaced by or filled with calcite in the backreef facies. The coarsely crystalline calcite cement that is replacive of evaporites is associated with meteoric waters (Ulmer-Scholle et al. 1993).

Dolomites

Dolomitization has affected most of the carbonates on the entire shelf from the tidal flats and lagoons to the fore-reef facies. There has also been significant dolomitization in the reef itself, as well as in the fore-reef (King, 1948; Adams and Rhodes, 1960; Adams, 1965; Cys, 1971; Motts, 1972; Melim and Scholle, 2002).

Possible models for the dolomitization of these Permian sediments are the tidal flat/sabkha model and the seepage reflux model (Adams and Rhodes 1960, Patterson and Kinsman, 1982; Shinn 1983).

Tidal flats and sabkhas can be flooded by tides or storm waves. This seawater can be concentrated in brines through evaporation and drawn down into the sediments. The fluids can then drain toward the basin, dolomitizing as they go. Precipitation of evaporites can act as a catalyst for dolomite formation. Most of the dolomitization occurs in the first few meters of sediment in the upper intertidal and supratidal zones (Shinn, 1983). Dolomites formed in this type of environment are typically aphanocrystalline with a poorly ordered crystal structure (protodolomite); they tend to replace aragonite and retain fabrics (Shinn, 1983; Land, 1985).

With the seepage reflux model, evaporation of seawater on a shelf or behind a barrier reef lowers water levels landward of the reef. As in the tidal flat/sabkha model, during evaporation, the waters become increasingly concentrated, producing brines with high specific gravities. The brine sinks to the bottom of the water column and drains seaward down the shelf slope and through the sediments, following permeability

pathways such as fractures (Adams and Rhodes, 1960). Again, in this model, precipitation of evaporites acts as a catalyst for dolomite formation. Although, a restricted carbonate lagoon environment can be dolomitized by seepage reflux even if no evaporites are present in the area (Adam and Rhodes, 1960; Melim and Scholle, 2002). The fluid dolomitizes the fractures and fills pore spaces in the subsurface as it moves through the units. The amount of dolomitization depends on how much pore or fracture space is present at any given location, since the dolomitizing fluid must have some space to migrate through in the subsurface. This process can take place over thousands of years (Adams and Rhodes, 1960). Dolomites associated with burial (and the seepage reflux model) are typically intermediate to coarsely crystalline with a well ordered structure. They can be fabric retentive, but are commonly fabric destructive when replacing calcite or aragonite (Radke and Mathis, 1980).

Dolomitization can also occur in reducing, anoxic conditions, making it possible for iron to be more easily incorporated into the crystal lattice (Dix, 1993; Vasconcelos and McKenzie, 1997; Warthmann et al., 2000; van Lith et al., 2002). These reducing conditions could be caused either by bacteria or decomposing organic matter. An experimental study by Warthmann et al., (2000) found that sulfate reducing bacteria can create an anoxic environment and induce dolomite precipitation. Another study by Vasconcelos and McKenzie, which took place in Lagoa Vermelha, Brazil, found dolomite precipitation associated with reducing condition caused by decomposing organic matter. In a later study done in Lagoa Vermelha, high salinity was attributed to providing the necessary ions required for dolomite to precipitate. This coupled with bacterial sulfate reduction helps to drive dolomitization in that location (van Lith et al., 2002).

Dolomites mediated by microbial activity in hypersaline, anoxic conditions were found to have a highly ordered crystal structure. Under SEM, these dolomites are dumbbell shaped. This morphology is indicative of rapid crystal growth (Warthmann et al., 2000).

Replacement of cements

After their formation, aragonitic cements have been replaced with calcite and dolomite. Preservation of aragonitic fabrics ranges from well-preserved to poorly preserved (Mazzullo and Cys, 1977; Melim and Scholle, 2002). The neomorphosed aragonite tends to have well preserved fabrics (Mazzullo and Cys, 1977), as does some of the dolomite analyzed by Melim and Scholle (2002).

Using Holocene analogues, Mazzullo and Cys (1977) suggest that fresh water played a part in the Neomorphism of aragonite to calcite, and that some of the inversion could have been driven by algae or bacteria. Mazzullo and Cys (1977) have suggested that the aragonite has undergone the following diagenesis:

1. Aragonitic cement formed syndepositionally.
2. The aragonitic cement underwent mineralogic stabilization to calcite via paramorphic inversion. The fabrics are preserved.
3. Excess calcite is produced during neomorphism.

4. The excess calcite precipitates as syntaxial overgrowth where there is space for it to grow.

Based on the petrographic study by Melim and Scholle (2002), the fabric-preserving dolomite was determined to have formed while the originally aragonitic cements were undergoing neomorphism to calcite. The fabric-preserving dolomite ranges in size from 5 to 50 micrometers (Melim and Scholle, 2002). Crystals are anhedral and tend to replace botryoidal and isopachous cements, as well as detrital grains and micrite. The objects replaced by this dolomite are easily recognized even though the original material is gone (Melim and Scholle, 2002).

The fabric-destroying dolomite is thought to have formed during deep burial of the reef complex. Some of the later fabric destructive dolomite may have replaced some of the early dolomite. The crystal size of the fabric destroying dolomite ranges from 30 to 200 micrometers and can be anhedral to euhedral (Melim and Scholle, 2002)

Late Calcite Cement

The last diagenetic cement is coarsely crystalline, sparry calcite cement that fills void space and is replacive of- or pore filling after the dissolution of evaporites (Scholle et al., 1992). Mruk (1985, 1989) identified two types of this late-stage calcite. The first, Spar II, is coarsely crystalline poikilotopic calcite that can be up to a centimeter across. This generation of calcite spar is zoned and varies from non-luminescent to brightly luminescent with up to six luminescent bands (Mruk, 1985, 1989). It mostly fills pore space but can be replacive. This was observed in the forereef facies (Mruk, 1985, 1989; Scholle et al., 1992)

Spar III is also very coarsely crystalline. It is distinguished from Spar II by being non-luminescent. This calcite is not as widespread as the earlier generation of calcite cement (Spar II). Both generations of calcite have “floating fabrics” where grains are floating in calcite cement (Mruk 1985, 1989, Scholle et al., 1992).

Spar III calcites are thought to have precipitated after dolomitization occurred. This calcite fills in almost all pore space and may be replacive of evaporite nodules that were once in the subsurface (Scholle et al., 1992). The late calcite cement is thought to have occurred during uplift and exposure of the Capitan Formation (Ulmer-Scholle et al., 1993).

Geochemistry

There are numerous sets of isotope data for surficial carbonates in the Permian Reef Complex (Allan and Matthews, 1982; Given and Lohmann, 1985, 1986; Scholle et al., 1992; Ulmer, 1992; Mazzullo, 1999; Chafetz et al., 2008; Budd et al., 2013, Bishop et al., 2014). Figure 4 is a compilation of all $\delta^{13}\text{C}$ and $\delta^{18}\text{O}$ data from the Tansill and Yates Formations in or near Dark Canyon.

Aragonite

Chafetz et al. (2008) studied relict and preserved aragonite in tepee structures in the Yates and Tansill Formations. Samples were collected in Walnut Canyon and Dark

Canyon. In Dark Canyon, the $\delta^{18}\text{O}$ signal of aragonite ranges from -3.13‰ to 0.93‰ PDB, and the $\delta^{13}\text{C}$ values range from 5.2‰ to 7.75‰ PDB. For carbonates with such low values for the $\delta^{18}\text{O}$ to precipitate, the water they precipitated from must also have a low $\delta^{18}\text{O}$ signature (such as meteoric water) or be at high temperature (Chafetz et al., 2008). The compositions of the least altered aragonite samples are -1.6‰ $\delta^{18}\text{O}$ and 5.8‰ $\delta^{13}\text{C}$ (Chafetz et al., 2008). These compositions indicate precipitation directly from seawater, (Mazzullo, 1999) so marine waters at high temperature (40°C or higher) is the most likely source for the aragonite. This temperature is higher than expected for aragonite precipitated during the Permian (Chafetz et al., 2008), but in a restricted shallow lagoon located 10-15° north of the Permian equator (Ross, 1978) temperatures could probably get that high.

Calcite

Calcite that precipitated directly from Permian seawater has isotopic signatures of -2‰ to -3‰ $\delta^{18}\text{O}$ and 5‰ to 6‰ $\delta^{13}\text{C}$ PDB (Given and Lohmann, 1986; Mruk, 1985). Late-stage calcites studied by Scholle et al. (1992) have lower in $\delta^{18}\text{O}$ and $\delta^{13}\text{C}$ values. Their samples collected from the Yates and Tansill Formations in Dark Canyon yield average values of -10.7‰ $\delta^{18}\text{O}$ and -15.9‰ $\delta^{13}\text{C}$ PDB. These low $\delta^{18}\text{O}$ values indicated that the calcites probably precipitated from meteoric waters. The low $\delta^{13}\text{C}$ signatures were attributed to the incorporation of organically sourced carbon dioxide (Scholle et al., 1992), such as decomposing organic matter or the break-down of hydrocarbons in the subsurface (this can be a bacterial or thermal process). Bacterial breaking-down of hydrocarbons is thought to be the cause of the low $\delta^{13}\text{C}$ in these late calcites. Hydrocarbons have moved through the reef and backreef facies in the Permian Reef Complex, leaving trace amounts behind. The reef complex was buried to a maximum depth of approximately 1 km, so the thermal break-down of the self-sourced hydrocarbons is unlikely (Scholle et al., 1992).

Like Mruk (1985, 1986), Budd et al. (2013) and Frost et al. (2012) also analyzed calcites from the Dark Canyon near backreef facies (the Yates and Tansill Formations). Using cathodoluminescent petrography (CL), they found both luminescent and non-luminescent phases of calcite in evaporite pseudomorphs and interparticle pore spaces. The non-luminescent calcite ranges from -10.1‰ to -16.2‰ $\delta^{18}\text{O}$ and 1.9‰ to -18.1‰ $\delta^{13}\text{C}$ VPDB. The luminescent phase is younger than the non-luminescent phase and ranges from -8.8‰ to -12.9‰ $\delta^{18}\text{O}$ and -4.6‰ to -13.8‰ $\delta^{13}\text{C}$ VPDB. Both phases are interpreted to have originated from meteoric waters (Budd et al., 2013; Frost et al., 2012).

Three late calcite spars from Slaughter Canyon were analyzed by Bishop et al. (2014). Spar 1 fills in primary and secondary pore space and forms syntaxial overgrowths on inclusion-rich prismatic cements. Spar 1 isotopic values for $\delta^{18}\text{O}$ are -5‰ to -8‰ and 1‰ to -4‰ $\delta^{13}\text{C}$ (PDB). These are interpreted as meteoric phreatic cements. Spar 2 is also found filling most primary and secondary pore space and is commonly in the form of equant crystals. The boundaries between this spar and Spar 1 usually involves corroded and fractured Spar 1. Spar 2 has $\delta^{18}\text{O}$ values of -2.3‰ to -11.1‰ and 2.3‰ to 3.1‰ $\delta^{13}\text{C}$ (PDB). This spar is thought to be meteoric cement that replaced evaporites. Spar 3 fills fractures in both Spars 1 and 2 and also interpreted as

meteoric cement. The $\delta^{18}\text{O}$ values for Spar 3 range from -7.5‰ to -9.2‰ and 3.7‰ to -5‰ for $\delta^{13}\text{C}$ (PDB) (Bishop et al., 2014; Scholle et al., 1992).

Bishop et al. (2014) also examined early marine cements from Slaughter Canyon, about 25 km (15 miles) south of Dark Canyon. Most of the material analyzed is former aragonite that has neomorphosed into calcite. The $\delta^{18}\text{O}$ signature of this material ranges from -6‰ to 0‰ (PDB), and the $\delta^{13}\text{C}$ values vary from 0‰ to 6‰ (PDB).

Calcitized Evaporites

The calcites on the shelf of the Permian Reef Complex have slightly higher $\delta^{18}\text{O}$ values than those found on the fore-reef slope (Scholle et al., 1992). Massive evaporites and large hydrocarbon deposits on the shelf could have slowed meteoric fluid flow through the shelf, delaying the calcitization and causing the slight enrichment of $\delta^{18}\text{O}$ of the evaporites in the shelf. It is also possible that the calcitization process could have taken a longer time due to these massive evaporites retarding the flow of meteoric fluid. The evaporites that are preserved in the shelf and not the slope facies supports this hypothesis (Scholle et al., 1992).

Dolomite

Melim and Scholle (2002) analyzed samples of replacive dolomites ranging from fabric retentive to fabric destructive. They also compared dolomites from the near backreef (lagoon) facies to the near backreef facies, as well as a few from farther backreef. A compilation of their average $\delta^{18}\text{O}$ and $\delta^{13}\text{C}$ values for these dolomites is shown in Table 2 (Melim and Scholle, 2002).

Table 2: Average $\delta^{18}\text{O}$ and $\delta^{13}\text{C}$ of dolomites in the forereef and near-backreef facies in Dark Canyon (from Melim and Scholle, 2002).

Sample Type	$\delta^{18}\text{O}$	$\delta^{13}\text{C}$
Fabric-preserving	5.8	0.9
Mostly fabric-preserving	5.8	0.4
Mostly fabric-destroying	5.4	-0.8
Fabric-destroying	5.2	-3.3
Near backreef	5.9	2.3
Far backreef	6.3	3.6

The fabric-destroying dolomites have the highest $\delta^{18}\text{O}$ values (PDB). This is thought to indicate either higher temperatures during formation or a fluid with a low $\delta^{18}\text{O}$ signature, or some combination of the two. Higher formation temperatures are more likely the case here. Dolomitization probably occurred at the surface in a sabkha, tidal flat, or lagoon environment (Melim and Scholle, 2002). Using surface temperatures to calculate fluid compositions at the time of dolomitization (30° C in the Permian), the far backreef water was probably about 2.5‰ $\delta^{18}\text{O}_{\text{SMOW}}$. Near backreef water compositions were calculated to be within the range of 1.4‰ to 2.8‰ $\delta^{18}\text{O}_{\text{SMOW}}$ (Melim and Scholle, 2002).

There was probably a difference in the water temperatures from the near to far backreef, with the far backreef being shallower and therefore warmer. This could account for differences in the $\delta^{18}\text{O}$ of the near vs. far backreef dolomites (Melim and Scholle, 2002). The spread in $\delta^{18}\text{O}$ values could also be caused by a difference in salinity between the near and far backreef environments (Melim and Scholle, 2002). The far backreef lagoon was interpreted to be hypersaline, and the near backreef mesosaline based on mineralogical and faunal studies by Sarg (1977) and Hurley (1989).

The carbon isotope values of the dolomites analyzed by Melim and Scholle (2002) are typical for late Permian dolomites (Bein and Land, 1983; Veizer et al., 1986; Scholle 1995; etc.). These high, positive values were probably caused by an increase in the rate of burial of organic carbon sources during this time (Bernier and Lasaga, 1989; Kump, 1989; Scholle 1995; Melim and Scholle, 2002).

Budd et al. (2013) and Frost et al. (2012) examined dolomite that lines the walls of syndimentary fractures as well as dolomitized cements. The isotopic values of this dolomite are concurrent with those of early replacive dolomites that were reported by Frost et al. (2012) as well as earlier studies in Dark Canyon (Rudolph, 1978; Mazzullo 1999). The $\delta^{18}\text{O}$ values range from 1.2‰ to 3.3‰ VPDB, and the $\delta^{13}\text{C}$ values range from 5.1‰ to 7.1‰ VPDB (Budd et al., 2013; Frost et al., 2012).

Bishop et al. (2014) isotopically analyzed a range of dolomites (fabric-preserving to fabric-destroying) in the backreef setting in Slaughter Canyon. The fabric retentive dolomites have $\delta^{18}\text{O}$ signatures from 1.4‰ to 2.1‰ and $\delta^{13}\text{C}$ values from 6.1‰ to 6.3‰ (PDB). Fabric destructive dolomites are from -0.5‰ to -1.8‰ $\delta^{18}\text{O}$, and 5.5‰ to 5.9‰ $\delta^{13}\text{C}$ (PDB). From this data and numerical models for fluid-rock interaction, they infer that the early diagenetic fluids were mostly meteoric with a contribution from lingering marine fluids during sea-level low stands, and dolomitizing fluids during sea-level highs (Bishop et al., 2014). Previous studies agree that diagenesis continued through periods of exposure (Scholle et al., 1992, 2002).

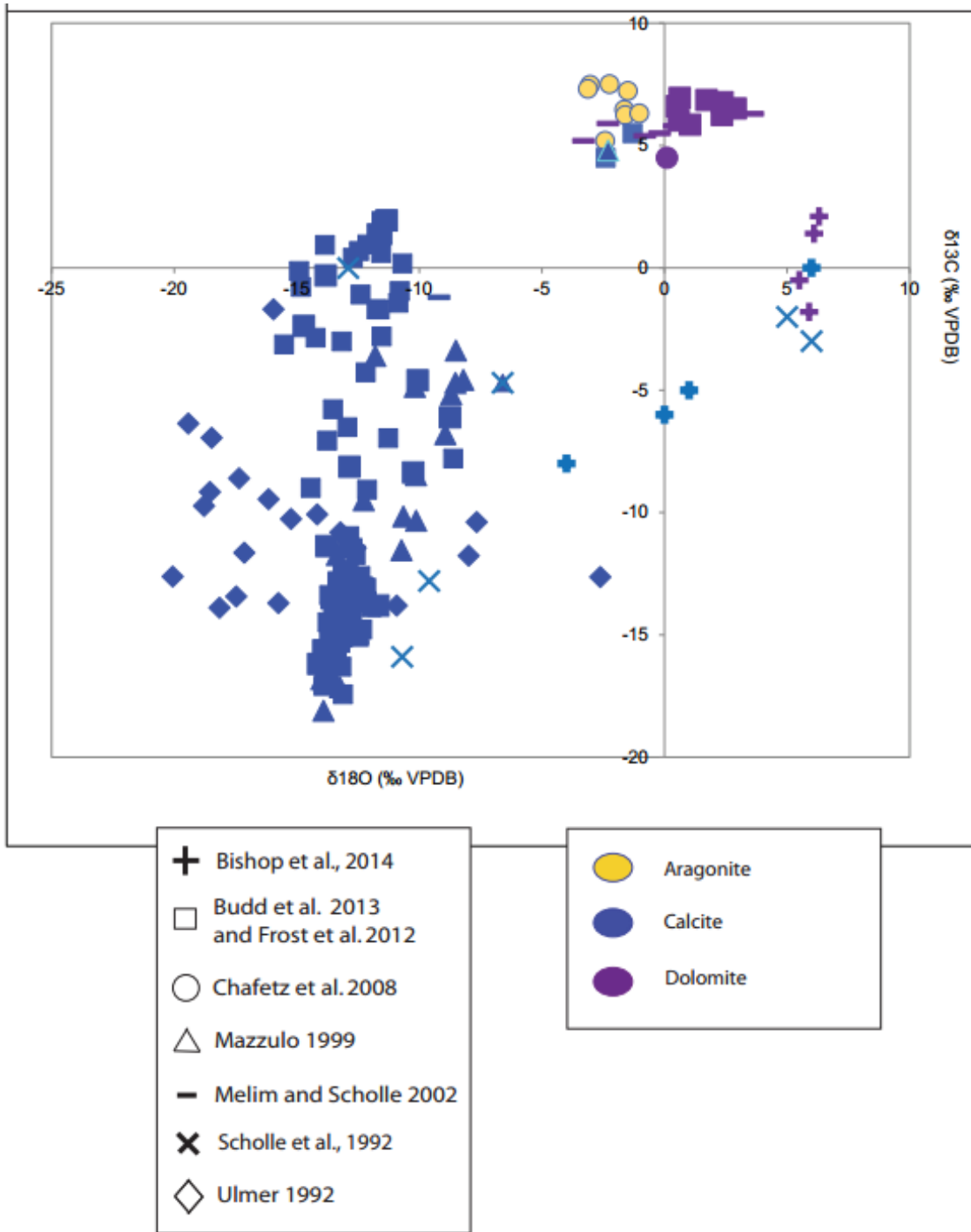


Figure 4: $\delta^{13}\text{C}$ and $\delta^{18}\text{O}$ for cements in Dark Canyon. Calcite is represented by various shades of blue symbols (so that they are more visible), calcitized evaporites by purple, and dolomites are in grey.

Dedolomitization

Dedolomitization is the process by which a fluid with a high $\text{Ca}^{2+}/\text{Mg}^{2+}$ ratio interacts with dolomite to form calcite. The result is dedolomite, or calcitized dolomite. Dedolomite is generally recognized by calcite in the distinctive rhombic shape of dolomite (Von Morlot, 1847). Dedolomitization can affect the dolomite rhombs from the outside inward (centripetal dedolomitization) or from the inside outward towards the margins of the crystals (centrifugal dedolomitization) (Khwaja, 1983). Dedolomite from the Late Devonian Martin Formation (Arizona) examined by Kenny (1992) consists of “cloudy core dolomite rhombs are preferentially calcitized,” as well as entire rhombs of dolomite replaced with polycrystalline or monocrystalline calcite. Grumeleuse texture (micrite clots surrounded by coarser calcite crystals) was also noted in dedolomites from that study. Dedolomite in the Mississippian Madison Formation examined by Budai et al. (1984) dominantly appears as corroded edges on dolomite rhombs, partial dolomite rhombs suspended in a calcite matrix, and patches of calcite within rhombic dolomite cores. It is also observed as calcite rhombs after dolomite and granular calcite that fills in rhomb-shaped pores; these are classic dedolomite fabrics, which were described by Von Morlot (1847).

Early studies found the formation of dedolomite to be associated with evaporites and CaSO_4 -rich fluids (Von Morlot, 1847; Tatarskiy, 1949; Lucia, 1961; Shearman et al., 1961; Evamy, 1967; Goldberg, 1967; Folkman, 1967; Warrak, 1974). These studies did not fully understand the exact reaction pathways for dedolomitization; they suggested that dolomite reacted with CaSO_4 rich fluids. This process could have produced CaCO_3 and MgSO_4 .

Experimental studies on the formation of dedolomite were conducted both at low temperature (De Groot, 1967) and at higher temperatures up to 200°C (Kastner, 1982). These studies concluded that the dedolomitization process can happen during shallow and/or deep burial, as well as at the surface. Back et al., (1983) found that the driving mechanism behind the dedolomitization process to be calcium (limestone) rich fluids associated with sulfates derived from evaporites, such as gypsum. Dissolution of evaporite minerals saturates the dissolving fluids with calcium, which decreases the magnesium to calcium ratio and causes calcite to precipitate. The precipitation of calcite, in turn, lowers the CO_2 content in the system and the pH, which causes the dissolution of dolomite (Back, 1983; Ulmer and Laury, 1984).

Budai et al. (1984) discovered some dedolomite that was associated with burial, thrusting, fracturing and uplift in the Mississippian Madison Limestone in Wyoming and Utah. Fracture associated dedolomite was found to be related to shallow and deep burial. Nodular dedolomite could be associated with shallow burial or thrusting. This dedolomite was found within anhydrite nodules that had been replaced with calcite. Stylolite related dedolomite is associated with deeper burial. The isotopic signatures of each were very distinct. Table 3 shows the average compositions of each of the types of dedolomite analyzed from a core in the Mississippian Madison Limestone, Wyoming and Utah (Budai et al., 1984).

Table 3: Average isotopic compositions of dedolomites associated with different diagenetic environments analyzed by Budai et al., (1984).

Dedolomite type	Average $\delta^{18}\text{O}$ (PDB)	Average $\delta^{13}\text{C}$ (PDB)
Fracture related (Shallow and deep burial/uplift)	-6.3	1
Nodular (Burial/thrusting)	-8.1	-17.5
Stylolite (Burial)	-8.0	-8.6

Spötl et al. (1998) also examined dedolomite that is associated with deeper burial. In this case, dedolomite formed in an evaporitic mélangé in the Permian Haselgebirge (Austrian Alps). It is the only study with isotopic signatures for dedolomite in Permian units; the $\delta^{13}\text{C}$ ranges from -2.8‰ to 0‰ (VPDB) and -10‰ to -7.8‰ $\delta^{18}\text{O}$. Spötl et al. determined that this dedolomite formed during deep burial from Ca-rich brines that dissolved anhydrite. This is based on several lines of evidence: 1. The dedolomite is intergrown with minerals that are unrelated to near surface formation. 2. Meteoric water had limited access to the dedolomitized rocks due to a gypsum caprock. 3. The dedolomite is finely crystalline. Jones et al. (1989) and Cañaveras et al. (1996) found dedolomite and calcite associated with near surface formation to be coarsely crystalline.

Some authors (Katz, 1971; Al Hashimi and Hemingway, 1973; Frank, 1981) found that ferroan dolomites or calcium- rich dolomites (Katz, 1968) tend to be calcitized preferentially in oxidizing environments near the surface. These processes are thought to produce iron oxides and hydroxides as a byproduct. Dedolomite has also been associated with subaerial exposure coupled with an influx of low $\delta^{18}\text{O}$ (meteoric) water and/or dolomite interactions with groundwater that descended from paleoaquifers (Kenny, 1992) and karstification (Canaveras et al., 1996).

Dedolomitization has been found to increase porosity in some cases (Ayora et al., 1998). This can happen when the amount of dissolution of dolomite is much greater than the precipitation of, and replacement by, calcite (Deike, 1990). Increase in porosity has also been attributed to the dissolution of evaporites (Crestin-Desjobert et al., 1988; Bischoff et al., 1994) prior to dedolomitization. Removal of calcite (i.e. in an open system) after dedolomitization could also increase porosity. The volume change during replacement of dolomite with calcite does not seem to have an effect (Ayora et al., 1998).

Dedolomite in the Tansill Formation in the backreef setting of the Permian Reef Complex was first suggested by Lucia (1961). His assumption is based on a decreasing amount of dolomite inclusions toward the edges of calcite crystals that he examined. Mazzullo (1999) discover dedolomite in the Tansill Formation in Dark Canyon. It is only briefly mentioned in the paper, not discussed in detail.

METHODS

Two research cores were drilled in 1965 by Amoco Production Company on the north side of Dark Canyon (Figures 5 and 6) sixteen kilometers (ten mi) south of Carlsbad, NM. Amoco No.1 goes down approximately 120 meters (400 ft) from the surface and is located close to the mouth of Dark Canyon. Amoco No. 2 was also drilled from the surface down to about 140 meters (465 ft) about 0.9 km (0.5 mi) west, further up the canyon. These provide a window into the shallow subsurface for study of diagenetic features within the Tansill and Upper Yates formations, and the Capitan Massive facies.

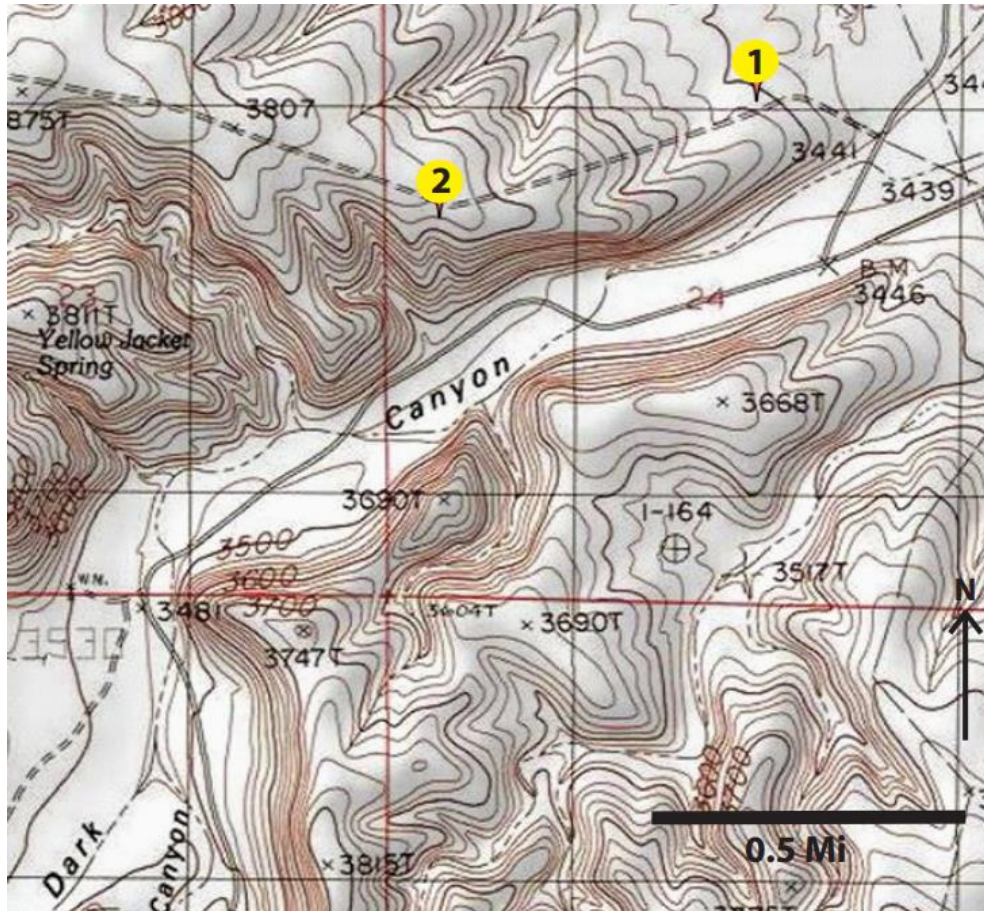


Figure 5: Location of Amoco cores No.1 and No. 2 on a topographic map near the mouth of Dark Canyon. Unpublished Amoco Core Report (1965).

Amoco No.1 penetrates the Upper Tansill Formation and some of the Capitan Reef Formation in the shelf reef margin and the outer shelf facies. Amoco No. 2 goes through the Tansill Formation and the Upper Yates Formation (Figure 6; Unpublished Amoco Core Report, 1965).

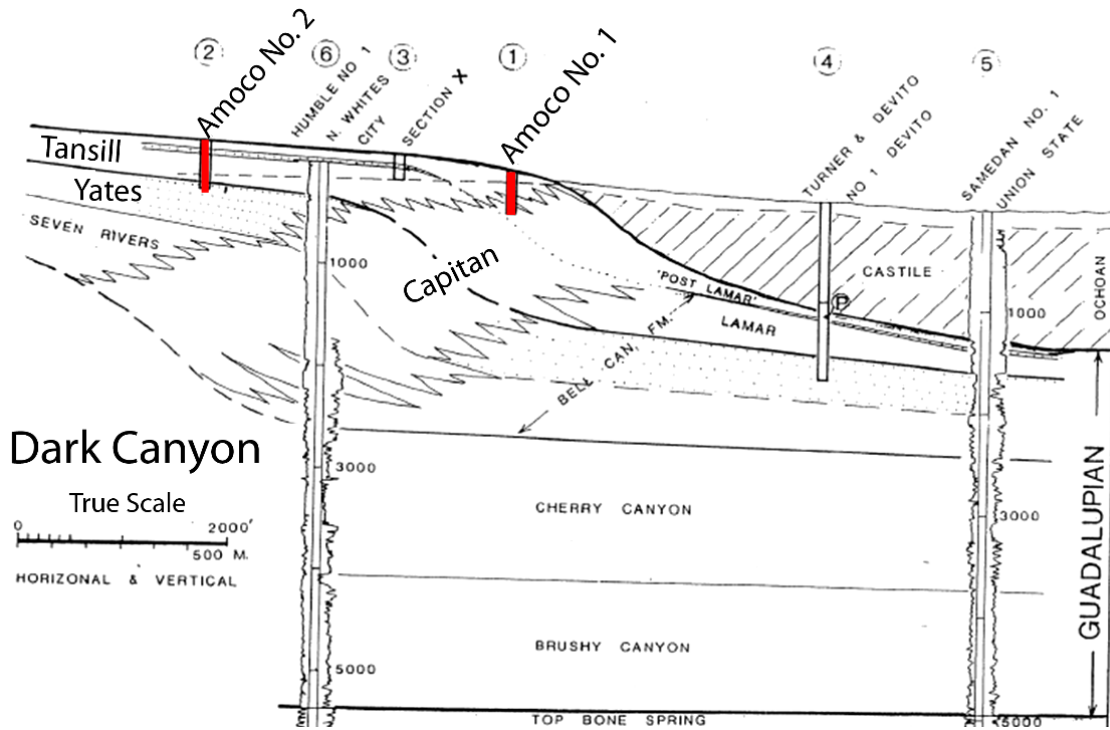


Figure 6: A schematic cross section through the facies present in Dark Canyon with the locations of Amoco cores No.1 and No. 2. Unpublished Amoco Core Report 1965.

Both cores drilled by Amoco on the north side of Dark Canyon were briefly described, particularly cements and replacement phases and their relationships to their surroundings (Appendix 1). Petrographic analysis was conducted on the thin sections from both research cores as well as on those taken from the surface samples using BX-53 and CX-31 Olympus Microscopes. Photomicrographs of thin sections were taken with an 18 MP Canon Rebel T2i. From the petrographic studies, paragenetic relationships were established for both surface and subsurface samples.

Two days were spent in Dark Canyon examining surface features and collecting samples for analysis. The outcrop samples were taken from the Tansill Formation in Dark Canyon, above the Tansill/Yates contact. This is analogous to approximately 115 meters (380 ft) depth in Amoco No. 2.

Thirty-six thin sections from various depths in both cores were made to examine diagenetic textures. Thirty of these were made for a previous uncompleted M.S. thesis; 15 were taken from Amoco No.1, and 15 from Amoco No. 2, and an additional six were taken from the Amoco No. 2 core for this project. Two thin sections were made from the

surface samples. Thin sections taken from Amoco No.1 bear the sample name in the following format: DC-1 sample depth (ft). Those from Amoco No. 2 are named DC-2 sample depth (ft). The thin sections were stained with Alizarin red S (to distinguish calcite from dolomite) and potassium ferricyanide (to detect iron) (Dickson, 1966).

Based on observations made from the thin sections, three samples were selected for microprobe analyses on a CAMECA SX-100 electron microprobe at the New Mexico Bureau of Geology and Mineral Resources at the New Mexico Institute of Mining and Technology. The CAMECA SX-100 is equipped with three wavelength dispersive spectrometers. Samples were cut to fit into a one inch round epoxy base, and then polished flat and carbon coated. Backscattered electron imaging (BSE) was used to examine the calcite and dolomite cements, replacive dolomites, and dedolomites to determine which crystals to choose for quantitative analyses. Quantitative analysis was done on all diagenetic cements and dedolomite crystals. Analytical standards included the following: amphibole, calcite, dolomite, and siderite. An accelerating voltage and probe current of 15 kV and 20 nm, respectively, were used under a general carbonate label. The elements analyzed are Ca, Mg, Sr, Ba, Fe, Mn, S, and Si as oxides. Only Ca, Mg, and Fe are above the detection limit of the microprobe. Results were given in weight percent of oxide, then converted to parts per million (ppm). Totals of 100% ± 3% are considered within error. See Appendix 2 for raw microprobe data.

The $\delta^{13}\text{C}$ and $\delta^{18}\text{O}$ were determined for eight samples (Table 4): One calcite sample, three dedolomite samples, and two samples each of the early and late dolomites. These samples were drilled from rock chips left over from thin sectioning. Table 3 is a list of these samples and the core depth from which they were collected. The powdered samples were analyzed at the Stable Isotope Laboratory of the University of New Mexico by continuous flow elemental analyzer-isotope ratio mass spectrometry (EA-IRMS) using a Costech ECS 4010 Elemental Analyzer coupled to a Thermo-Finnigan Delta Plus mass spectrometer. The laboratory standard used is Vienna Pee Dee Belemnite (VPDB); all isotope data is reported in parts per thousand (‰) relative to VPDB. These measurements are accurate to within 0.1‰.

Table 4: Isotopically analyzed samples and their depths in the Amoco No. 2 core.

Sample Type	Core Depth (ft)
Calcite	62
Early Dolomite	47
Early Dolomite	76
Late Dolomite	47
Late Dolomite	76
Dedolomite	62

RESULTS

The sequence of diagenetic events for these units is based on the petrography of the Amoco cores No.1 and No. 2 and Dark Canyon outcrops as well as core and field descriptions. Table 5 is a summary of the diagenetic events noted in this study.

Table 5: A summary of diagenetic events noted in Amoco research cores in Dark Canyon (this study).

Diagenetic Event	Appearance
Early cement	-Aragonite: Fibrous botryoidal cement, fibrous isopachous crusts, square tipped crystals -Possible high-Mg calcite: isopachous fibrous to bladed, pointed crystal tips
Dolomite	-Aphanocrystalline to medium crystalline, cloudy brown dolomite replacing fossil organisms and marine cement or lining voids (mostly fabric preserving). -Coarser, clear crystals replacing cement or lining voids as cement (somewhat fabric preserving to fabric obliterating)
Replacement of aragonitic cement	-Long, broad calcite crystals replacing fibrous aragonite -Aphanocrystalline to medium crystalline, cloudy dolomite replacing fibrous aragonite
Evaporites	-Cauliflower-shaped nodules replaced with coarsely crystalline calcite. Some contain floating dolomite.
Dedolomite	Euhedral dolomite-shaped rhombs made of calcite. Some remnant dolomite cores and/or rims.
Coarsely crystalline calcite/Calcitized evaporites	Coarsely crystalline, blocky calcite filling nodular vugs and pore space
Caliche (Surface)	Aphanocrystalline concentric pendant cements

Marine Cementation

Aragonite

Marine cement is observed in both the reef and the backreef. This cement commonly forms botryoids with radial fibrous crystals in botryoids range in length from 0.1 mm to 3 cm and are subhedral to euhedral. In thin section, the square tips on the ends of the fibrous crystals are characteristic of aragonitic crystal structure (Figure 7).

In the backreef Tansill and Yates Formations, botryoidal cements are present mostly within tepee structures, along with later diagenetic cements (such as dolomite and coarsely crystalline calcite). As the tepee structures were forming, the crust they were forming in (dominantly algally laminated carbonates) was expanding and being pushed incrementally upwards by upwelling waters or thermal expansion, which could have created space for the botryoidal cement to form in within the tepees (Kendall and Warren, 1987). Figure 8 is one such tepee structure, and Figure 9 is a photograph of a dolomitized botryoid in a tepee structure in Walnut Canyon near the headquarters of Carlsbad Caverns.

These botryoidal cements are inferred to be originally aragonitic. The aragonite examined in the backreef of the Permian Reef Complex in previous studies, like that of this study, tends to encrust allochems with isopachous needle fringes that have square tipped crystals. This cement also forms fan druses and botryoids and fills in most of the primary pore space, even cementing organisms in their living positions (King, 1942; Mazzullo and Cys, 1977; Cys, 1979; Chafetz et al., 2008).

Many of the delicate organisms that lived in the reef complex facies, such as crinoids and phylloid algae, are preserved in living position by this cement. As the aragonitic cements filled in the primary porosity within the reef, organisms, such as *Archaeolithoporella* sp., continued to grow on and be encrusted by later episodes of cementation (Figures 10 and 11). This indicates that the aragonitic cements were precipitating during deposition (syndepositional).

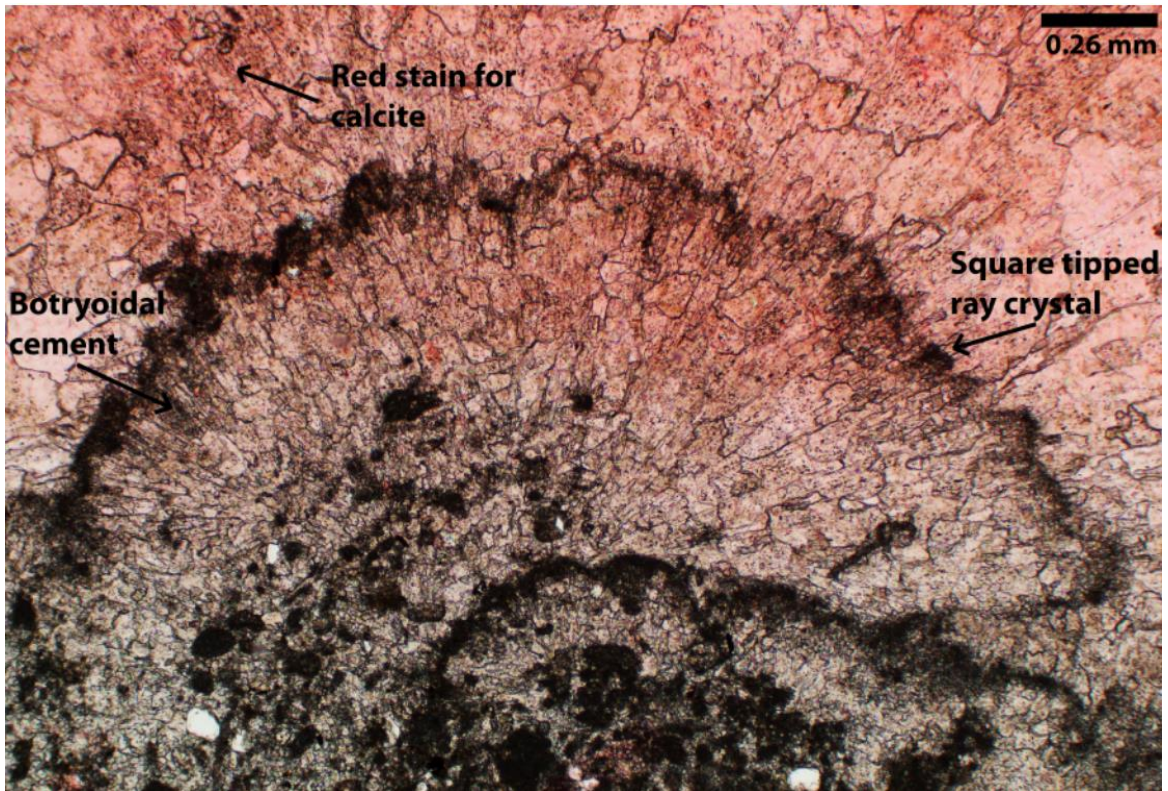


Figure 7: Amoco No. 1, 245 ft (DC-1 245). Formerly aragonitic botryoidal cement. Square tipped crystals, which are diagnostic of aragonite, are evident. The radial fibrous nature of the original aragonite is extremely subtle, as this cement has neomorphosed to calcite since its formation, a process in which the original radial fibrous fabric has been somewhat preserved. During neomorphism, the crystals became wider and less fibrous. There are at least three generations of aragonite visible here.

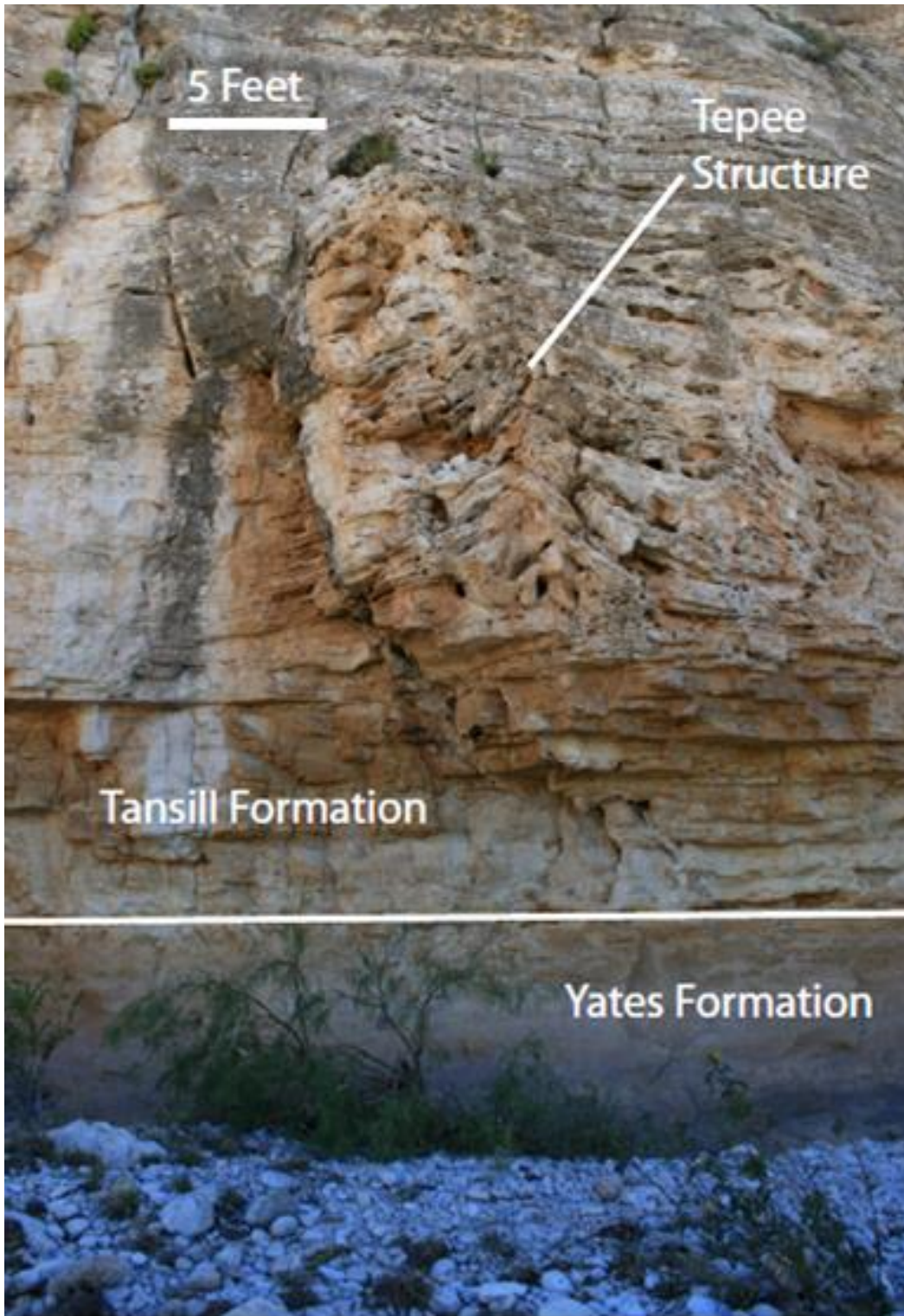


Figure 8: The contact between the Tansill and Yates Formations is visible at the base of the tepee structure. This tepee is approximately 5 m (15 ft) tall. From the backreef facies in Dark Canyon (mile 0.6).

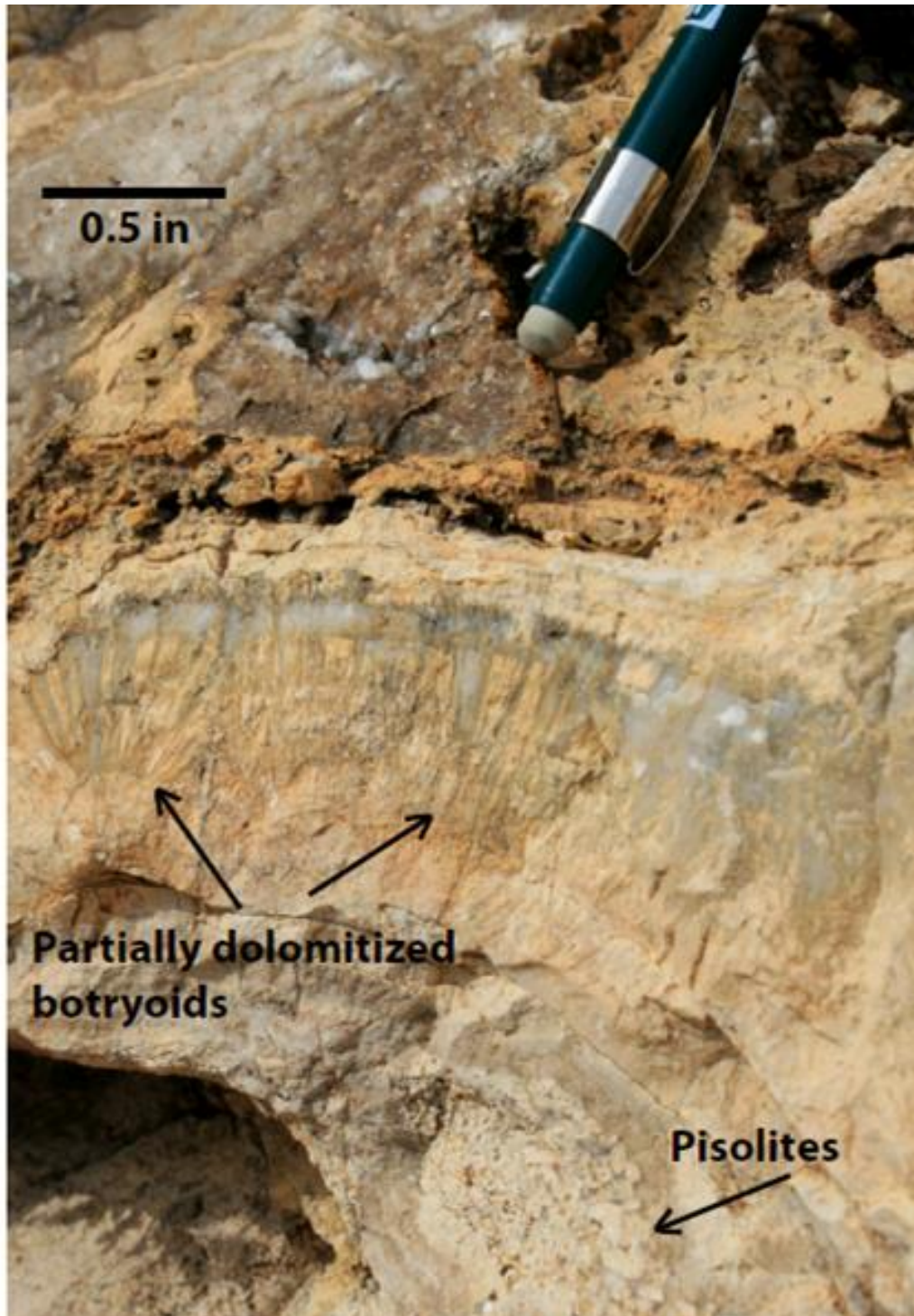


Figure 9: Dolomitized aragonite botryoids in a tepee structure. Square tipped crystals indicate that the botryoids were originally aragonite. The white cement at the tips of the botryoids is medium crystalline calcite. These calcites could either be replacive or void filling. The calcite here is thought to be replacive, as is somewhat fabric preserving. Pisolites can be seen below the botryoids. Yates Formation in Walnut Canyon (mile 0.8).



Figure 10: Originally aragonitic cement forms botryoids growing on, and intergrown with, *Archaeolithoporella* sp. The brown area underneath the pencil is partly dolomitized and partly calcitized botryoidal cement that was formerly aragonite. From the reef facies in Walnut Canyon, approaching the backreef facies (mile 0.5).

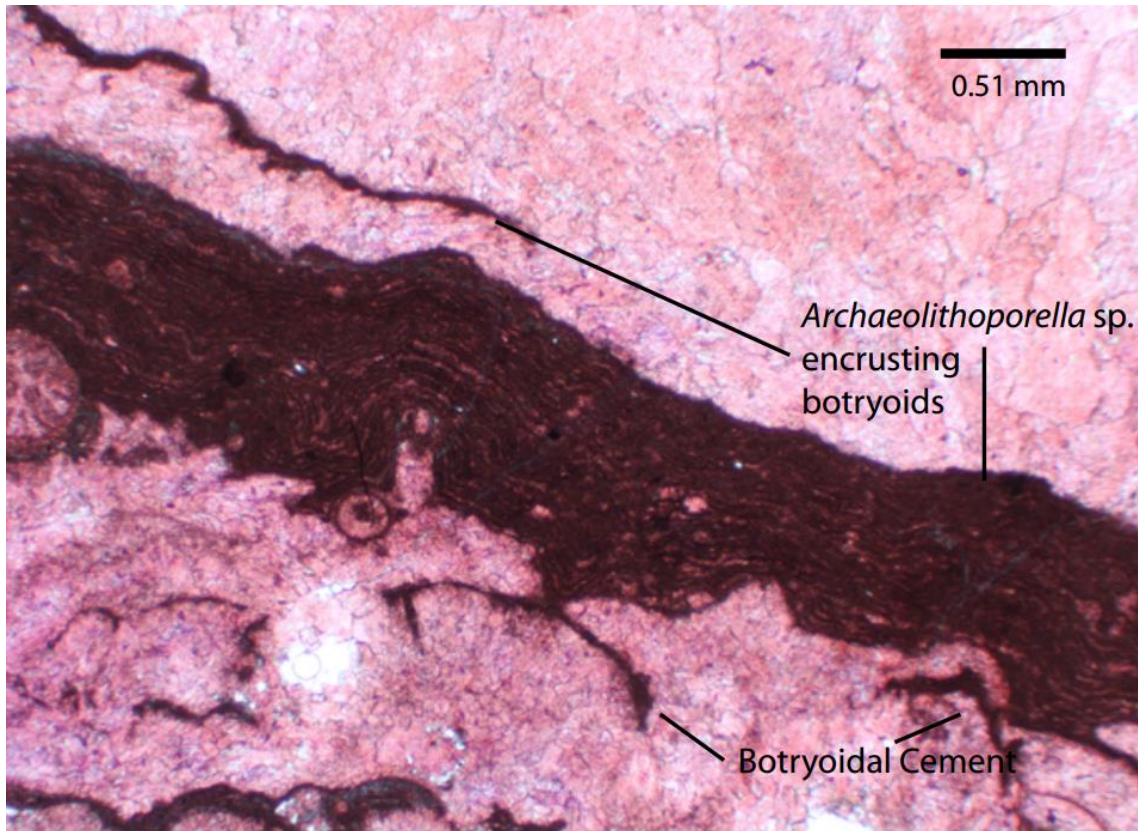


Figure 11: Amoco No.1, 300 ft (DC-1 300). *Archaeolithoporella* sp. encrusting formerly aragonitic botryoidal cements. The *Archaeolithoporella* sp. is also encrusted by aragonitic cement, indicating that the aragonite cement was penecontemporaneous with deposition in a marine environment.

Possible High-Mg Calcite

Isopachous fibrous calcite cement is also observed lining pore spaces and encrusting organisms in the reef and backreef grainstones. These crystals are anhedral to euhedral and range in size from 0.005 to 0.05 mm across (Figures 12, 13, and 14). Crystal shape is generally fibrous with pointed tips (Figures 12 and 13) although it can be more bladed (Figure 14). The more bladed nature of the crystal shape and the pointed tips on the ends of the crystals indicate that these cements could have originally been high magnesian (high-Mg) calcite (Scholle and Ulmer-Scholle, 2003). Alternatively, they could have originally been aragonite.

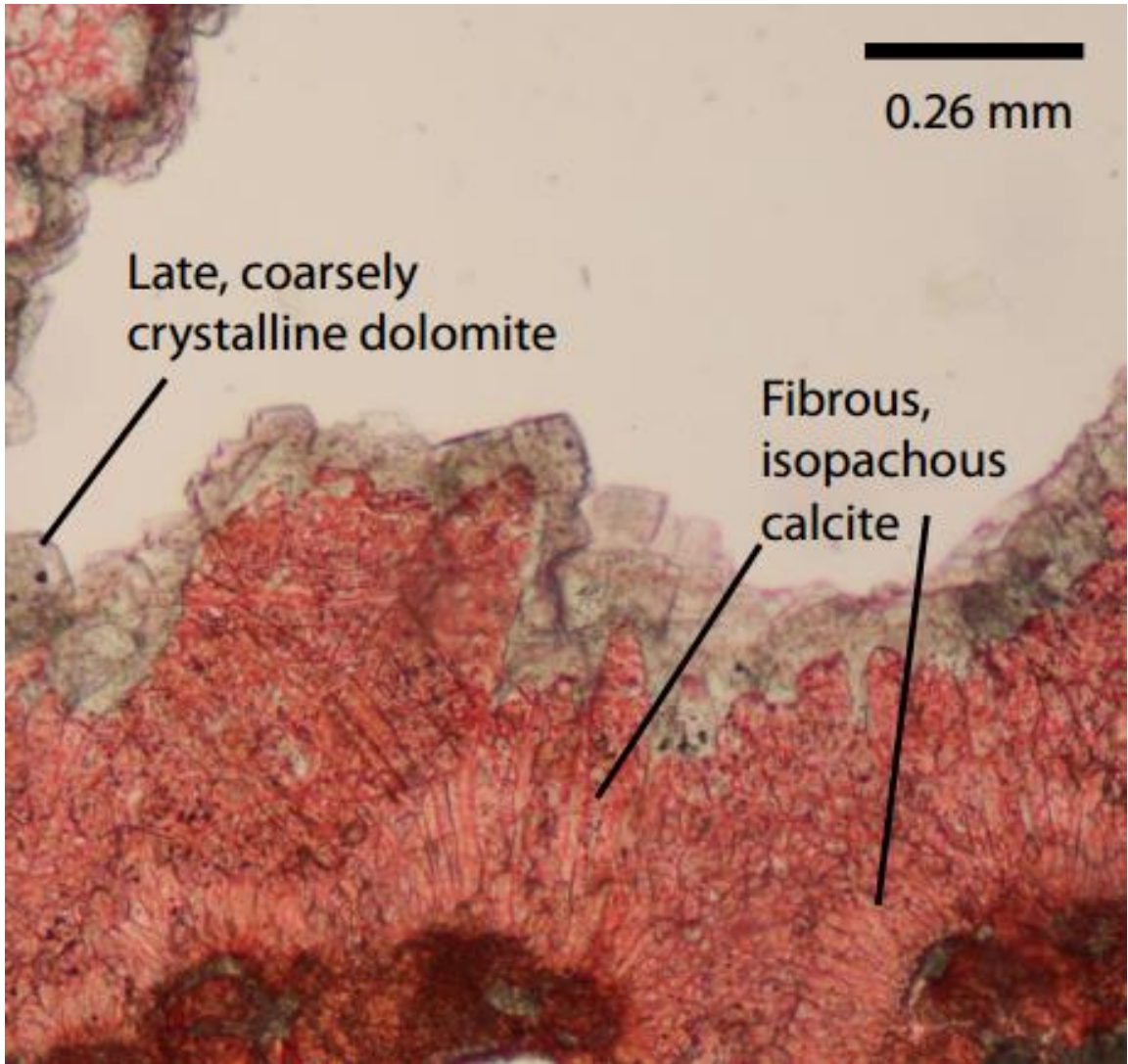


Figure 12: Amoco No.1, 56 ft (DC-1 56). Fibrous high-mg calcite cement precipitated on the edge of a void (in this case, the osculum of a sponge that has been dolomitized). This cement forms an isopachous crust on the sponge. The crystals have pointed tips, indicating that it is not aragonite

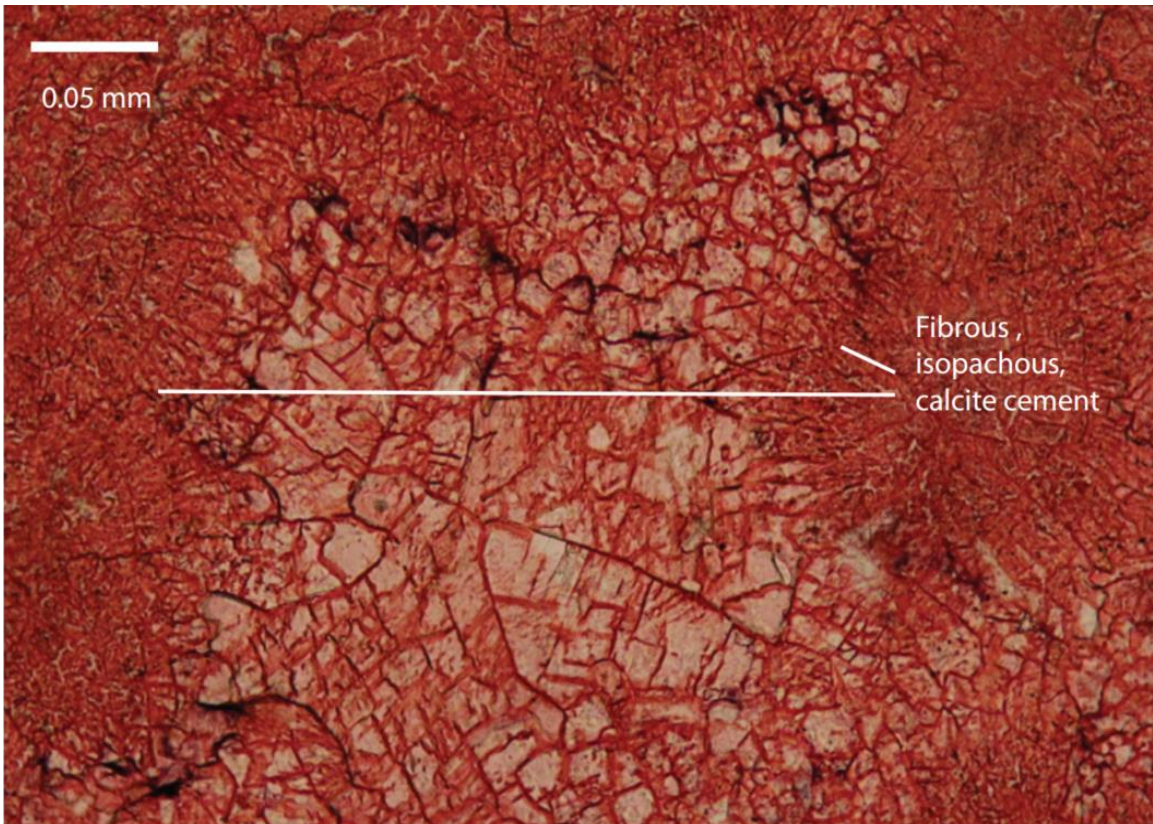


Figure 13: Amoco No. 2, 55 ft (DC-2 55). Fibrous, isopachous calcite cement lining what used to be a pore space (now filled in with coarser crystalline calcite cement). The fibrous nature of these crystals and pointed tips could indicate that this might be high magnesian calcite. Alternatively, it could be former aragonite, which is also fibrous.

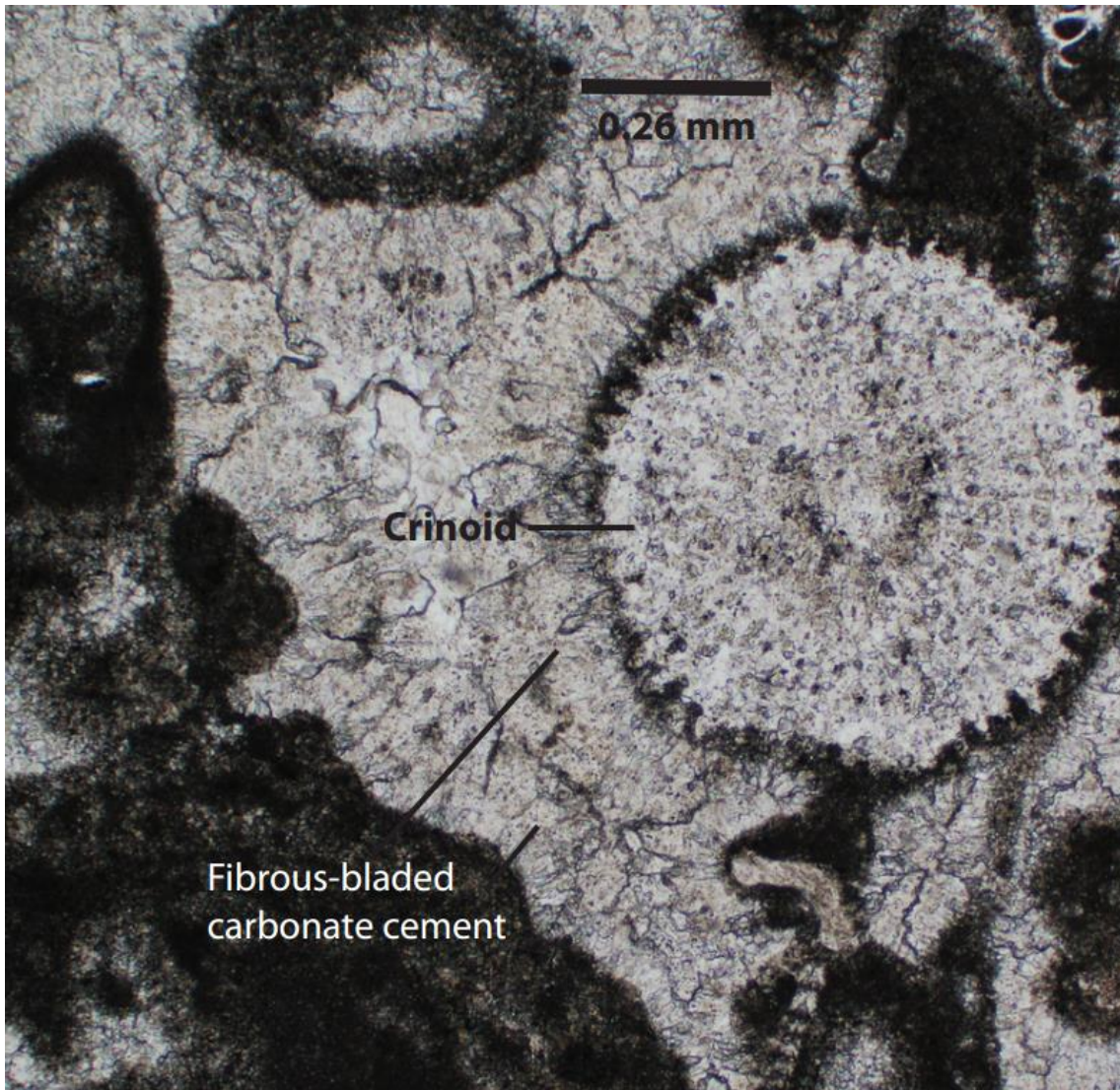


Figure 14: Amoco No. 1, 128 feet depth (DC-1 128). Isopachous calcite cement coats a section of a crinoid. This cement is more bladed than fibrous, which could indicate that it was originally high-Mg calcite. Alternatively, the crystals could have originally been fibrous and only became bladed after diagenesis. If this is the case, it was probably originally aragonitic and has converted to low-Mg calcite. This photomicrograph was taken in an unstained portion of the thin section.

As this cement, like fibrous aragonitic cement, isopachously lines voids and organisms, it too could be considered syndepositional. It is known that aragonite and high-Mg calcite precipitate together based on modern analogues (Scholle and Ulmer-Scholle, 2003). Prior study of this type of cement found it to be syndepositional (Mazzullo and Cys, 1977).

Dolomite Cementation

Dolomite cement is sometimes observed lining the walls of pore spaces and voids as an isopachous crust (Figure 15). This cement is medium crystalline, equant, and subhedral to euhedral. The crystal shape, isopachous nature, and larger crystal size possibly indicate precipitation from fluids rather than replacement of an earlier isopachous cement. These characteristics could be an indicator that this dolomite formed at depth, while the reef was in a burial stage (Adams and Rhodes, 1960; Shinn, 1983). Alternatively, this cement could have occurred at or near the surface during sea level fluctuations and the mixing of marine and meteoric waters. Clear, equant dolomite crystals can precipitate slowly from solutions with low salinity, such as marine/meteoric mixed waters (Folk and Land, 1975; Weaver, 1975; Humphrey, 1988), or form during seepage refluxion of brines in the subsurface (Adams and Rhodes, 1960, Melim and Scholle, 2002).

The dolomite cement has precipitated on top of early marine cements that have isopachously lined and organisms (Figure 15). This indicates that the dolomite cement occurred after the early aragonite and high-Mg calcite cements were already in place. Alternatively, this dolomite cement could be replacing some of the early marine cements. In either case, this dolomite occurred later than the syndepositional marine cementation. Coarsely-crystalline calcite is observed filling in pore space and growing over and around the dolomite cement crystals, which indicates that the dolomite cement is younger than the coarsely crystalline calcite (see section on coarsely-crystalline calcite).

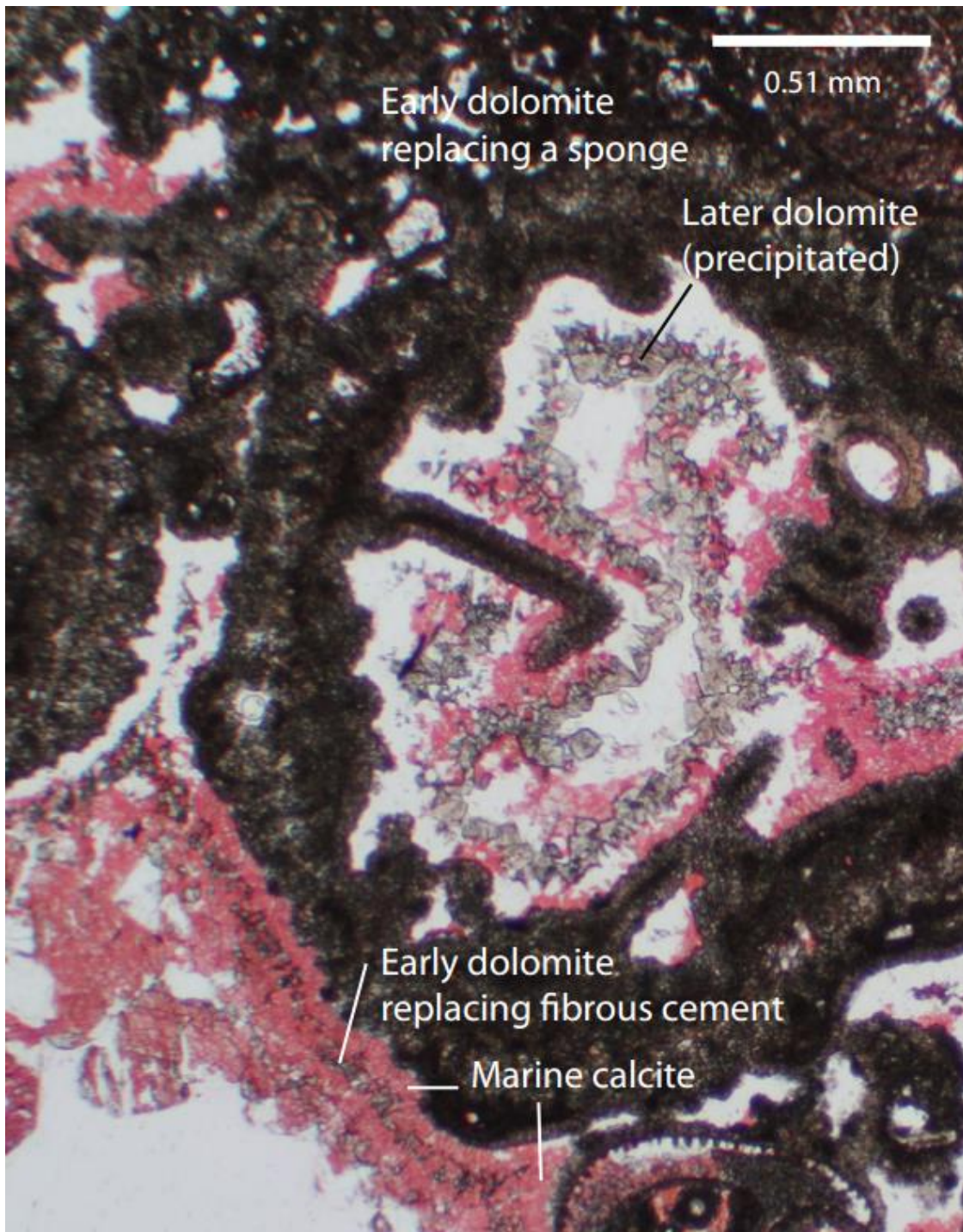


Figure 15: Early dolomite replacing a sponge. In the lower left, isopachous calcite cements line the edge of the sponge. A layer of dolomite replacing the isopachous fibrous cement overlies the first layer of marine cement. This sequence is repeated at least once; it is barely discernible outside this sponge.

Dolomite Replacement

Two types of replacive dolomite are present in the backreef facies: aphanocrystalline to medium-crystalline (dominantly finely-crystalline), cloudy dolomite and coarser crystalline, clear dolomite. Both types of replacive dolomite were examined with backscattered electron imaging (BSE) for comparison.

Early/Syn depositional Dolomite

The first type of dolomite is 0.03 to 0.1 mm approximately and cloudy brown. This dolomite is generally fabric preserving and replaces fossils, like sponges, as well as aragonite and high-Mg calcite cements (Figures 15 and 16). In general, during dolomitization, dolomite preferentially replaces aragonite (Scholle and Ulmer-Scholle, 2003).

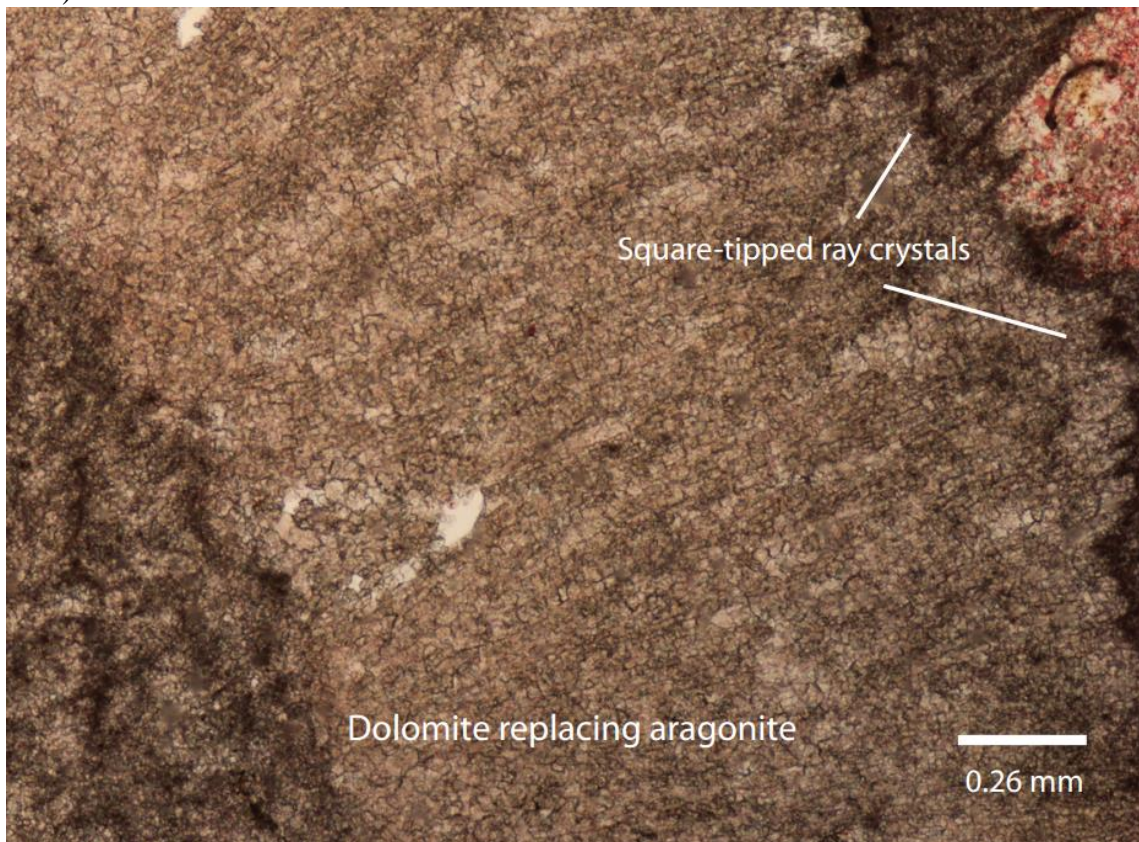


Figure 16: Amoco No. 2, 76 ft (DC-2 76). Finely-crystalline dolomite directly replacing an aragonitic botryoid. Square tipped crystals indicate former aragonite. The original fibrous fabric of the aragonite is well preserved.

Under BSE, the more finely crystalline dolomite displays slightly more porosity than the more coarsely crystalline dolomite (discussed in the next section) (Figure 17).

This could be causing the cloudy appearance of the finely-crystalline dolomite. Alternatively, the cloudiness could be due to inclusions or trace elements.

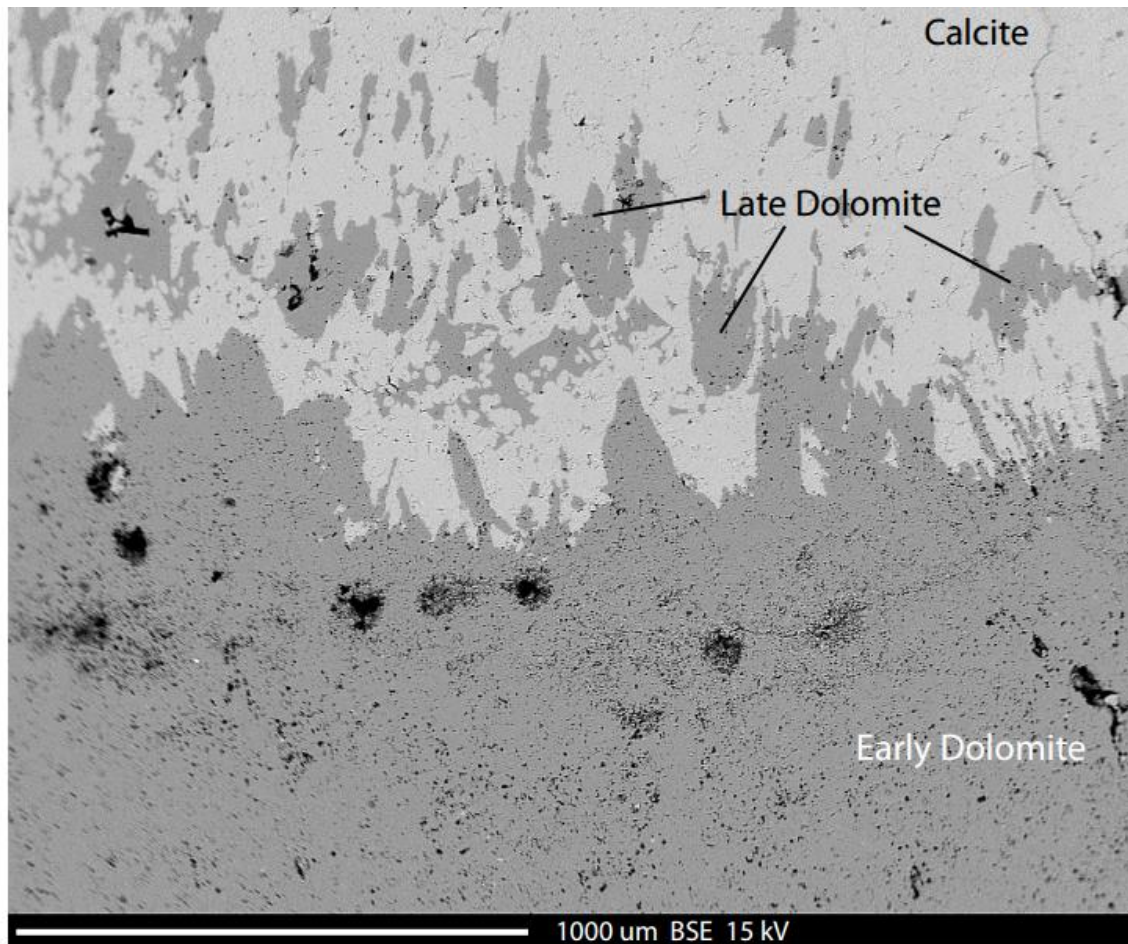


Figure 17: A backscatter electron image. Calcite displays the lightest color; dolomite is the darker grey. The black spots represent porosity. Note that the early dolomite has much more porosity (the black spots) than the later dolomite. From DC-2 76.

In high-gain mode backscattered electron imaging (BSE), both the early and later replacement dolomites exhibit subtle chemical variations (Figure 18), which are represented by the slight color differences within the crystals. Although quantitative analyses were completed to determine the cause of the color variation, the elemental difference between the lighter and darker phases was too subtle to be detected by the microprobe.

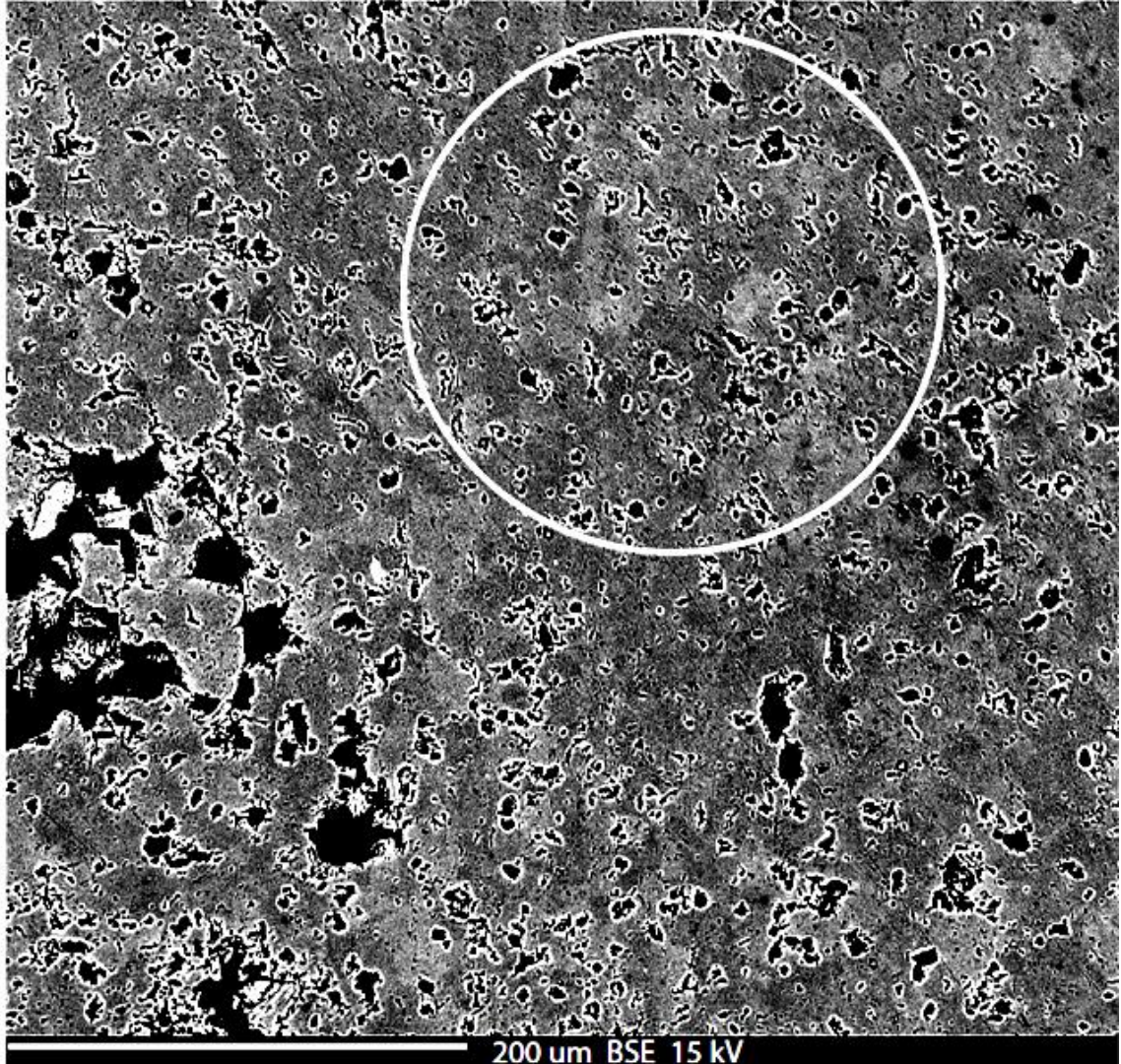


Figure 18: High gain BSE image of the older dolomite. Note the subtle differences in color within the circle. These represent slight chemical differences within the dolomite. These subtle chemical differences can also be seen in the younger dolomite and the calcite. They look the same as in the BSE image above. From DC-2 76.

Since this type of dolomite replaces aragonite and marine organisms, it can be inferred that it occurred after these were in place. It is possible that it was occurring while deposition was still going on. Figure 19 is a photomicrograph of dolomite that has replaced a sponge. The sharp, clean border between the dolomitized sponge and the high-Mg calcite that isopachously lines it suggests that the sponge was dolomitized before the high-Mg calcite precipitated. If the sponge had been dolomitized after the high-Mg calcite was in place, this border would not be so clean. This implies that the early replacive dolomite was likely syndepositional.

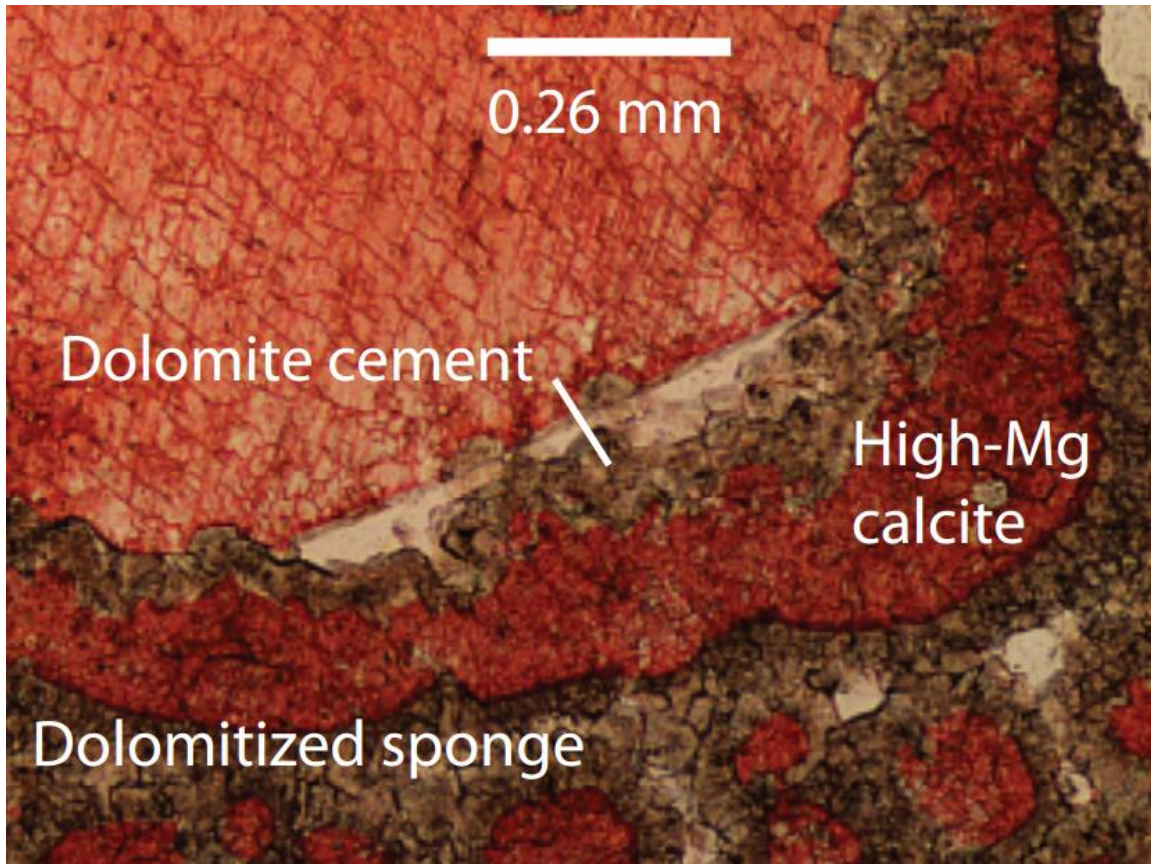


Figure 19: Amoco No.1, 56 ft (DC-1 56). Photomicrograph of possible high-Mg calcite isopachously lining a dolomitized sponge. The clean border between the sponge and the calcite suggests that the sponge was dolomitized before the calcite precipitated on top of it. The high-Mg calcite above has been replaced with low-Mg calcite. This replacement did not preserve the fibrous character of the original calcite. Alternatively, the cement isopachously lining the sponge could have been aragonite. Dolomite cement precipitated on the possible high-Mg calcite (or aragonite) cement after it was in place and before the coarsely crystalline calcite formed.

Later Dolomitization

The next type of dolomite is more coarsely crystalline and clearer. Crystals range from subhedral to euhedral and 0.01 to 0.5 mm in size. It is dominantly fabric preserving but can be fabric destructive. Figure 20 is a photomicrograph of the coarser dolomite replacing calcite. Note that some is fabric preserving, and some is euhedral, obliterating previous textures.

This coarser, clearer replacive dolomite is observed growing around the more finely crystalline, cloudy dolomite (Figure 21). This implies that it came later than the aphanocrystalline dolomite. The clear, coarse nature of this dolomite, like the dolomite cement, could indicate that it formed from mixed marine-meteoric waters (Folk and Land, 1975; Weaver, 1975; Humphrey, 1988), or from seepage refluxion of brines

(Adams and Rhodes, 1960). Melim and Scholle (2002) concluded that this type of dolomite occurred during deeper burial of the Permian Reef Complex.

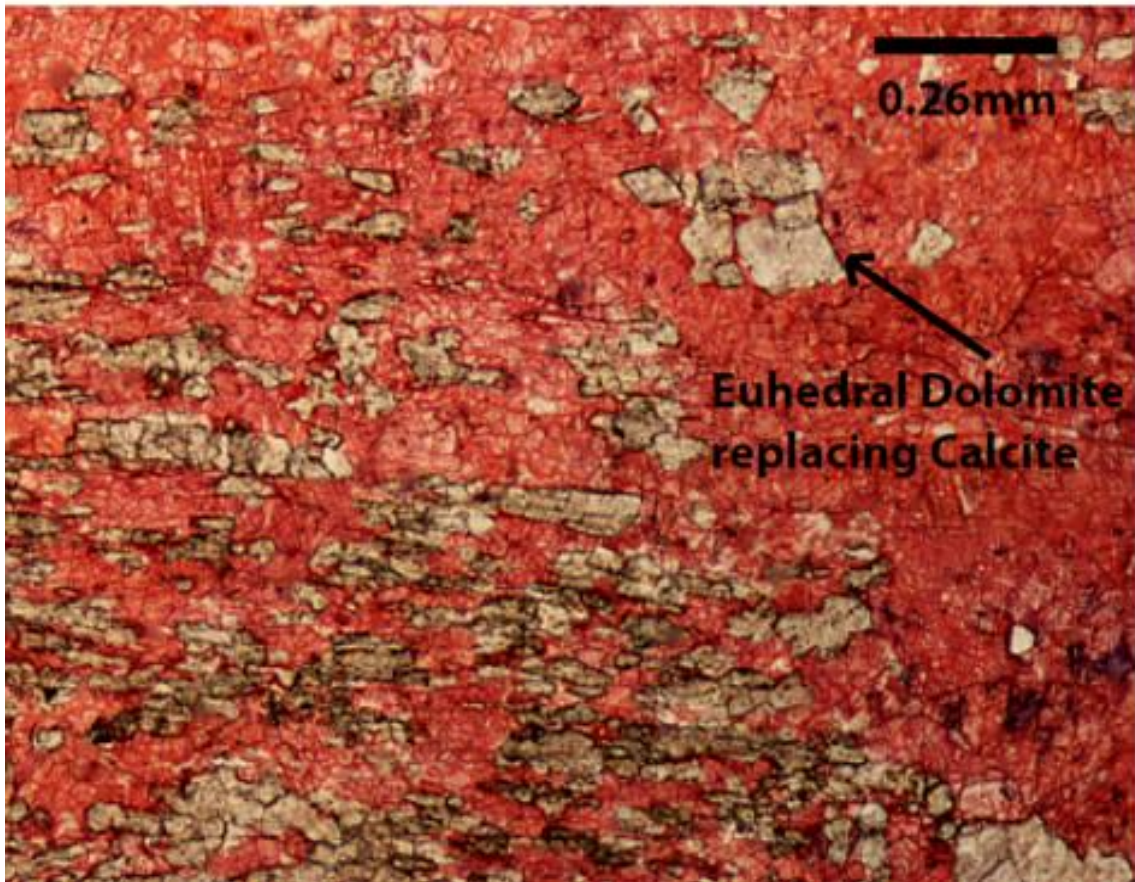


Figure 20: Amoco No. 2, 76 ft (DC-2 76). This is the second type of replacive dolomite. Euhedral dolomite rhombs (upper right) replace calcite cement. In the lower left, the dolomite is less euhedral and appears to also be replacing calcite. Note the elongated, almost bladed appearance of the replacement dolomite. This could indicate that this dolomite is replacing original aragonitic cement and somewhat preserving the fibrous nature of the aragonite crystals. Alternatively, when the aragonite neomorphosed to calcite (discussed later), the crystals became wider and more bladed than fibrous. The dolomite could be replacing this neomorphosed fabric. More study is necessary to be certain.

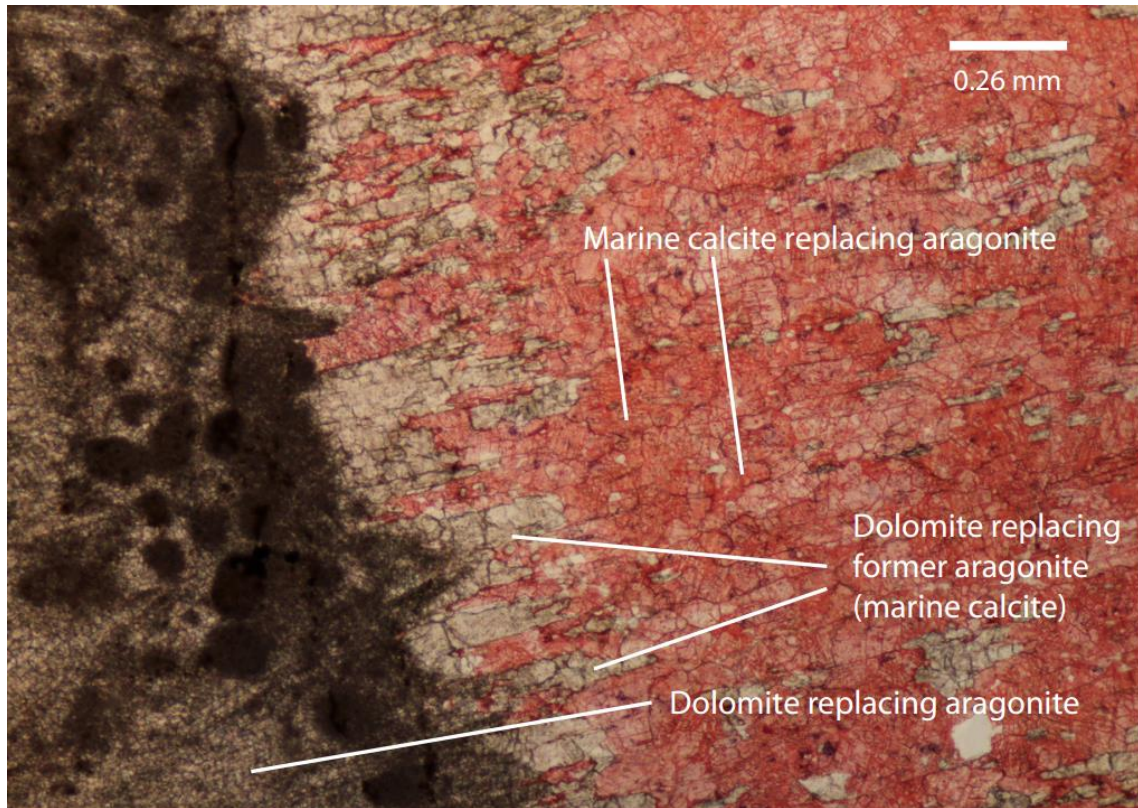


Figure 21: Amoco No. 2, 76 ft (DC-2 76). Photomicrograph of aragonitic cements that have been directly replaced by finely-crystalline dolomite (far left), marine cement that has been neomorphosed into/replaced by calcite (far right), and coarser, clearer dolomite replacing either aragonite or the later calcite. Note that the coarser dolomite appears to grow around the finer, cloudier dolomite.

Geochemistry of Replacive Dolomites

Quantitative analysis of both the early, finely-crystalline dolomite and the later more coarsely crystalline dolomite reveals that the early dolomite, overall, has a higher iron content (Figure 22). The Ca/(Ca+Mg) is narrow for both the early and later dolomites, ranging from 0.622 to 0.641. The later dolomite has a slightly lower Ca/(Ca+Mg) than the earlier dolomite, indicating higher magnesium content, making them closer to a stoichiometric dolomite. Table 6 shows these data and the depths of the three samples from Amoco No. 2.

Stable isotope analyses ($\delta^{18}\text{O}$ and $\delta^{13}\text{C}$) of the two types of replacive dolomite (two samples for each type of dolomite) show that the early dolomite ranges from -0.51‰ to 1.15‰ , and the $\delta^{13}\text{C}$ for those samples are 6.31‰ to 6.68‰ (Figure 23). The later dolomites have a slimmer range for $\delta^{18}\text{O}$: -0.2‰ to 0.52‰ , and a wider range for $\delta^{13}\text{C}$, from 5.76‰ to 6.89‰ .

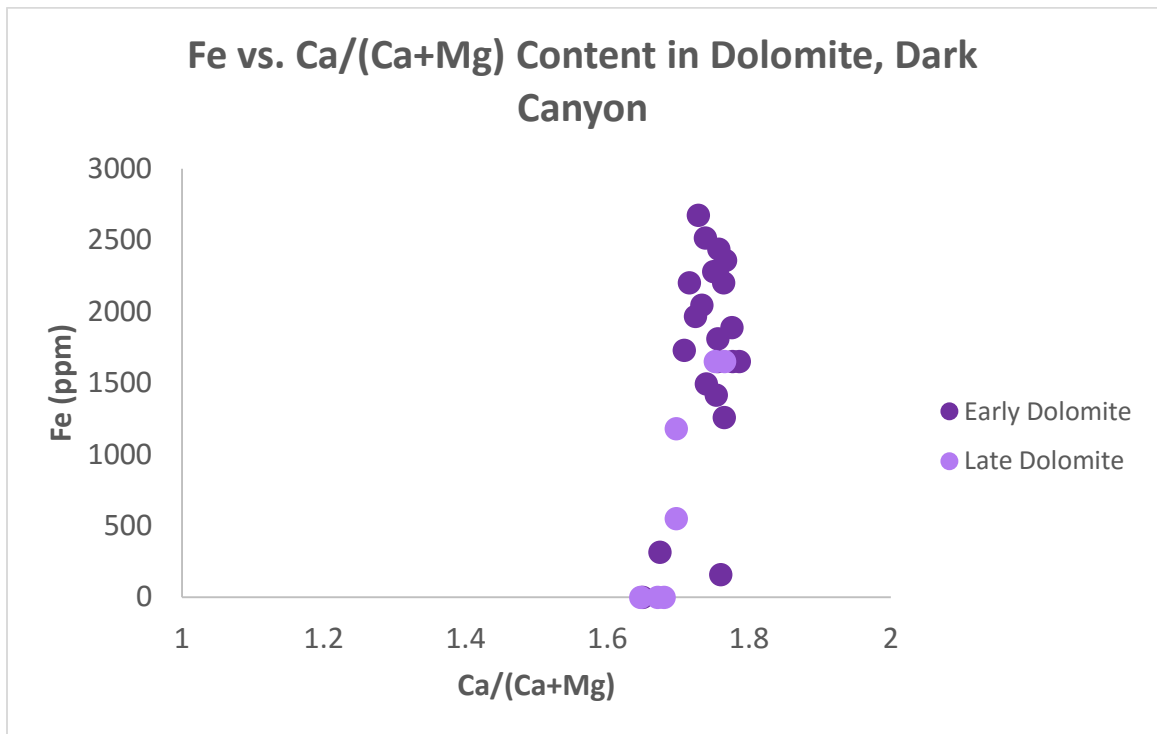


Figure 22: Data from the quantitative analysis of both types of dolomite in parts per million (ppm). The Ca/(Ca+Mg) range for both dolomites is very narrow, ranging from 0.622 to 0.644. Overall, the early dolomite has a higher iron content and Ca/(Ca+Mg) than the later dolomite.

Table 6: Quantitative microprobe analysis for dolomite samples in parts per million (ppm). The light and dark labels are referring to the subtle color differences noted in high-gain mode.

Sample Type	Ca/(Ca+Mg)	Fe (ppm)	Depth (ft)
Early Dolomite	0.639	2359.717	76
Early Dolomite	0.641	1651.802	76
Early Dolomite	0.626	314.6289	47
Early Dolomite	0.623	0	47
Early Dolomite	0.631	1730.459	108
Early Dolomite	0.637	1415.83	108
Early Dolomite (dark)	0.637	2438.374	76
Early Dolomite (dark)	0.636	2281.06	76
Early Dolomite (dark)	0.638	2202.403	76
Early Dolomite (dark)	0.638	1258.516	76
Early Dolomite (dark)	0.640	1887.774	76
Early Dolomite (dark)	0.632	2202.403	76
Early Dolomite (dark)	0.634	2045.088	76
Early Dolomite (dark)	0.637	1809.116	76
Early Dolomite (light)	0.635	2517.032	76
Early Dolomite (light)	0.640	1651.802	76
Early Dolomite (light)	0.637	2281.06	76
Early Dolomite (light)	0.638	157.3145	76
Early Dolomite (light)	0.633	2674.346	76
Early Dolomite (light)	0.633	1966.431	76
Early Dolomite (light)	0.635	1494.487	76
Early Dolomite (light)	0.637	1651.802	76
Late Dolomite	0.638	1651.802	76
Late Dolomite	0.622	0	47
Late Dolomite	0.637	1651.802	108
Late Dolomite	0.629	1179.859	108
Late Dolomite (euhedral)	0.629	550.6006	47
Late Dolomite (euhedral)	0.627	0	47
Late Dolomite (euhedral)	0.626	0	47

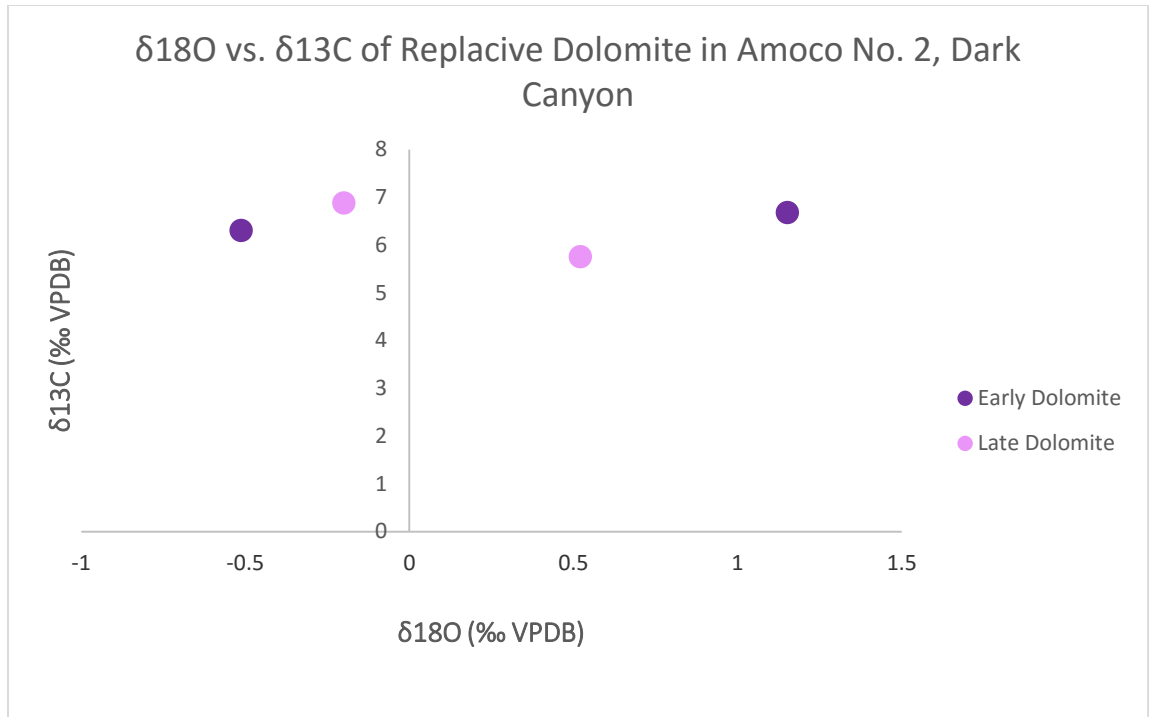


Figure 23: Stable isotope data for replacive dolomites (in parts per mil- ‰). Early dolomites range from -0.51‰ to 1.15‰ $\delta^{18}\text{O}$ and 6.31‰ to 6.68‰ $\delta^{13}\text{C}$. Later dolomites vary from -0.2‰ to 0.52‰ $\delta^{18}\text{O}$ and from 5.76‰ to 6.89‰ $\delta^{13}\text{C}$. These values are consistent with those from previous studies (see Figure 4 and Discussion section).

Calcite Replacement of Aragonite (Neomorphism)

Some of the aragonitic cement neomorphosed into calcite. It partially retains the original fibrous character of the aragonite (Figure 24). The calcite crystals that replaced the aragonite are coarser than the original fibrous aragonite crystals. In some places it has become more bladed than fibrous during the transition from aragonite to calcite (Figure 24). This could be an effect of recrystallization (Mazzullo, 1980). Low-Mg calcite tends to have a more bladed than fibrous crystal morphology. Original aragonite and high-Mg calcite generally converts to low-Mg calcite during diagenesis of older limestones (Scholle and Ulmer-Scholle, 2003).

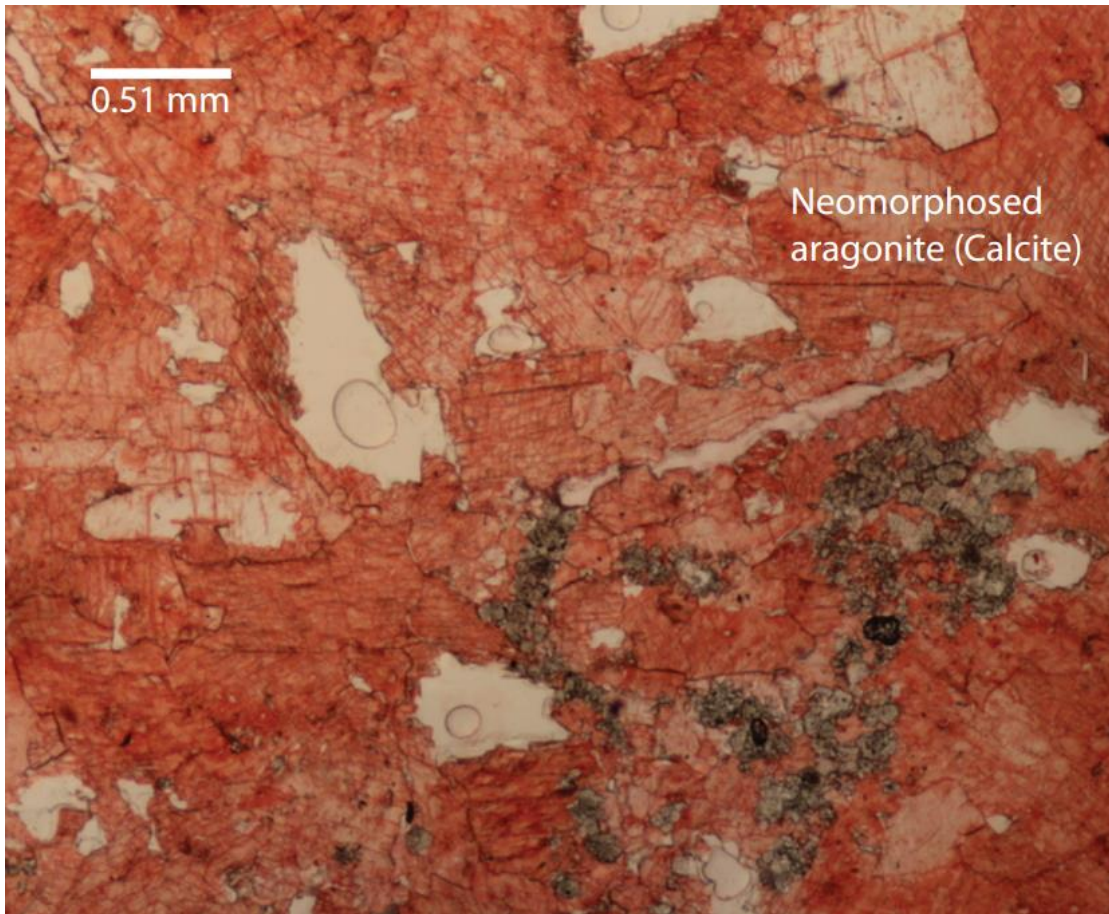


Figure 24: Amoco No. 2, 247 ft (DC-2 247). Aragonite that has neomorphosed into calcite. During neomorphism, the crystals became less fibrous and more wide and bladed.

Neomorphism of aragonite to calcite probably happened after early dolomitization- some of the observed former aragonite was directly replaced by finely-crystalline, fabric-preserving dolomite. This type of dolomite is interpreted to be very early in the diagenetic sequence, perhaps even syndepositional. The broader, more bladed crystals that were neomorphosed are not seen replaced with the finely-crystalline dolomite. Based on the petrographic study by Melim and Scholle (2002), the fabric-preserving dolomite was determined to have formed while the originally aragonitic cements were undergoing neomorphism to calcite. More evidence is necessary in order to be certain about the exact timing of the neomorphism of aragonite to calcite relative to dolomitization.

Evaporite Precipitation

Direct evidence of evaporite minerals was not found in either of the two Amoco cores from Dark Canyon. There may be minute evaporite inclusions in the later coarsely-

crystalline calcite (Figure 25), but microprobe analysis is necessary to correctly identify these inclusions. Instead, fabrics indicative of evaporites, such as cauliflower-shaped nodular vugs, have mostly been replaced with calcite or dissolved away, leaving voids (Figure 26). Figure 27 is an image of the “floating dolomite” which was described by Scholle et al. (1992) as evidence for prior evaporites. The dolomite is contained within coarsely crystalline calcite crystals, which appears to have replaced the evaporite, or at least filled voids that were once occupied by evaporite minerals. Because the evaporites do not appear to be contained to any specific facies, more thin sections are needed to fully understand their distribution throughout the core.

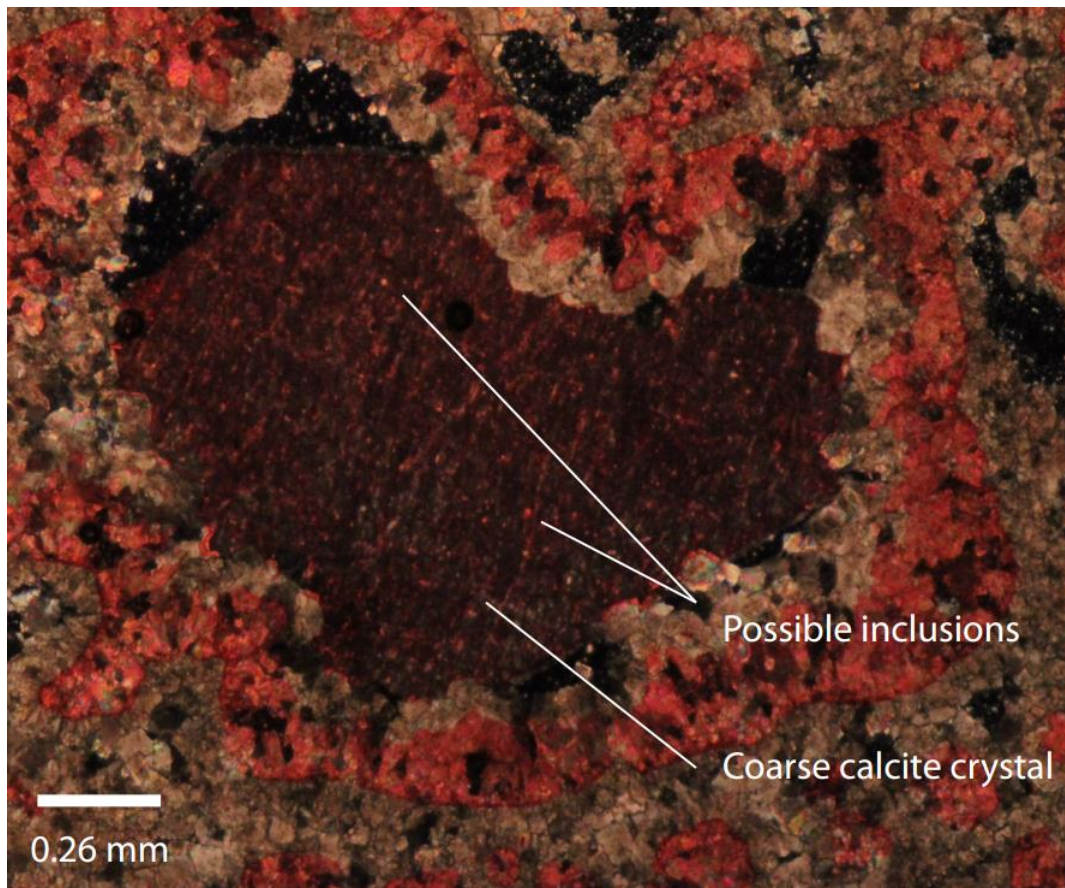


Figure 25: Amoco No. 2, 73 ft (DC-2 73). In cross-polarized light, it is possible to see bright spots contained within most of the coarsely crystalline calcites (red stain). These could be inclusions of evaporites. This coarse crystal of calcite is located in the osculum of a dolomitized sponge. The dolomite replacing the sponge is finely crystalline and cloudy (early). Fibrous to bladed calcite isopachously lines the osculum. This was probably originally high-Mg calcite based on the bladed character of the crystals. Coarser, clearer dolomite crystals overlie the isopachous calcite, concentrically lining the osculum of the sponge. This dolomite occurred after the calcite cement was in place. The coarse calcite crystal filling in the rest of the sponge osculum occurred the latest.



Figure 26: Photograph from the south side of Dark Canyon approximately 0.25 miles behind the reef. Cauliflower-shaped nodular vugs are indicative of the past presence of evaporites. These have been dissolved away and then partially or completely filled with coarsely crystalline calcite cement.

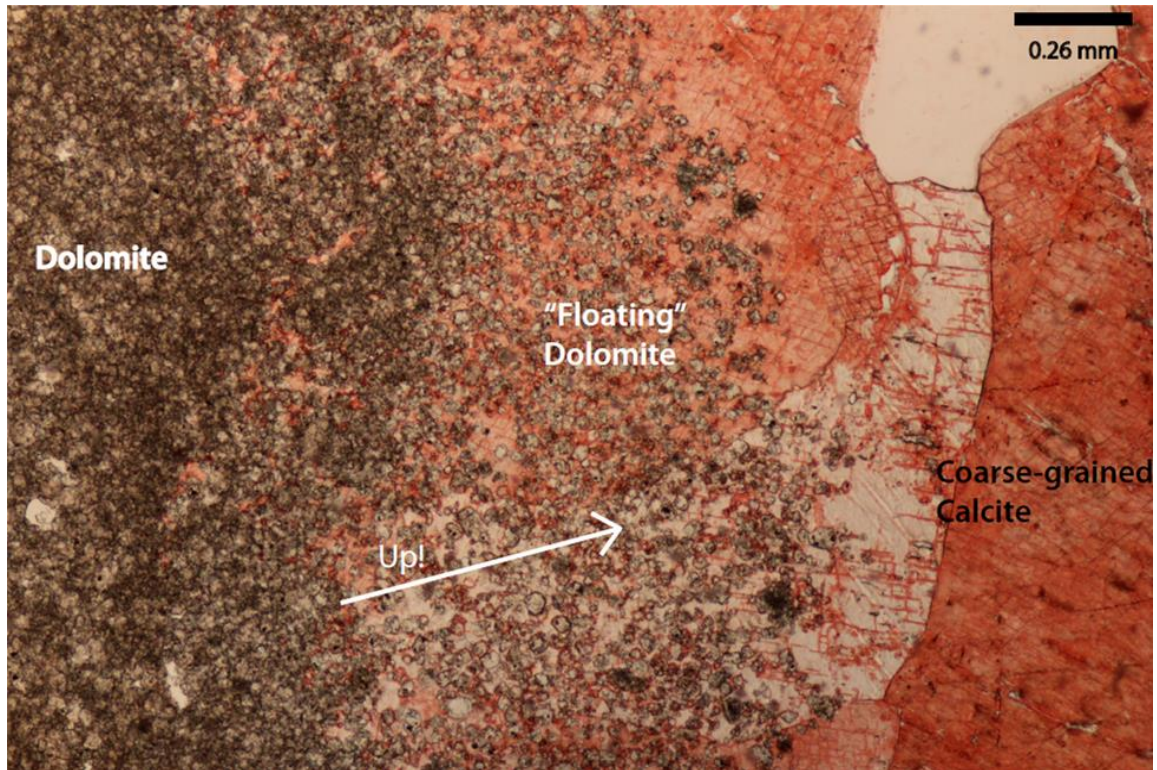


Figure 27: Amoco No. 2, 207 ft (DC-2 207). Floating dolomite crystals contained in the late, coarsely crystalline calcite. This could be “floating dolomite” (Scholle et al., 1992), indicative of evaporite replacement by the coarsely crystalline calcite.

The timing of evaporites is difficult to constrain precisely. As seen in Figure 25, while the evaporite was growing displacively, it included some of the early dolomite into the nodule. This indicates that the evaporites (at least this particular one) grew after the early dolomite was in place. Since the evaporites have been replaced with coarsely-crystalline, blocky calcite, they had to have occurred before the calcite came in.

Euhedral rhombs of calcitized dolomite (dedolomite, discussed in the next section) are present in some of the replaced evaporite nodules. This could either imply that euhedral rhombs of what was originally dolomite replaced the original evaporite or that it was replacing the calcite that replaced the evaporite. The former is more likely as the coarsely crystalline calcite replacing the evaporites is interpreted by previous studies (and discussed later) to be very late in the diagenetic sequence. This interpretation is based on the assumption that the calcite precipitated from meteoric fluids that were present during the uplift and exposure of the Permian Reef Complex after it was buried by the Castille Formation (Scholle et al., 1992; Ulmer-Scholle, 1993).

Dedolomitization

Within the upper and middle Tansill Formation in Amoco No. 2, there are areas containing euhedral dolomite-shaped rhombs that are stained red by Alizarin red-S stain; these rhombic crystals are actually calcite filled (Figure 28). Based on their shape and remnant dolomite cores and rims, the rhombic calcite crystals were originally dolomite and have been calcitized (also known as dedolomitization). Calcitized dolomites, or dedolomites, have not been extensively studied in the Yates Formation in Amoco No. 2 or in outcrops in Dark Canyon.

Dedolomite crystals in Amoco No. 2 range in size from 0.01 to 0.15mm. Some of the dedolomites have a cloudy or inclusion-filled appearance (Figure 29). These could be inclusions of remnant dolomite or other contaminants that were in the original dolomite. Some of the dedolomite crystals retain remnant cores of dolomite (Figure 30). This represents an incomplete calcitization of the dolomite from the outside of the crystal towards the center. Most dedolomites appears within the coarsely crystalline calcite (discussed later) or in close proximity to porosity.

In BSE, some of the dedolomite appears to have remnant dolomite rims surrounding it (Figure 31). In the thin sections taken from the Amoco No. 2 core, these dolomite rims were not observed. This could be due to a different cut through the rock, as the thin section itself was not used in microprobe analysis. Or, the staining in the thin section may not be fine enough to pick up on submicron-sized inclusions, which can be seen easily with the microprobe. Dedolomitization could have also affected some crystals from the inside out towards the rims (centrifugal dedolomitization (Khwaja, 1983)), as relict dolomite cores are also visible in some of the dedolomites examined with BSE (Figure 31).

There is possible evidence for dolomite being completely dissolved away before being partly filled in with calcite. For example, Figure 32 is an image of a euhedral rhomb shaped void space. Along the lower left side of the void, finely-crystalline calcite has started to fill it in. Alternatively, this finely-crystalline calcite could be dissolving away, and the void could just be coincidentally rhomb-shaped. No dolomite crystals observed in this study were as large as the void in Figure 32.

Quantitative analysis of the dedolomite shows that the Ca/(Ca+Mg) is slightly more variable than in the replacive dolomites, ranging from 0.96 to almost 1 (Figures 33 and 34, Table 7). This is a wider range than in both the early and later dolomites, which indicates more variance in magnesium content. One of the dedolomites analyzed has a lower Ca/(Ca+Mg) ratio than the others, indicating higher levels of magnesium. Alternatively, a dolomite core or rim could have been included in that analysis, skewing the results. The iron concentration varies from 0 to 157.3 ppm.

Three samples of dedolomite were analyzed for $\delta^{18}\text{O}$ and $\delta^{13}\text{C}$ (Figure 35). $\delta^{18}\text{O}$ values range from -5.07‰ to -4.03‰. $\delta^{13}\text{C}$ of the dedolomites vary from 0.61‰ to 2.14‰. Both the $\delta^{18}\text{O}$ and $\delta^{13}\text{C}$ values for the dedolomites are much lower than those for the replacive dolomites mentioned earlier (Figure 36).



Figure 28: Amoco No. 2, 62 ft (DC-2 62B). Dedolomite present around a void space. Most dedolomite is present as euhedral rhombs, but some is subhedral. Note the inclusion-rich cores in some of the dedolomite crystals.

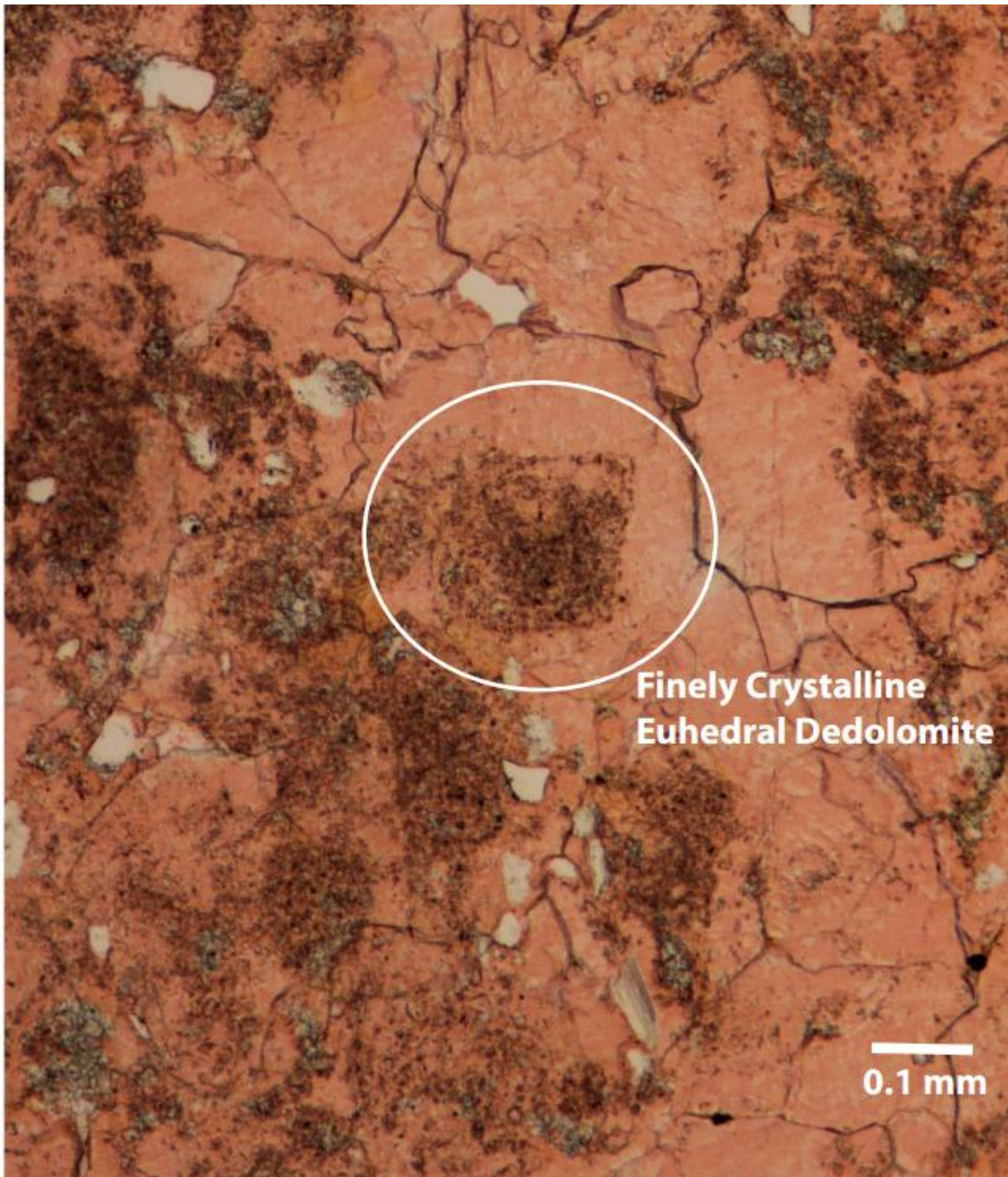


Figure 29: Amoco No. 2, 62 ft (DC-2 62B). A medium-sized euhedral dedolomite crystal in a void-filling coarsely-crystalline calcite. The cloudy core may be remnant inclusions of dolomite (note how some of the cloudy areas do not take a stain) or other inclusions. The original dolomite crystals may have had cloudy cores and limpid rims that were later preserved during dedolomitization.

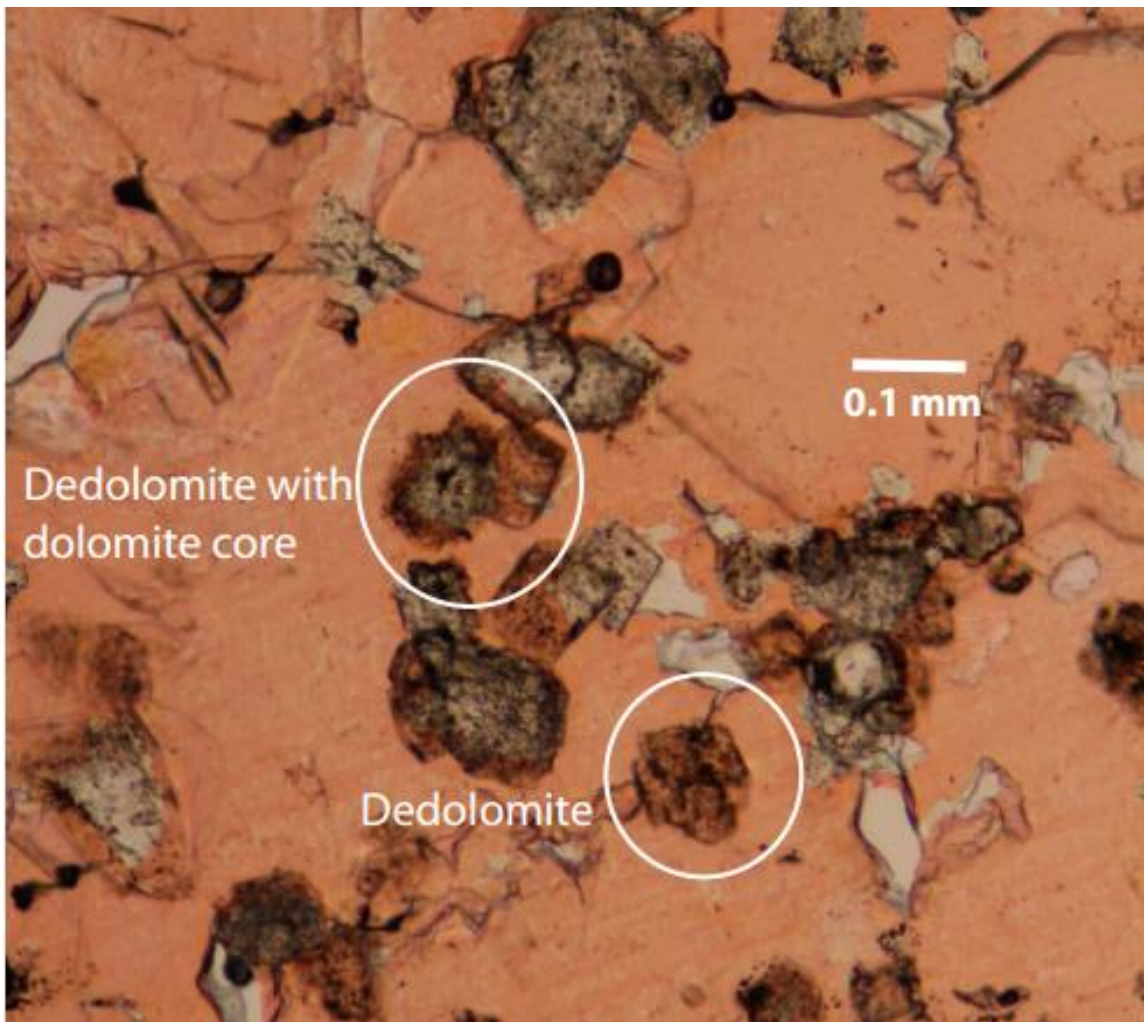


Figure 30: Amoco No. 2, 108 ft (DC-2 108B). Photomicrograph showing euhedral dedolomite rhombs and partially calcitized dolomite rhombs. The dedolomites are contained within coarsely crystalline pore-filling calcite.

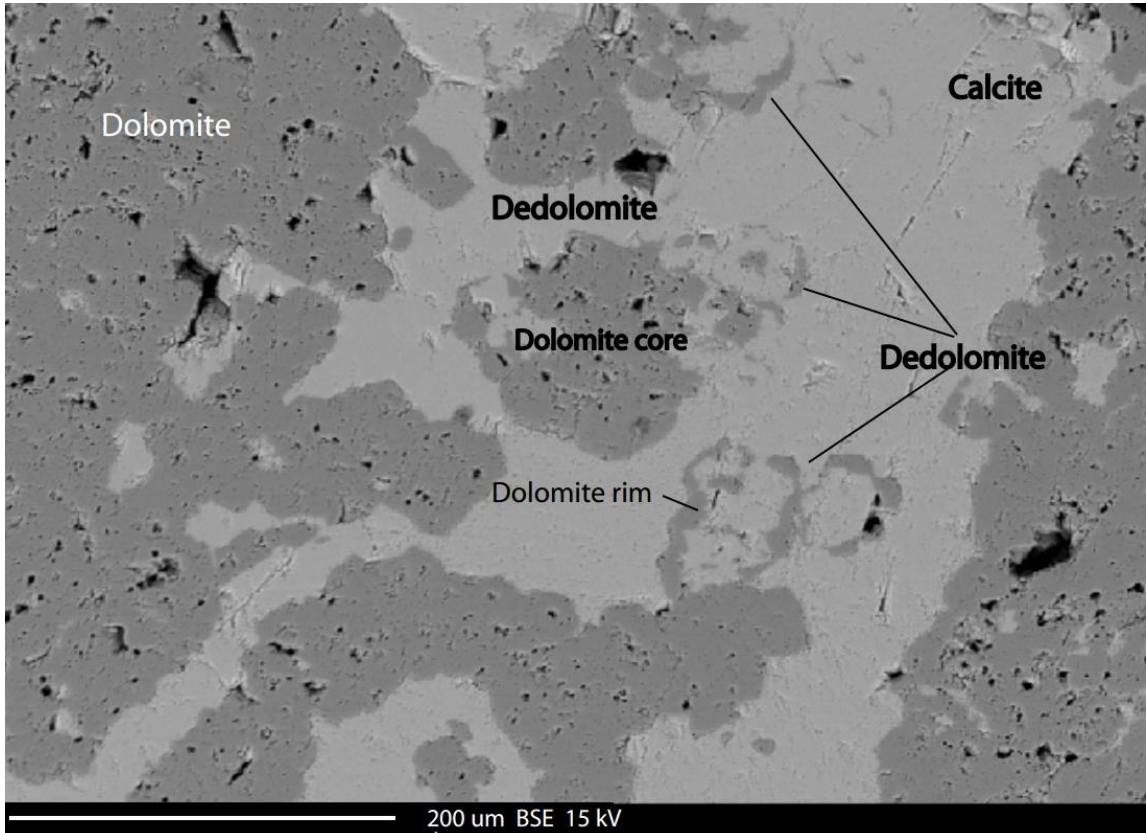


Figure 31: Backscattered electron image of dedolomite with dolomite cores and rims. From DC-2 47A.

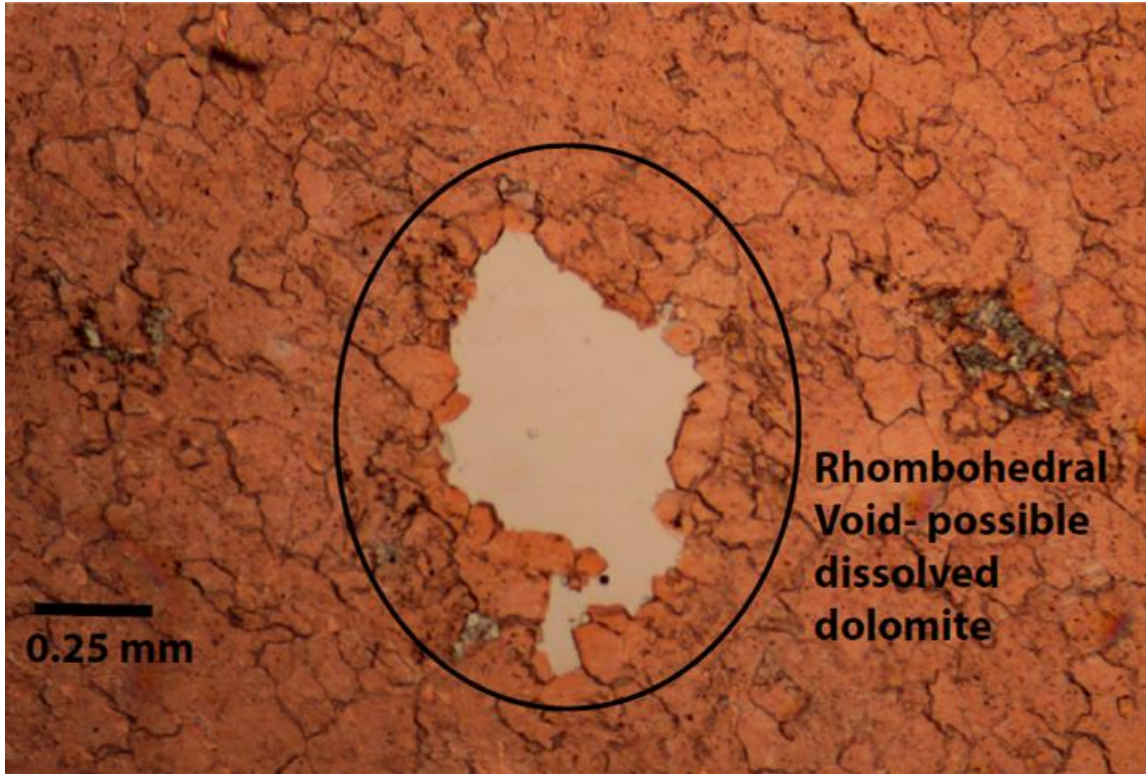


Figure 32: Amoco No. 2, 70 ft (DC-2 70). A rhomb-shaped void possibly in the midst of being filled with calcite. It is conceivable that this void was once filled with dolomite, which has since been dissolved away. It could also just be a nicely shaped void, since dolomite crystals as large as this void have not been found in the thin sections from Amoco No. 2.

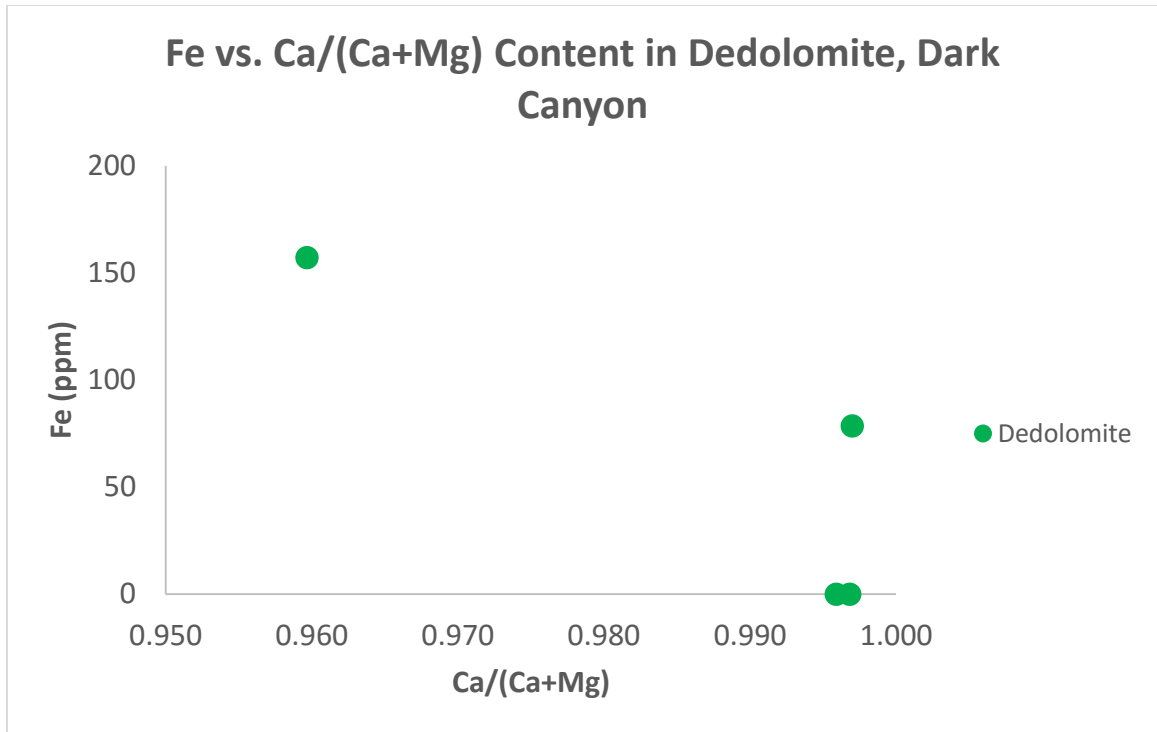


Figure 33: Data from the quantitative microprobe analysis of dedolomites in ppm. The Ca/(Ca+Mg) ratio is much more variable than in the dolomites; it ranges from 0.96 to almost 1. Fe content varies from 0 to 157.3 ppm.

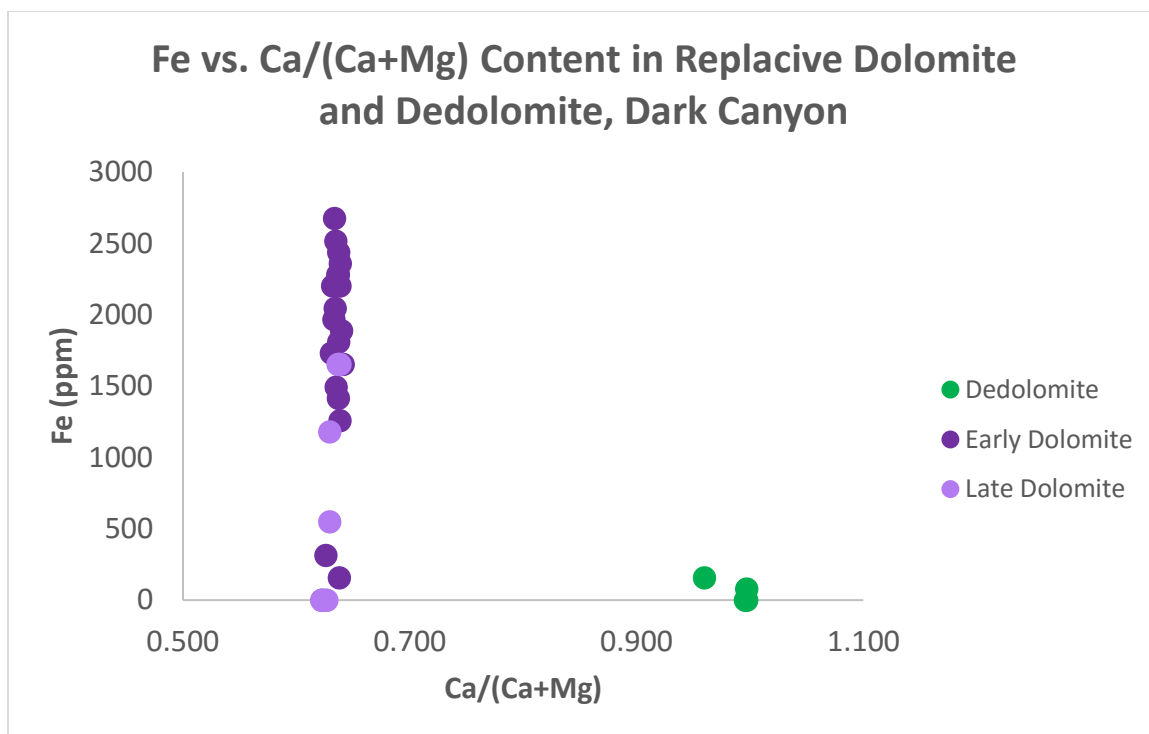


Figure 34: Data from the qualitative analysis of dedolomites plotted with those of the replacive dolomites. Most of the dedolomite plots with calcite in terms of the $\text{Ca}/(\text{Ca}+\text{Mg})$ (approximately 0.99), except for one, which is slightly higher in Mg. That point has a $\text{Ca}/(\text{Ca}+\text{Mg})$ of 0.96

Table 7: Quantitative microprobe analysis for dedolomite samples in parts per million (ppm).

Sample Type	$\text{Ca}/(\text{Ca}+\text{Mg})$	Fe (ppm)	Depth (ft)
Dedolomite	0.996	0	47
Dedolomite	0.997	0	47
Dedolomite	0.997	78.65723	47
Dedolomite	0.960	157.3145	108

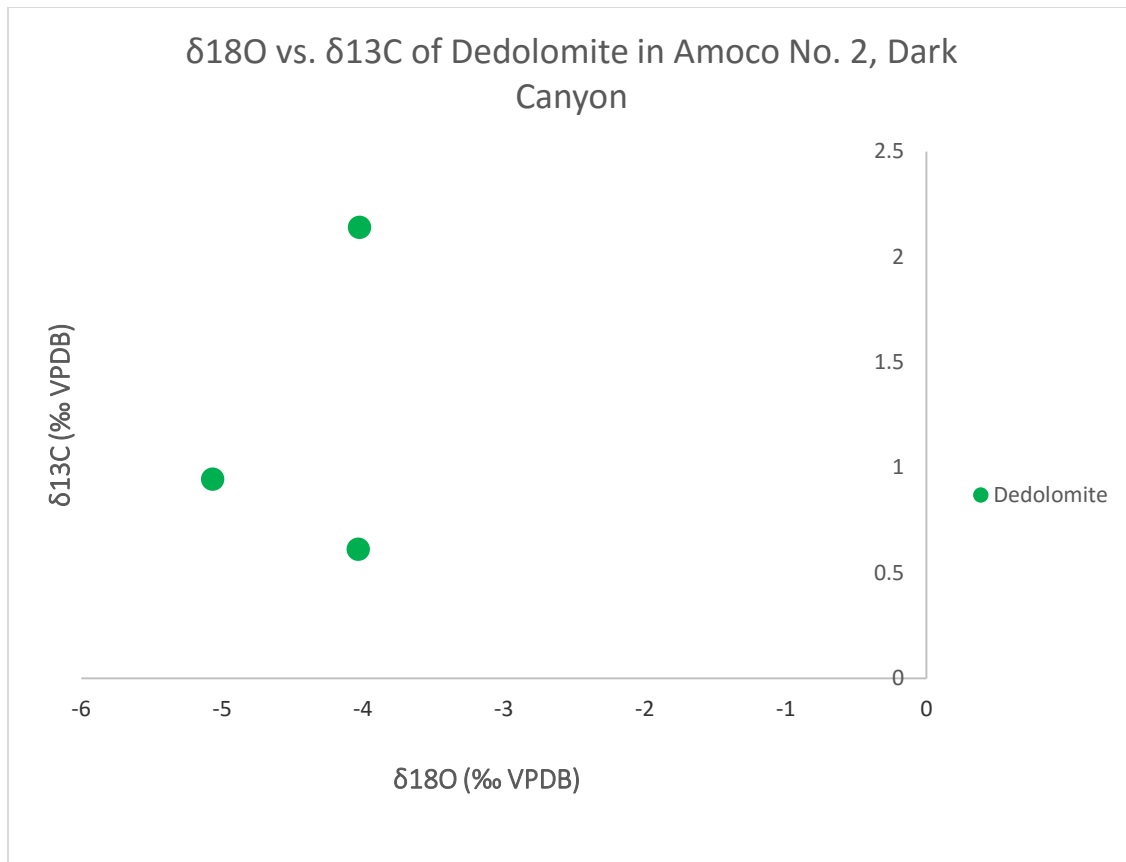


Figure 35: Stable isotope data from the analysis of dedolomite samples. $\delta^{18}\text{O}$ values range from -5.07‰ to -4.03‰. $\delta^{13}\text{C}$ of the dedolomites vary from 0.61‰ to 2.14‰.

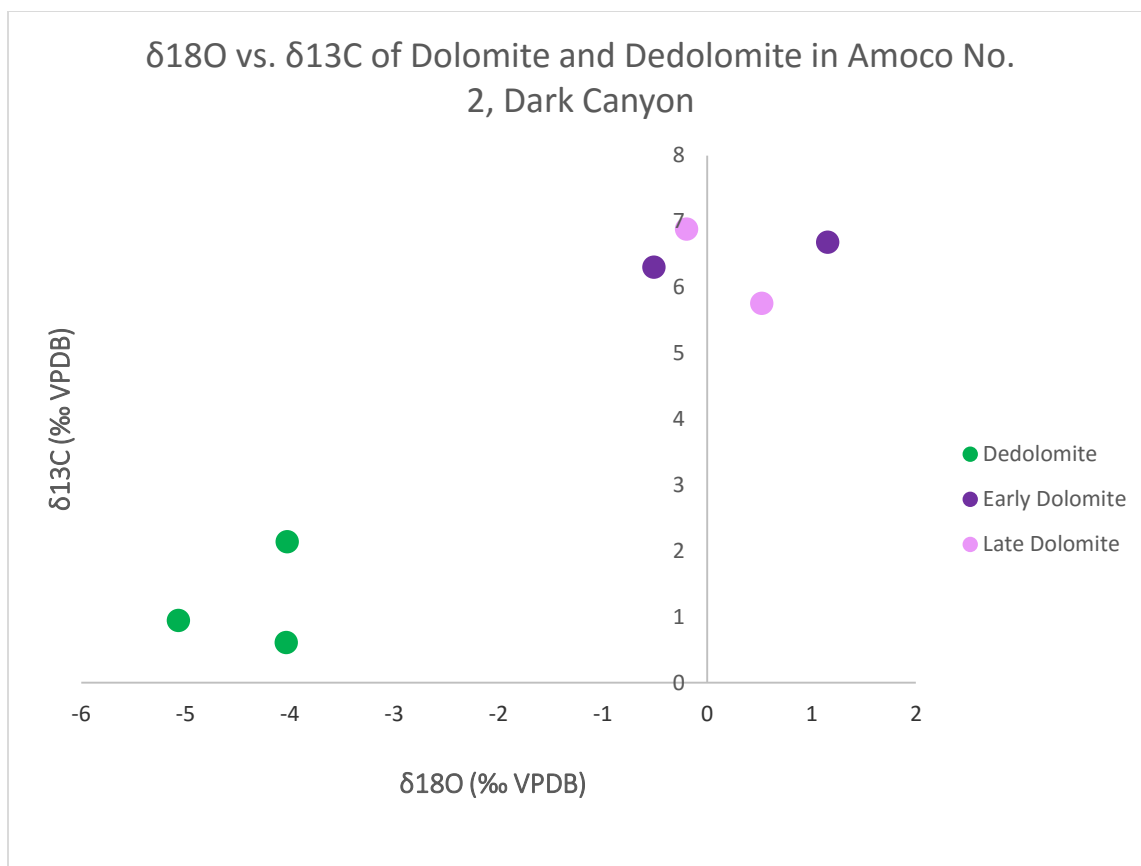


Figure 36: $\delta^{18}\text{O}$ and $\delta^{13}\text{C}$ values for the dedolomite samples compared with the early and late replacive dolomite samples.

Dedolomitization definitely occurred after the later episode of replacive dolomite was in place, as it is this type of dolomite that was locally calcitized (dedolomitized). Dedolomite is mostly found near pore spaces or fractures and contained within the coarsely-crystalline calcite that is interpreted to be replacive of evaporite nodules. This indicates that the later episode of replacive dolomite and dedolomitization occurred after evaporites were in place. It could also show that dedolomite is associated with the coarsely crystalline calcite (discussed in the next section). If this is the case, it would show that the coarsely-crystalline calcite directly replaced the evaporites, as opposed to the evaporites being partially or completely dissolved away before the calcite cement filled the void.

Calcite Spar Precipitation and Calcitization of Evaporites

Coarsely-crystalline blocky calcite, ranging in size from 0.5 cm to more than 1 centimeter across, is present as subhedral to anhedral crystals, filling in pores and fractures. Figure 37 shows a coarse calcite crystal contained within the osculum of a

sponge. The coarse calcites have not been dolomitized and are non-ferroan. Some calcites contain tiny inclusions of unknown composition (Figure 25).

These calcites fill the latest generation of pore space- after the latest dolomite precipitated on the edges of the voids. They also replace evaporite minerals and contain dedolomite crystals. These crystals mostly fill in the latest generation of pore space, and are inferred to be late in the diagenesis.

This type of calcite is comparable to that studied by Mruk (1985, 1989) and Scholle et al. (1992). The coarsely crystalline, blocky calcite from previous studies was also found to house floating fabrics and replace evaporites. Ulmer-Scholle et al. (1993) concluded that this type of calcite formed during the uplift and exposure of the Permian Reef Complex during the second half of the Tertiary.

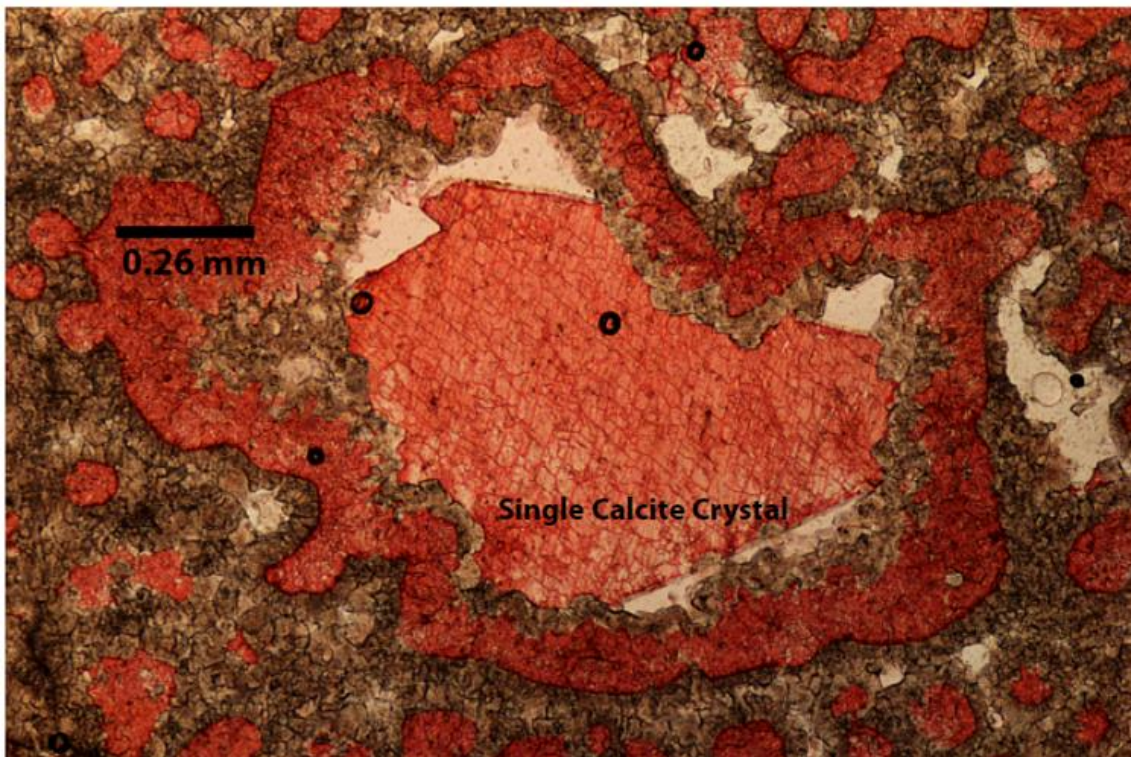


Figure 37: Amoco No.1, 56 ft (DC-1 56). A single coarse calcite crystal inside a void space within the osculum of a dolomitized sponge. The white is porosity. Note the cross-cutting relationship between the dolomite and the coarse crystal of calcite; the calcite grew inside the osculum of the sponge after it was dolomitized as it has grown around the dolomite crystals. Based on the clean contact between the dolomitized sponge and the high-Mg calcite growing isopachously on it, it is likely that the sponge was dolomitized before the high-Mg calcite cement precipitated. If this is the case, the early replacive dolomite was syndepositional.

Quantitative analysis shows that the calcite values have a slim range for Ca/(Ca+Mg) (0.993 to 0.998). The high ratio and short range indicates that Mg values are low and not very variable (Figure 38, Table 8). The iron concentration in the calcite crystals, which ranges from 0 to 393.2 ppm, is much less than in the dolomites. The calcite mostly plots within the range of the dedolomite in regards to both Ca/(Ca+Mg) and Fe content (Figure 39).

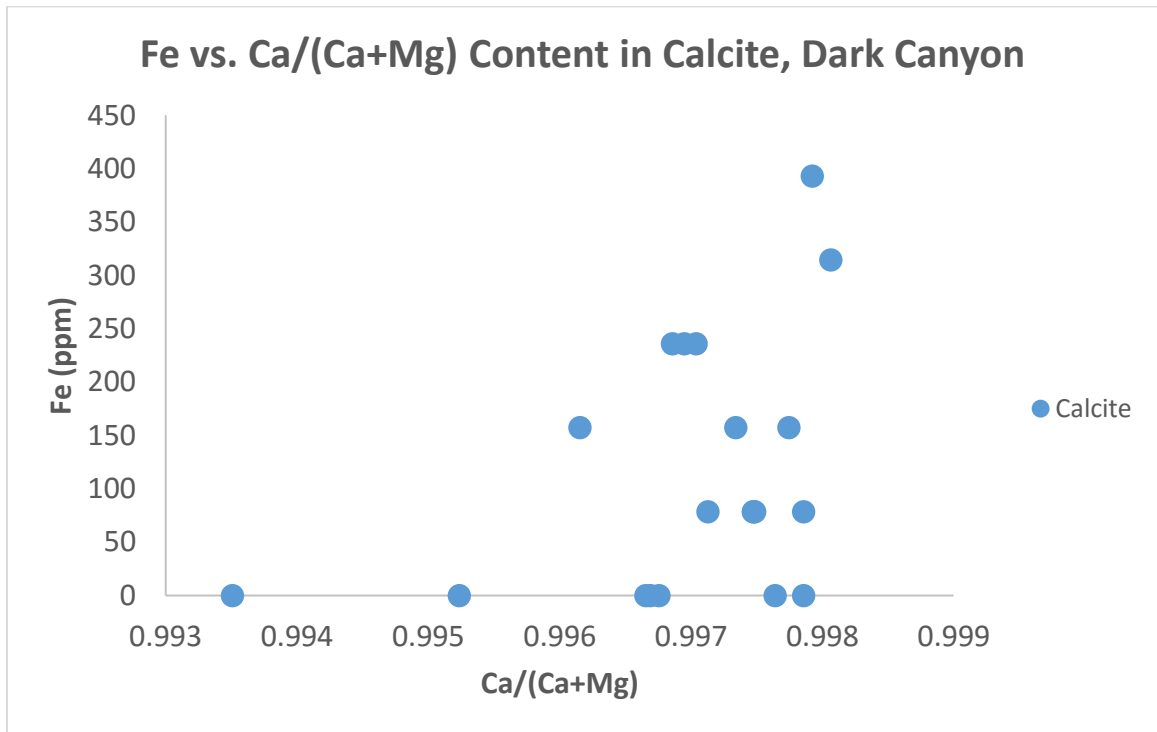


Figure 38: Data from the quantitative microprobe analysis of calcite. Ca/(Ca+Mg) has a very narrow range (0.993 to 0.998). Iron content varies from 0 to 393.3 ppm.

Table 8: Data from quantitative analysis on diagenetic cements (ppm). Light and dark calcite refers to the subtle color variations in high gain mode under BSE.

Sample Type	Ca/(Ca+Mg)	Fe (ppm)	Depth (ft)
Calcite	0.997	78.65723	76
Calcite	0.996	157.3145	47
Calcite	0.998	78.65723	47
Calcite	0.997	0	47
Calcite	0.998	0	47
Calcite	0.995	0	108
Calcite	0.997	0	108
Calcite	0.997	235.9717	108
Calcite (dark)	0.998	0	76
Calcite (dark)	0.997	235.9717	76
Calcite (dark)	0.997	235.9717	76
Calcite (dark)	0.997	0	76
Calcite (dark)	0.997	78.65723	76
Calcite (light)	0.994	0	76
Calcite (light)	0.997	78.65723	76
Calcite (light)	0.998	314.6289	76
Calcite (light)	0.997	157.3145	76
Calcite (light)	0.997	78.65723	76
Calcite (light)	0.998	157.3145	76
Calcite (light)	0.998	393.2862	76

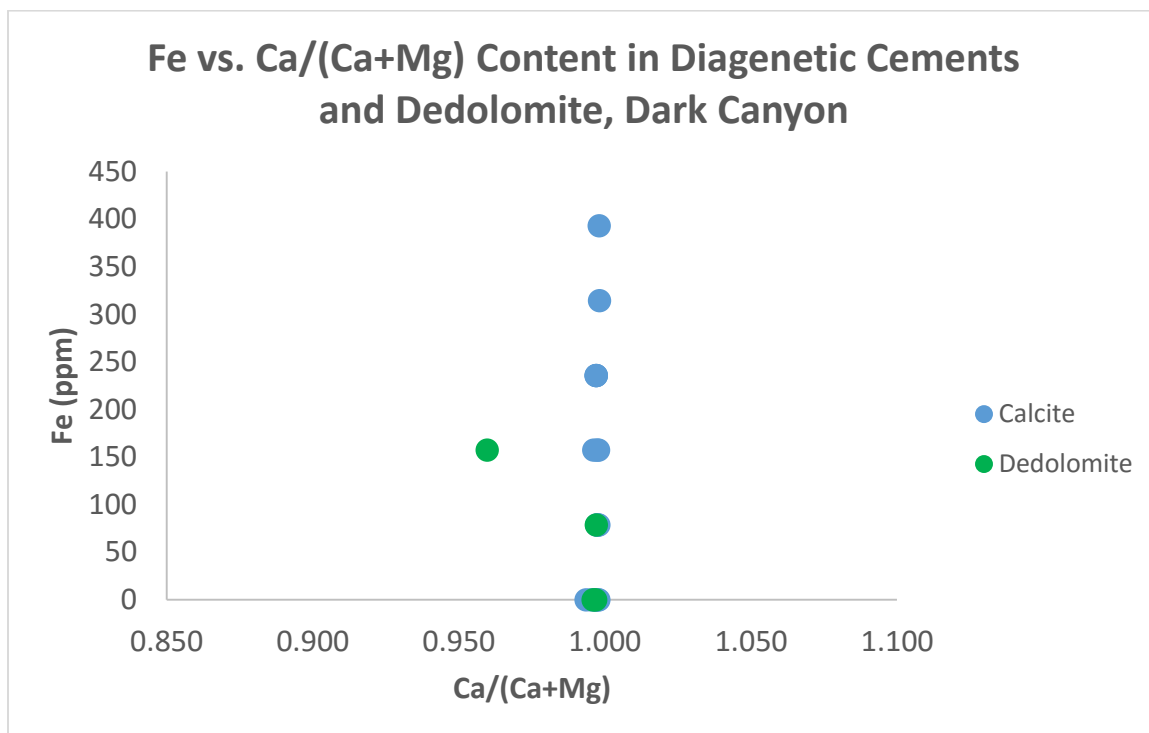


Figure 39: Quantitative analysis for calcite plotted with dedolomite. The dedolomite mostly plots with the calcite in terms of Ca/(Ca+Mg), except for one outlier, which is slightly more Mg-rich. The calcites analyzed contain more iron than the dedolomites.

The coarsely-crystalline calcite definitely occurred after the both the dolomite cement and evaporites. The calcite is observed filling voids and growing around the dolomite cement crystals the isopachously line pore walls (Figures 25 and 37), and is interpreted to have replaced the evaporites that were present in Amoco No. 2. Scholle et al. (1992) and Ulmer-Scholle et al. (1993) found it to be very late in the diagenetic sequence during the uplift and exposure of the Permian Reef Complex after it was buried by the Castille Formation.

Surface Weathering

Thin sections from the surface revealed that most of the diagenetic cements have been overprinted with or obliterated by meteoric weathering. Figure 40 is a photomicrograph of one of the surface samples taken from the Tansill Formation in Dark Canyon, approximately half a mile into the canyon. This image is characteristic of both thin sections. Modern caliche is present as pendant cements on the calcite crystals and in voids (Figure 40). The caliche is inferred to be the latest diagenetic cement, as it appears as pendant cements on the late coarsely crystalline calcite spars.

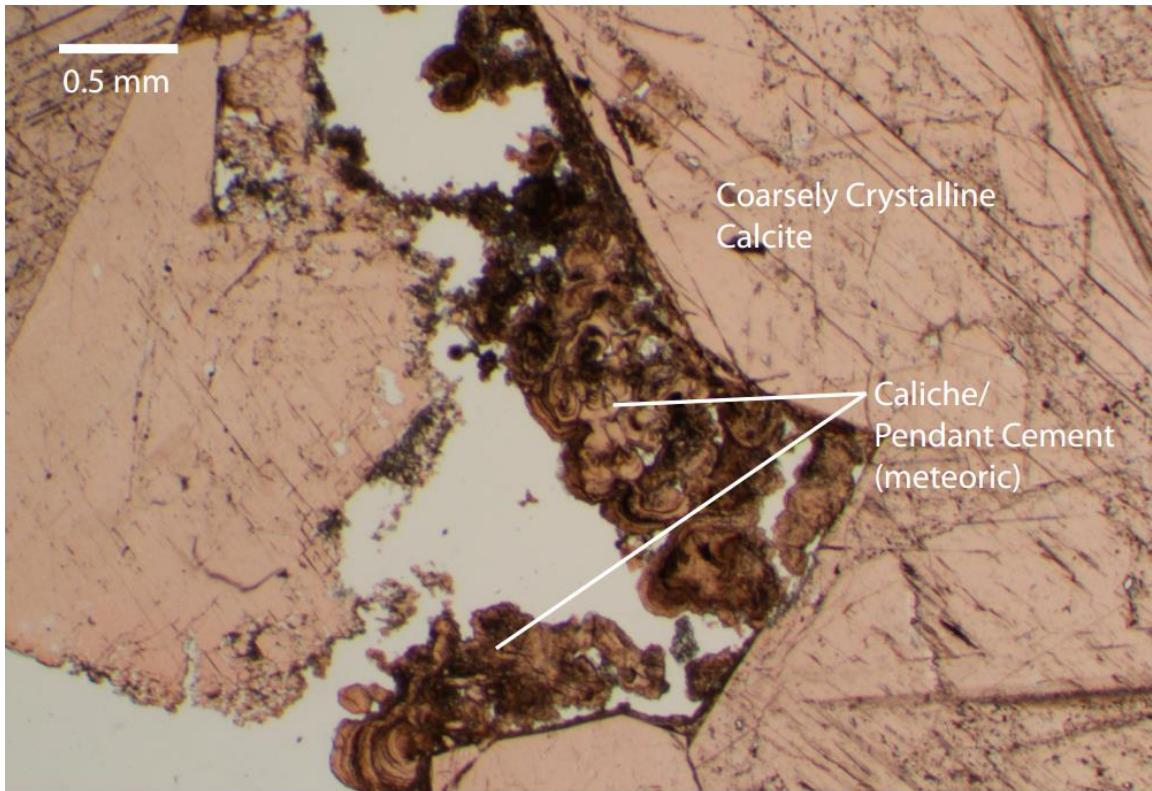


Figure 40: Surface sample from the Tansill Formation, Dark Canyon. Coarsely-crystalline calcite with modern caliche forming in void space as pendant cements. This implies that the caliche is younger than the coarsely crystalline calcite.

Observed Paragenetic Sequence

The paragenetic sequence observed in this study is briefly summarized below. Figure 41 is a chart depicting the order of diagenetic events.

- 1) Syndepositional aragonitic cement precipitated from seawater as evidenced by *Archaeolithoporella* sp. encrusting the tips of and being encrusted by aragonitic cement. Fibrous aragonite also lines pore spaces and form botryoids in larger pore spaces. Early calcite (possibly high-Mg calcite) precipitated isopachously on the edges of voids and on organisms. This too is thought to be syndepositional as aragonite and high-Mg calcite tend to precipitate together based on modern analogues (Scholle and Ulmer-Scholle, 2003).
- 2) At least one episode of replacive dolomitization occurred, replacing fossils, aragonitic cement and the early (high-Mg?) calcite cement with anhedral to medium-crystalline, cloudy crystals. Possibly syndepositional.
- 3) Dolomite cement precipitated isopachously along the edges of voids, overlaying the syndepositional marine cement.
- 4) Evaporites grew displacively after at least one episode of dolomite, as fragments of the early replacive dolomite was observed inside one of the replaced evaporite nodules.
- 5) The aragonite probably recrystallized to calcite after, or possibly during (Melim and Scholle, 2002), at least one episode of dolomitization. More study is necessary to narrow down when the aragonite neomorphosed to calcite.
- 6) The later episode of dolomitization (clear, coarsely crystalline) occurred after most of the evaporite precipitation. Finely-crystalline dolomite is sometimes included in former evaporites, not the coarser dolomite. This later replacive dolomite is observed growing in euhedral rhombs inside the evaporite nodules, though, suggesting that it replaced either the evaporites or the calcite that replaced the evaporites
- 7) Coarsely crystalline, sparry calcite filled pore spaces, replaced anhydrite, and possibly dedolomitized some of the euhedral dolomites present in and around pores.
- 8) Modern caliche formed along the edges of the coarsely crystalline calcite as pendant cements in surface samples. Caliche is not observed in the core.

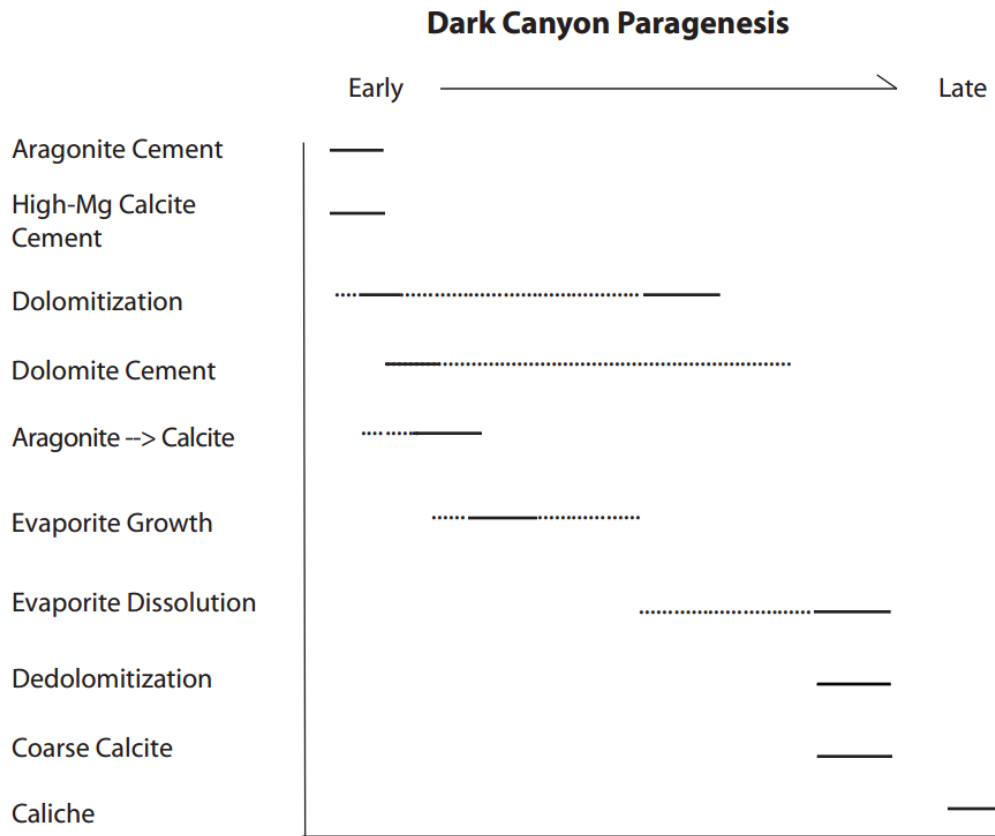


Figure 41: A paragenetic sequence for the rocks in Dark Canyon, based on petrographic analyses, field work, and previous studies. Aragonite and calcite cement, as well as at least one episode of dolomitization occurred early in the sequence. Evaporites were probably also relatively early, although more examination is required to know for certain. Aragonite neomorphosed to calcite probably after the early dolomitization took place. Dissolution of evaporites, dedolomitization, and the coarsely crystalline calcite cementation occurred later in the paragenetic sequence, followed by caliche precipitation at or near the surface.

Discussion

This section deals primarily with dolomitization and calcitization of dolomites (dedolomitization). Understanding the timing, methods, and geochemistry of dolomitization and dedolomitization can lead to a better understanding of the depositional and diagenetic environments and possibly fluids and fluid pathways present during their emplacement. This understanding, in turn, would lead to a better picture of the diagenetic history of the Permian Reef Complex. Knowing the diagenetic history of this area is important for understanding the presence of hydrocarbons and their movements within the Permian Basin.

Dolomitization

As noted in the results section, dolomitization consisted of multiple episodes in the backreef units that occurred over a period of time. The earliest identified replacive dolomite, cloudy and finely-crystalline, may have been syndepositional. This type of dolomite is fabric preserving and directly replaces originally aragonitic material (Figures 16, 21).

The cloudiness of the early replacive dolomite could be due to the presence of inclusions (solid or fluid) or pores. Porosity is visible under BSE. These are an indication that the dolomite is probably not stoichiometric, or the crystal structure is not very ordered, which makes these dolomites protodolomites. Protodolomites are defined as an “imperfectly ordered dolomite” (Gaines, 1977), which means that it is not stoichiometric.

One possible model for early replacive dolomitization is the sabkha/tidal flat model. In this model, sea water that is brought up onto the sabkha by tidal forces becomes concentrated through evaporation. The resulting brine is dense and infiltrates down into the sediment, dolomitizing up to the first few meters of sediment it encounters. This process is typically syndepositional and forms aphanitic to finely-crystalline, poorly ordered dolomites (Shinn, 1983; Land, 1985). It is likely that the dolomites observed in this study formed in similar conditions. The depositional environments of the Tansill and Yates Formations are analogous to the modern Persian Gulf (Abu Dhabi) with widely spread intertidal to supratidal carbonates and sabkha sands (Scholle et al., 2007). Most of the dolomites in this study are aphanitic to finely-crystalline dolomites that preserve the original fabrics of precursor carbonates; this is supportive of a tidal flat/sabkha model for dolomitization. The timing of the early dolomitization in this study suggests a syndepositional origin. Other methods of dolomitization that would produce similar

fabrics are possible (such as seepage refluxion), but based on the depositional setting and the timing, the tidal flat/sabkha model is most likely.

The later replacive dolomite is more coarsely crystalline and clearer in appearance than the earlier dolomite (Figures 20, 21). The crystal structure may be more ordered judging by the large, clear, euhedral crystals. It is fabric preserving up to a certain point; this dolomite also grows euhedrally in formerly aragonitic calcite (fabric obliterating), and tends to replace either the calcite that the originally aragonitic material neomorphosed into or aragonitic material. This later dolomite could have formed during shallow burial. In the seepage reflux model for dolomitization, evaporation of seawater on a shelf or in a lagoon causes the seawater to become dense and briny. These dense brines can then sink to the bottom of the water column and work their way downward through pores and/or fractures, dolomitizing the rocks as it drains basinward. The rocks affected by this process are generally buried in the subsurface (Adams and Rhodes, 1960; Shinn, 1983). Alternatively, it could have formed from mixed marine-meteoric fluids. Clear, euhedral dolomite has been found to precipitate from such fluids (Folk and Land, 1975; Weaver, 1975; Humphrey, 1988).

The later replacive dolomite could represent a completely separate episode of dolomitization from the earlier dolomites. Alternatively, it could be a continuation of this first dolomitization event in some drawn out combination of the tidal flat/sabkha and seepage reflux models. In the seepage reflux model for dolomitization, brines moving through the subsurface can dolomitize over long distances and periods of time (Adams and Rhodes, 1960).

The dolomites, both early and late, from this study plot with the dolomites from other studies (Budd et al., 2013; Chafetz et al., 2008; Frost et al., 2012; Melim and Scholle, 2002) (Figure 42). Their $\delta^{13}\text{C}$ values are consistent with those considered typical for late Permian dolomite that formed from brines (Bein and Land, 1983; Melim and Scholle, 2002; Scholle, 1995; Veizer et al., 1986).

After the early replacive dolomitization and before the later replacive dolomite, evaporite precipitation occurred in both the reef and backreef facies, as evidenced in outcrop by cauliflower-shaped vugs (Figure 26). Evaporites grew displacively within the sediment and formed cauliflower-shaped nodules that include surrounding matrix (like finely-crystalline dolomite).

In the tidal flat/sabkha and seepage reflux models for dolomitization and seepage reflux dolomitization models, seawater is concentrated into brines through evaporation, driving the precipitation of evaporite minerals. Evaporite precipitation is nearly always necessary to lower kinetic barriers that sulfate produces for dolomite precipitation from seawater. So, the evaporites may have predated at least one episode of dolomite (Adams and Rhodes, 1960; Shinn 1983).

The presence of evaporites indicates a warm, shallow lagoon or sabkha type environment. There was probably a lot of evaporation and concentrating of elements in the seawater happening in the backreef setting during the Permian, which would have allowed evaporites to grow and precipitate in remaining pore and void spaces. This process took place either at or very close to the surface, and fits with the tidal flat/sabkha model for dolomitization (Adams and Rhodes, 1960, Shinn, 1983).

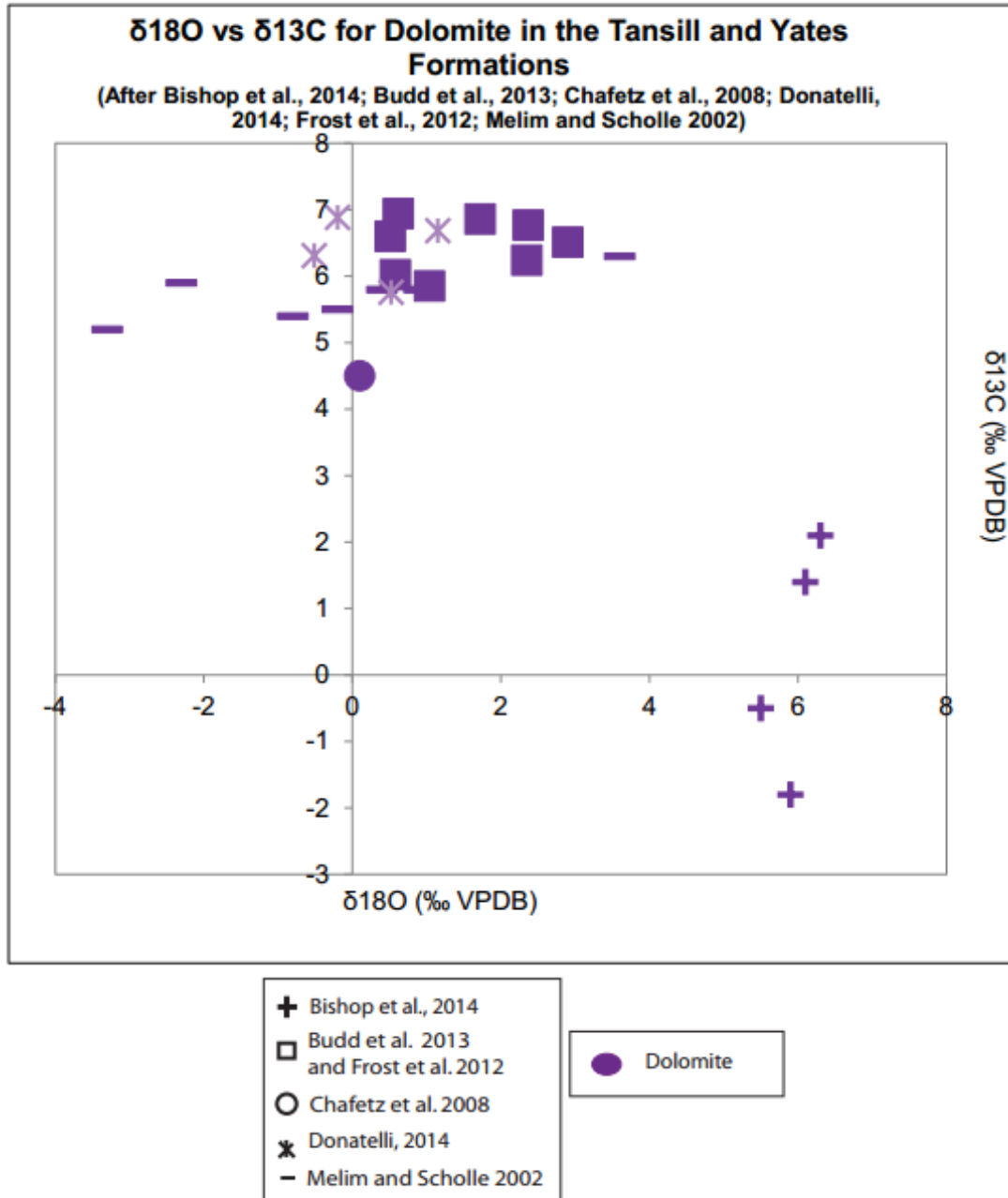


Figure 42: Isotope data for dolomites studied in Dark Canyon and Slaughter Canyon from previous studies and this study.

The high iron content in the early replacive dolomite is unusual (Figure 22). Normally, later dolomites are more iron rich (Land, 1980; Warren, 2000). Based on the high iron content, the formation environment of the early dolomite could have been reducing, as reducing conditions favor the precipitation of iron from solution (Dix, 1993, Warthmann et al., 2000). An experimental study by Warthmann et al., (2000) found that sulfate reducing bacteria can create an anoxic environment and induce dolomite precipitation. One possible explanation for this is that some kind of bacteria were able to produce anoxic, reducing conditions making it possible for the Fe to be able to come out of solution and into the dolomite structure. This could have been possible locally where a source of iron existed in the backreef setting during deposition.

Alternatively, the decomposition of organics could have produced an anoxic and reducing environment, as in a study by Vasconcelos and McKenzie (1997) in Lagoa Vermelha, Brazil. Again, decaying organic matter present within or on the backreef sediments during deposition could have been responsible for local dolomitization.

Another alternative is that the early replacive dolomite neomorphosed at depth. Iron could have been incorporated into the crystal structure as the dolomite was stabilizing and becoming more stoichiometric. This would imply that the fluids interacting with the dolomite as it neomorphosed had significant iron content (Gregg and Sibley, 1984; Land, 1980; 1985; Sibley and Gregg, 1987), such as basinal fluids (Amthor and Friedman, 1992)

The source of this iron in the early replacive dolomites is unclear. There are a couple of possibilities: terrigenous sediments or pyrite produced by microbial activity. The terrigenous sediment present around the Capitan Shelf during the Permian consisted dominantly of sand and silt (mostly quartz, but some feldspar) redbeds (the red implies significant iron content). During low stands of sea level, this sediment could have migrated out over the shelf and into the basin (reciprocal sedimentation). Some of this sediment remains within the backreef marine sediments (Scholle et al., 2007, Mutti and Simo, 1994). None of this terrigenous sediment was observed near the dolomites that were quantitatively analyzed in this study. That is not to say there wasn't any nearby; the core that the samples came from can only reveal so much. It is possible that there were terrigenous sediments trapped nearby, but were not captured by the core.

The iron could also have come from pyrite produced by microbial activity. Certain microbes which reduce sulfur could have been present in the backreef during the Permian. This reduced sulfur produced by the microbes can combine with iron that comes from detrital iron bearing minerals (such as terrigenous sediments) forming pyrite (Berner, 1970; 1974; Cansfield et al., 1996). No definite pyrite was observed in or near the dolomite samples quantitatively analyzed in this study. Again, this is not to say that there is no pyrite nearby. More study is necessary to determine the source of the iron that is present in the early replacive dolomites.

It is also possible that the locations picked for quantitative analysis were all, coincidentally, anomalously high in iron. It is assumed that the high iron content in the early dolomite is a local phenomenon. However, there is not enough data to come to any solid conclusions. More quantitative analysis on more samples of both the early and later replacive dolomites from different locations is the only way to tell.

Dedolomitization

After dolomitization, some of the dolomites were locally calcitized (dedolomitized). Most of the calcitized dolomite is inferred to have formed by direct replacement of dolomite by calcite based on the euhedral rhombic shape of the calcite crystals, the equal crystal size associated with associated dolomite (Evamy, 1967), and the presence of dolomite cores in many of the dedolomite crystals (Figure 28). The dedolomitization process appears to have affected the dolomite crystals from the outside toward the center with remnant dolomite cores at the centers of many dedolomite crystals are compelling evidence (Figure 28).

Remnant dolomite cores within many of the dedolomite crystals are also evidence for incomplete dedolomitization. BSE images of dedolomite crystals are somewhat contradictory to the idea that the dedolomitization process affected the dolomite crystals from the outside of the crystals towards the center. They do show the remnant dolomite at the center of the dedolomite crystals, but they also reveal dolomite rims. This might suggest that the dedolomitization process occurred from the center outward. It is possible that the dedolomitization process worked on the dolomite crystals both from the core out and from the rim in. Dedolomitization has been known to affect the dolomite rhombs from the outside inward (centripetal dedolomitization) and/or from the inside outward towards the margins of the crystals (centrifugal dedolomitization) (Khwaja, 1983). Alternatively, the dolomite crystals could have had zones of different compositions and dedolomitization acted preferentially on certain zones. R. Kenny found this to be the case in some of the dedolomites examined in his 1992 study. Further examination is required for conclusive evidence.

Dedolomites within the core mostly plot within the range of the Ca/(Ca+Mg) of the calcite. This is expected, as it is calcitized dolomite. There is one point that plots closer to dolomite in terms of Ca/(Ca+Mg) (Figure 39). This could indicate a possible remnant core of dolomite or that there is more Mg left over in the calcite crystal lattice. It could also have included an accidental sampling of dolomite, or even a dolomite core or rim. The low iron content of the dedolomite indicates formation in an oxidizing environment. This could imply that it formed at or near the surface.

The isotopic signatures of the dedolomite plot between the bulk of the calcite and the dolomite data, from 0.61‰ to 2.14‰ $\delta^{13}\text{C}$ and -5.07‰ to -4.03‰ $\delta^{18}\text{O}$ (VPDB) (Figure 43). In relation to the dolomite, the dedolomites have lower $\delta^{18}\text{O}$ and $\delta^{13}\text{C}$ values. Diagenesis tends to lower $\delta^{18}\text{O}$ and $\delta^{13}\text{C}$ signatures (O'Neil, 1987). Dolomite interacting with an isotopically lighter fluid, such as calcite-rich meteoric water, could replace the dolomite with calcite and lower the isotopic signatures (Sharp, 2007). Alternatively, formation at higher temperatures could have produced the isotopic signatures of the dedolomite, as in the 1984 study by Budai et al.

Variations in $\delta^{18}\text{O}$ and $\delta^{13}\text{C}$ within dedolomite could be due to differences in the degree of diagenetic alteration, local variations in the isotopic signatures of the fluids as they are precipitating the carbonates, or some combination of both. Alternatively, it could just be a mixture of the calcite and dolomite values, as there are still pieces of dolomite that have not been calcitized. More refined analyses are necessary to be certain.

Since dedolomitization is presumed to have occurred after dolomitization was complete, it is probably associated with either the burial/stabilization or the uplift of the Permian Reef Complex back to the surface after burial (discussed in the next section). Studies by De Groot (1967) and Kastner (1987) concluded that the dedolomitization process can happen during shallow and/or deep burial, as well as at the surface. Budai et al. (1984) analyzed dedolomite within the Mississippian Madison Limestone associated with burial (temperatures of 75-100°C) and found the carbon and oxygen isotopic values to be very low (mean -8.1‰ $\delta^{18}\text{O}$ and -17.5‰ $\delta^{13}\text{C}$). Burial dedolomite from the 1998 study by Spötl et al. in a Permian evaporite mélange also has low isotopic signatures also ($\delta^{13}\text{C}$ ranges from -2.8‰ to 0‰ (VPDB) and -10‰ to -7.8‰ $\delta^{18}\text{O}$). Dedolomites associated with fractures have mean values of -6.3‰ $\delta^{18}\text{O}$ and 1.0‰ $\delta^{13}\text{C}$ and are very close to dedolomite analyzed in this study (averages -4.4‰ $\delta^{18}\text{O}$ and 1.2‰ $\delta^{13}\text{C}$) (Budai et al., 1984). The fracture-related dedolomites from their study are thought to be associated with meteoric water and karsting as well as shallow burial (Budai et al., 1984). It is possible that dedolomitization in the backreef setting in Dark Canyon could be related either to the burial of the reef complex (and higher formation temperatures) or to uplift and meteoric fluid flow. The latter is more likely based on the low iron content of the dedolomite, which indicated formation in an oxidizing (probably near surface) environment.

Back et al. (1983) determined that one of the driving mechanisms behind dedolomitization is the interaction of pore fluids with sulfate minerals, such as evaporites. Dissolution of evaporite minerals saturates the dissolving fluids with calcium, which decreases the magnesium to calcium ratio and causes calcite to precipitate. The precipitation of calcite, in turn, lowers the CO_2 content in the system and the pH, which causes the dissolution of dolomite (Back, 1983; Ulmer and Laury, 1984). The latest coarse calcite event is associated with meteoric waters and the dissolution of evaporites (Ulmer-Scholle et al., 1993), and therefore is probably also be associated with near surface formation. It is probable that the dissolution of evaporites, dedolomitization, and late calcite diagenetic events took place simultaneously in the Permian Reef Complex and were formed from similar fluids.

Coarsely crystalline calcite spar is interpreted to be late in the diagenetic sequence. This cement replaces evaporites and filled in most of the secondary/tertiary porosity (Figure 37). None of the observed coarse calcites are dolomitized, but some contain euhedral dolomite rhombs. This could be evidence that the late calcite directly replaced the evaporites as opposed to the evaporites being dissolved away completely before the calcite was emplaced. Alternatively, there could have been multiple episodes of coarsely-crystalline calcite. It is possible that the evaporites were replaced by calcite before the later episode of replacive dolomite occurred. Or there even could have been another episode of the dolomite after the coarsely crystalline calcite. This is possible, as the Permian Reef Complex went through multiple periods of exposure as sea levels rose and fell throughout the Permian. Times of low sea level, where the reef and backreef facies were exposed, could have provided opportunity for meteoric fluids to percolate through the subsurface and precipitate blocky calcite.

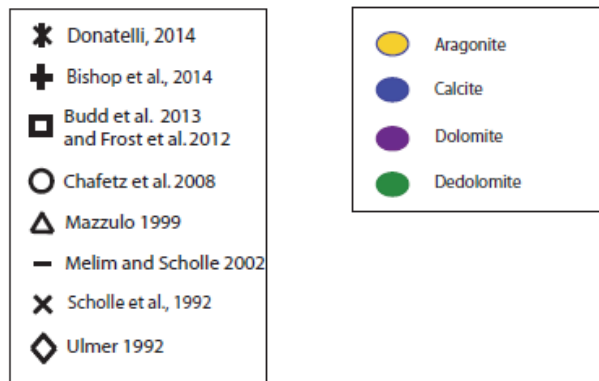
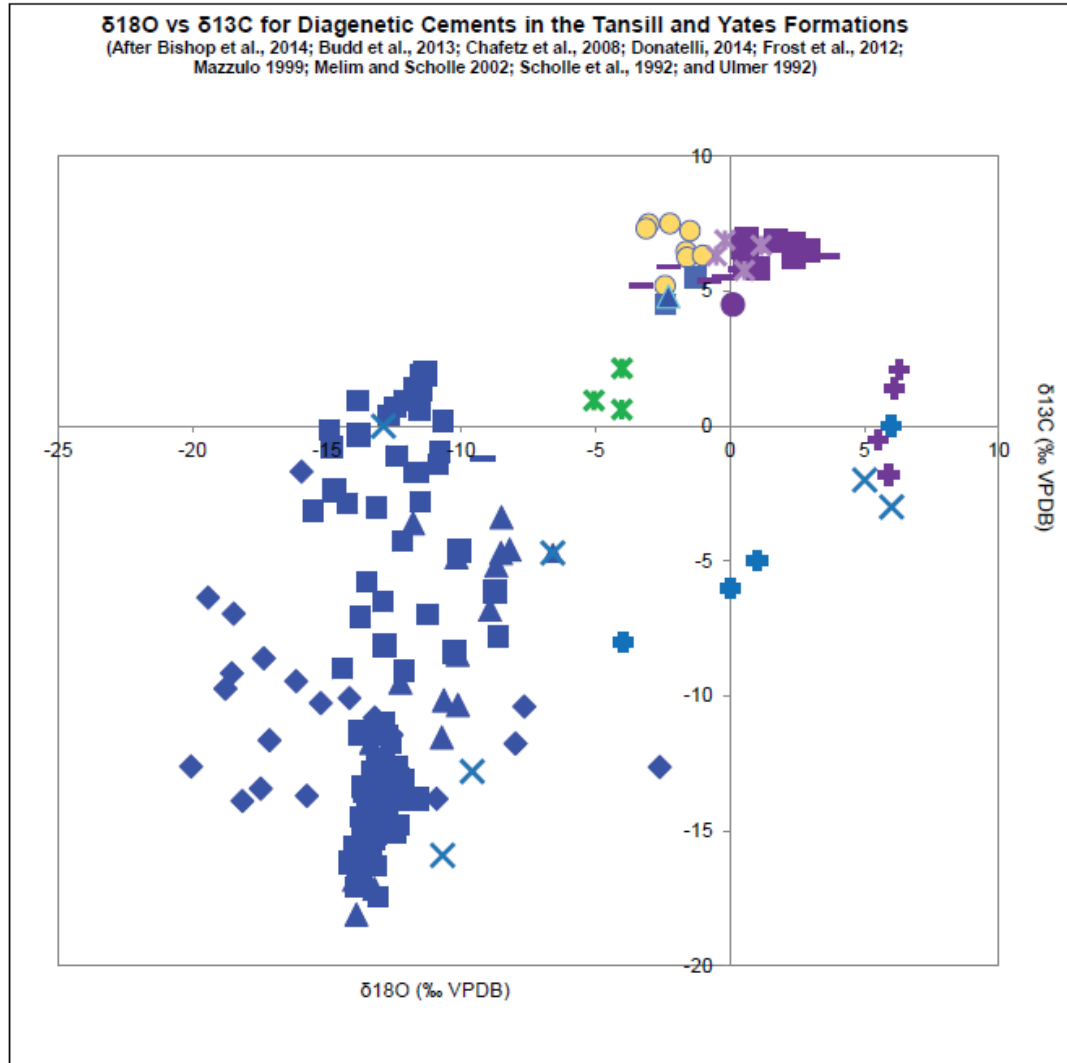


Figure 43: All previous isotope data from the Yates and Tansill Formations in Dark Canyon plotted with the analyses from this study. Some data from McKittrick Canyon and Slaughter Canyon is included. The dedolomites analyzed in this study plot between the bulk of the calcite and the dolomite data, from 0.61‰ to 2.14‰ $\delta^{13}\text{C}$ and -5.07‰ to -4.03‰ $\delta^{18}\text{O}$ (VPDB).

The floating dolomite described by Scholle et al. (1992) is interpreted to indicate the prior presence of evaporites that were replaced by the coarsely crystalline calcite. The evaporites in Amoco No. 2 were present as nodules that grew displacively, sometimes including the surrounding material as they expanded. Fluids later came through, partially or completely dissolving away the evaporites. The dolomite settled towards the bottom of the cavity before the coarsely crystalline calcite precipitated. As the fluids passed through the cavity, they could have been simultaneously dissolving the evaporite and precipitating calcite. This would give the dolomite an appearance of floating. The dissolution and replacement of the evaporites by calcite could be a telogenetic effect (Scholle et al., 1992; Scholle et al., 2007).

Late stage calcites studied by Scholle et al. (1992) have low $\delta^{18}\text{O}$ and $\delta^{13}\text{C}$ values. Their samples collected from the Yates and Tansill Formations in Dark Canyon yield average values of -10.7‰ $\delta^{18}\text{O}$ and -15.9‰ $\delta^{13}\text{C}$ PDB (Figure 46). These low $\delta^{18}\text{O}$ values indicated that the calcites probably precipitated from meteoric waters, as does the low iron content revealed by quantitative analysis (Figures 38, 39). The low amount of iron is evidence for formation in an oxidizing environment, such as a near surface one. The coarse, blocky nature could also indicate formation from meteoric fluids in a near surface environment.

The calcite sample analyzed in this study has an isotopic signature that plots with the dolomite both from this and previous studies (Figure 43). There are several possible reasons for this. Its isotopic composition could be closer to original marine cement, as opposed to calcite derived from meteoric fluids; or, there could have been a mistake during sampling and it could be actual dolomite. More isotopic analysis is the only way to confirm this. This single point for calcite is ignored here.

Dedolomite and Porosity

No increase in porosity due to dedolomitization was found in this study. The replacement of dolomite by calcite was a direct replacement (based on the euhedral nature of the crystals and remnant dolomite cores and rims) and no volume change caused by the change from dolomite to calcite was noted. In some places, porosity was preserved by the dedolomite (Figure 28). Preservation of porosity by dedolomitization has been observed in previous studies (Ayora et al., 1998; Evamy, 1967). In most cases, porosity was filled in with coarsely crystalline calcite (Figure 30), which may or may not be related to the dedolomitization in this study. In short, this is not a very good reservoir rock.

Diagenetic Events: Summary and Relation to Burial and Uplift

Figure 44 is a previously determined burial and uplift history diagram for the Permian Reef Complex from Crysdale et al. (1987), King (1948), and Scholle et al. (1992). This diagram was constructed based on an average surface temperature of 20°C and a geothermal gradient of 25°C per km. Burial depths were determined from thicknesses of units observed in the PDB-04 core (Garber et al., 1989, Scholle et al.,

1992). The diagenetic events observed in this study are superimposed on the diagram based on where they are inferred to have occurred.

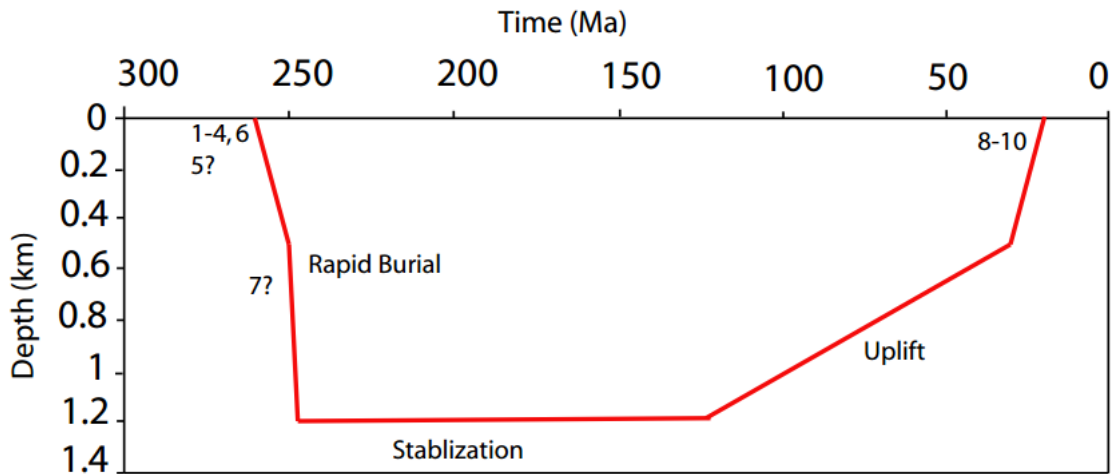
The aragonitic cement, early replacement dolomite, high-Mg calcite cement, neomorphism of aragonite to calcite, and the displacive growth of evaporite minerals are all inferred to be syndepositional or very soon after deposition. This implies that these events took place at the earth's surface or within a few meters of the surface.

Dolomite cement precipitation could have also occurred at or very near to the surface or during the burial of the Permian Reef Complex. Similar dolomite has been known to precipitate from mixed marine-meteoric fluids, (Folk and Land, 1975; Weaver, 1975; Humphrey, 1988) which would imply near-surface formation. Alternatively, it can form from brines percolating through the subsurface at depth (Adams and Rhodes, 1960; Melim and Scholle, 2002). The later replacive dolomite is inferred to have formed from such sinking brines and, therefore, during burial based on its isotopic signatures, which are typical of formation from brines.

During the Ochoan, the entire Delaware Basin and Permian Reef was infilled and buried by the Castile Formation very rapidly. This preserved the Reef Complex very well. The Castile Formation consists of bedded evaporites interlayered with organic matter and calcite that precipitated as the sea in the Delaware Basin dried up. During the Mesozoic, the Permian Basin was situated in a stable area with no subsidence, uplift, or deposition going on. Laramide deformation (a 5-10° eastward tilting of the units) led to Tertiary erosion and the eventual exposure of the Reef Complex and Basin (King, 1948).

Evaporite dissolution and (simultaneous) replacement with coarsely-crystalline, as well as dedolomitization, are inferred to have taken place at/near the surface after the Permian Reef Complex was uplifted and exposed. The blocky nature and stable isotope data of the coarsely-crystalline calcites, as well as the low iron content, indicate formation from meteoric waters. This implies an oxidizing, surface (or very near-surface) environment. Based on the timing of dedolomitization (later in the diagenetic sequence), it was probably associated with the dissolution of evaporites and coarsely-crystalline calcite formation. The low iron content, again, indicates an oxidizing, near surface formation environment. Therefore, it too probably occurred at or near the surface.

Capitan Burial/Uplift History



- 1) Aragonite cement
- 2) Early replacement dolomitization
- 3) High-Mg calcite cement
- 4) Aragonite --> calcite
- 5) Dolomite cement
- 6) Evaporite growth
- 7) Later replacement dolomitization
- 8) Evaporite dissolution
- 9) Blocky calcite replacement of evaporites/dedolomitization
- 10) Caliche (pendant cements)

Figure 44: Burial and uplift history diagram for the Permian Reef Complex with the observed and inferred diagenetic sequence from this study. Burial and uplift data from Scholle et al. (1992).

Conclusions

1. Within the Permian Reef Complex, numerous types of syndepositional cements precipitated, including aragonite (which is the dominant phase), dolomite, and high-magnesian calcite. Some replacive dolomite was syndepositional to early diagenetic. This dolomite cement was probably more poorly-ordered than the later replacive dolomite.
2. The high iron content in the early replacive dolomite could be an indicator that this dolomitization, at least locally, was triggered by microbial activity or decomposing organic matter in a reducing environment. Alternatively, this dolomite could have formed in an evaporitic sabkha or tidal flat environment (consistent with the tidal flat/sabkha model for dolomitization). Isotopic signatures are indicative of formation from brines. Another alternative theory is that the iron was incorporated into the dolomite crystal lattice when the dolomite neomorphosed at depth. Much more analysis is necessary to ascertain the origin of these “iron rich” dolomites.
3. The dolomite cement could have formed by mixing marine and meteoric waters or evaporative brines (based on the tidal flat and seepage reflux models for dolomitization).
4. Evaporites grew as cauliflower-shaped nodules sometime after the early replacive dolomitization. This assumption is based on the fact that there are pieces of the early replacive dolomite contained within some of the former evaporite nodules. The presence of evaporites supports the assumption that a tidal flat or sabkha type environment was present for at least some of the deposition.
5. The later replacive dolomite may have formed during the early surficial burial of the Permian Reef Complex. This would be in agreement with seepage reflux dolomitization studies by Adams and Rhodes (1960) and Melim and Scholle (2002). Isotopic signatures from this study indicate formation from brines.
6. Dedolomitization occurred after dolomitization. The dedolomite examined in this study is inferred to have formed via the direct replacement of dolomite with calcite based on remnant dolomite cores and rims. This event could be related to the replacement of evaporites with coarsely-crystalline calcite and the uplift and exposure of the Permian Reef Complex.
7. Coarsely crystalline calcite directly replaced some or all of the evaporites in the sections of rock examined in this study. This calcite is inferred to be late in the diagenetic sequence and associated with the uplift and exposure of the Permian Reef Complex.

Suggestions for Future Work

The early replacive dolomite is in need of much more analysis. More samples should be collected for quantitative analyses (microprobe). Iron should be closely examined with quantitative analysis to determine if the high iron content is local or widespread (or even real). Perhaps with more quantitative iron data, the source of the iron can be constrained.

All types of dolomite should be further analyzed for stable isotopes. This could help constrain the types of fluids that were present during dolomitization. Understanding the fluids would lead to a better comprehension of the types of environments and conditions that were contemporaneous with dolomitization.

Dedolomite and coarsely crystalline, blocky calcite should also be further analyzed for stable isotopes. Again, this could help constrain the types of fluids and environments that were present during their formation. More isotope data could either affirm or dispel the idea that these two events are connected.

References

- Adams, J. E., 1965, Stratigraphic-Tectonic Development of Delaware Basin: AAPG Bulletin, v. 49, no. 11, p. 2140–2148.
- Adams, J. E., and M. L. Rhodes, 1960, Dolomitization By Seepage Refluxion: AAPG Bulletin, v. 44, no. 12, p. 1912–1920, doi:10.1306/BC74368D-16BE-11D7-8645000102C1865D.
- Al Hashimi, W. S., and J. E. Hemingway, 1973, Recent dedolomitization and the origin of rusty crusts of Northumberland: Journal of Sedimentary Petrology, v. 43, p. 82-91.
- Allan, J. R., and R. K. Matthews, 1982, Isotope signatures associated with early meteoric diagenesis: Sedimentology, v. 29, p. 797-817.
- Amthor, J. E. and Friedman, G. M., 1992, Early- to Late-diagenetic Dolomitization of Platform Carbonates: Lower Ordovician Ellenburger Group, Permian Basin, West Texas: Journal of Sedimentary Petrography, v. 62, No. 1, p. 131-144.
- Assertero, R. L. A. M. and C. G. St. C. Kendall, 1977, Nature, origin and classification of peritidal tepee structures and related breccias: Sedimentology, v.24, p. 153-210.
- Ayora, C., C. Taberner, M. W. Saaltink, and J. Carrera, 1998, The genesis of dedolomites: a discussion based on reactive transport modeling: Journal of Hydrology, v. 209, p. 346-365.
- Babcock, J. A., 1974, The role of algae in the formation of the Capitan Limestone (Permian, Guadalupian) Guadalupe Mountains, West Texas-New Mexico: Unpublished Ph. D. Dissertation, University of Wisconsin, Madison, 241 p.
- Babcock, J. A., 1977, Calcareous algae, organic boundstones, and the genesis of the upper Capitan Limestone (Permian, Guadalupian), Guadalupe Mountains, West Texas and New Mexico: *in* Hileman, M. E., and S. J. Mazzullo, eds., Upper Guadalupian facies, Permian Reef Complex, Guadalupe Mountains, New Mexico

and West Texas, Field Conference Guidebook 77-16: Midland, Society of Economic Paleontologists and Mineralogists, Permian Basin Section, p. 3-44.

- Babcock, J. A., and D. Yurewicz, 1989, The massive facies of the Capitan Limestone, Guadalupe Mountains, Texas and New Mexico: *in* Harris, P. M., and G. A. Grover, eds., Subsurface and outcrop examination of the Capitan Shelf Margin, Northern Delaware Basin: Tulsa Society of Economic Paleontologists and Mineralogists Core Workshop 13, p. 365-371.
- Back, William, Bruce B. Hanshaw, L. Niel Plimmer, Perry H. Rahn, Craig T. Rightmire, and Meyer Rubin, 1983, Process and rate of dedolomitization: Mass transfer and ^{14}C dating in a regional carbonate aquifer: GSA Bulletin, v. 94, p. 1415-1429.
- Bein, A., and L. S. Land, 1983, Carbonate sedimentation and diagenesis associated with Mg-Ca-chloride brines: The Permian San Andres Formation in the Texas Panhandle: Journal of Sedimentary Research, v. 53, no. 1, p. 243-260.
- Berner, E. J., 1970, Sedimentary Pyrite Formation: American Journal of Science, v. 268, p. 2-23.
- Berner, E. J., 1984, Sedimentary Pyrite Formation, an update: *Geochemica et Cosmochimica Acta*, v. 48, p. 606-615.
- Berner, E. J., and A. C. Lasaga, 1989, Modeling the geochemical carbon cycle: *Scientific American*, v. 222, p. 74-82.
- Bischoff, J. L., Juliá, R., Shanks, W. C., and Rosenbauer, R. J., 1994, Karstification without carbonic acid: bedrock dissolution gypsum-driven dedolomitization: *Geology*, v. 22, p. 995-998.
- Bishop, J. W., D. A. Osleger, I. P. Montanez, D. Y. Sumner, 2014, Meteoric diagenesis and fluid-rock interaction in the Middle Permian Capitan backreef: Yates Formation, Slaughter Canyon, New Mexico: AAPG Bulletin, v. 98, no. 8, p. 1495-1519.
- Borer, J. M., and P. M. Harris, 1989, Depositional facies and cycles in Yates Formation outcrops, Guadalupe Mountains, New Mexico: Subsurface and Outcrop Examination of the Capitan Shelf Margin, Northern Delaware Basin, p. 305-317.
- Boyd, D. W., 1958, Permian Sedimentary Facies, Central Guadalupe Mountains, New Mexico: New Mexico Bureau of Mines and Mineral Resources Bulletin, v. 49, p. 1-100.

- Budai, Joyce M., Kyger C. Lohmann, and Robert M. Owen, 1984, Burial dedolomite in the Mississippian Madison Limestone, Wyoming and Utah Thrust Belt: *Journal of Sedimentary Petrology*, v. 54, p. 276-288.
- Budd, D. A., E. L. Frost III, K. W. Huntington, and P. F. Allwardt, 2013, Syndepositional deformation features in high-relief carbonate platforms: long-lived conduits for diagenetic fluids: *Journal of Sedimentary Research*, v. 83, no. 1, p. 12–36, doi:10.2110/jsr.2013.3.
- Cañaveras, J. C., S. Sanchez-Moral, J. P. Calvo, M. Hoyos, and S. Ordonez, 1996, Dedolomites associated with karstification, an example of early dedolomitization in lacustrine sequences from the Tertiary Madrid Basin, central Spain: *Carbonates and Evaporites*, v. 11, no. 1, p. 85-103.
- Candelaria, M. P., 1989, Shallow marine sheet sandstones, upper Yates Formation, northwest shelf, Delaware Basin, New Mexico: *SEPM Core Workshop No. 13*.
- Cansfield, D.E., Lyons, T. W., and Raiswell, R., 1996, A model for iron deposition to euxinic Black Sea sediments: *American Journal of Science*, v. 296, p. 818-834.
- Chafetz, H. S., Z. Wu, T. J. Lapen, and K. L. Milliken, 2008, Geochemistry of Preserved Permian Aragonitic Cements in the Teepees of the Guadalupe Mountains, West Texas and New Mexico, U.S.A.: *Journal of Sedimentary Research*, v. 78, no. 3, p. 187–198, doi:10.2110/jsr.2008.025.
- Crestin-Desjobert, S., Gout, R., Rey, J., 1998, Relations entre mur carbonaté et argilite dans les gisements de bauxite de l'Ariège (France). Distinction d'une dolomitisation par sédimentation régressive et d'une dédolomitisation par altération météorique: *C. R. Acad. Sci. Paris*, v. 306, p. 793-798.
- Crysdale, B. L., 1986, Fluid inclusion evidence for origin and diagenesis of sparry calcite cement in Capitan Limestone, McKittrick Canyon, Permian Basin, west Texas (abstract): *AAPG Bulletin*, v. 70, p. 578.
- Cys, J. M., 1979, Marine aragonite sea-floor growths and cements in Permian phylloid algal mounds, Sacramento Mountains, New Mexico: *Journal of Sedimentary Petrography*, v. 49, no. 3, p. 917-936.
- De Groot, K., 1967, Experimental Dedolomitization: *Journal of Sedimentary Petrology*, v. 37, p. 1216-1220.
- Deike, R. G., 1990, Dolomite Dissolution rate and possible Holocene dedolomitization of water-bearing units in the Edwards aquifer, south-central Texas: *J. Hydrol.*, v. 112, p. 335-373.

- Dickson, J. A. D., 1966, Carbonate Identification and Genesis as Revealed by Staining: *Journal of Sedimentary Petrology*, v. 36, no. 2, p. 491–505.
- Dix, G.R., 1993, Patterns of burial and tectonically controlled dolomitization in an Upper Devonian fringing-reef complex — Leduc Formation, Peace River Arch area, Alberta, Canada: *Journal of Sedimentary Petrology*, 63, 628–640.
- Esteban, M. and L. C. Pray, Origin of the pisolite facies of the shelf crest: *in* Hileman, M. E., and S. J. Mazzullo, eds., *Upper Guadalupian Facies, Permian Reef Complex, Guadalupe Mountains, New Mexico and West Texas*: SEPM, Permian Basin Section, Field Conference Guidebook, Publication 77-16, p. 479-486.
- Evamy, B. D., 1967, Dedolomitization and the Development of Rhombohedral Pores in Limestones: *Journal of Sedimentary Petrology*, v. Vol. 37, no. 4, p. 1204–1215, doi:10.1306/74D71870-2B21-11D7-8648000102C1865D.
- Folk, R. L., and Land, L.S., 1975, Mg/Ca ratio and salinity; Two controls over crystallization of dolomite: *American Association of Petroleum Geology Bulletin*, v. 59, p. 60-68.
- Folkman, Y., 1969, Diagenetic Dedolomitization in the Albanian-Cenomanian Yagur Dolomite on Mount Carmel (Northern Israel): *Journal of Sedimentary Petrology*, v. 39, p. 380-385.
- Frank, J. R., 1981, Dedolomitization in the Taum Sauk Limestone (Upper Cambrian), southeast Missouri: *Journal of Sedimentary Petrology*, v. 51, p. 7-18.
- Frost III, E. L., D. A. Budd, C. Kerans, 2012, Syndepositional deformation in a high-relief carbonate platform and its effects on early fluid flow as revealed by dolomite patterns: *Journal of Sedimentary Research*, v. 82, no. 12, p. 913-932.
- Garber, R. A., G. A. Grover, and P. M. Harris, 1989, *Geology of the Capitan Shelf Margin- Subsurface Data from the Northern Delaware Basin*: SEPM Core Workshop No. 13, v. 13, p. 3–253.
- Gaines, A. M., 1977, Protodolomite Redefined: *Journal of Sedimentary Petrography*, v. 47, no. 2, p. 543-546.
- Given, R. K., and K. C. Lohmann, 1985, Derivation of the original isotopic composition of Permian marine carbonates: *Journal of Sedimentary Petrology*, v. 55, p. 430-439.
- Given, R. K., and K. C. Lohmann, 1986, Isotopic Evidence for the Early Meteoric Diagenesis of the Reef Facies, Permian Reef Complex of West Texas and New Mexico: *Journal of Sedimentary Petrology*, v. 56, no. 2, p. 183–193.

- Goldberg, M., 1967, Supratidal dolomitization and dedolomitization in Jurassic rocks of Hamakhtesh Hagatan, Israel: *Journal of Sedimentary Petrology*, v. 37, p. 760-773.
- Gregg, J. M. and Sibley, D. F., 1984, Epigenetic dolomitization and the origin of xenotopic dolomite texture: *Journal of Sedimentary Petrology*, v. 54, p. 908-931.
- Handford, C. R., A. C. Kendall, D. R. Prezbindowski, J. B. Dunham, and B. W. Logan, 1984, Salina-margin tepees, pisoliths, and aragonite cements, Lake MacLeod, western Australia: Their significance in interpreting ancient analogs: *Geology*, v. 12, p. 523-527.
- Humphrey, J. D., 1988, Late Pleistocene mixing zone dolomitization, southeastern Barbados, West Indies: *Sedimentology*, v. 35, p. 327-348.
- Hurley, N. F., 1989, Facies mosaic of the lower Seven Rivers Formation, McKittrick Canyon, New Mexico: *in* *Subsurface and Outcrop Examination of the Capitan Shelf Margin, Northern Delaware Basin*, eds P.M. Harris and G.A. Grover: SEPM Core Workshop No. 13, p. 325-346.
- Jones, B., Pleydell, S. M., Ng, K. C. and Longstaffe, F. J., 1989, Formation of poikilotopic calcite-dolomite fabrics in the Oligocene-Miocene Bluff Formation of Grand Cayman, British West Indies: *Bull. Can. Petrol. Geol.*, v. 37, p. 255-265.
- Kastner, M., 1982, When does dolomitization occur and what controls it: 11th Intl. Cong. Sed. (Abst.), Hamilton, Ontario, Canada, p. 124.
- Katz, A., 1968, Calcian dolomites and dedolomitization: *Nature*, v. 217, p. 439-440.
- Katz, A., 1971, Zoned dolomite crystals: *Journal of Geology*, v. 79, p. 38-51.
- Kendall, C. G. S. C., 1969, An Environmental Re-interpretation of the Permian Evaporite/Carbonate Shelf Sediments of the Guadalupe Mountains: *GSA Bulletin*, v. 80, December, p. 2503-2526.
- Kendall, C. G. S. C., and J. Warren, 1987, A review of the origin and setting of tepees and their associated fabrics: *Sedimentology*, v. 34, p. 1007-1027.
- Kenny, R., 1992, Origin of disconformity dedolomite in the Martin Formation (late Devonian, northern Arizona): *Sedimentary Geology*, v. 78, no. 1-2, p. 137-146.
- Kerr, Jr., S. D., and A. Thomson, 1963, Origin of nodular and bedded anhydrite in Permian Shelf sediments, Texas and New Mexico: *Bulletin of the American Association of Petroleum Geologists*, v. 47, no. 9, p. 1726-1732.

- King, P. B., 1942, Permian of West Texas and Southeastern New Mexico (Part 1): AAPG Bulletin, v. 26, p. 535–592.
- King, P. B., 1948, Geology of the Southern Guadalupe Mountains, Texas (Part 2): USGS Professional Paper 215, p. 630-706.
- King, R., 1947, Sedimentation in Permian Castile Sea: AAPG Bulletin, v. 31, no. 3, p. 470-477.
- Kinsman, David J. J., 1969, Modes of Formation, Sedimentary Associations, and Diagnostic Features of Shallow-Water and Supratidal Evaporites: AAPG Bulletin, v. 53, no. 4, p. 830-840.
- Kirkland, B. L., S. A. Longacre, and E. L. Stoudt, 1993, Reef: *in* Bebout, D. G., and C. Kerans, eds., Guide to the Permian Reef Geology Trail, McKittrick Canyon, Guadalupe Mountains National Park, West Texas Guidebook 26: Austin, Bureau of Economic Geology, University of Texas, p. 23-31.
- Kump, L. R., 1989, Alternative modeling approaches to the geochemical cycles of carbon, sulfur, and strontium isotopes: American Journal of Science, v. 289, p. 390-410.
- Khwaja, A. A., 1983, Types of dedolomitization: Geol. Bull. Univ. Peshwar, v. 16, p. 51-53.
- Land, L.S., 1980, The isotopic and trace element geochemistry of dolomite: the state of the art: *in* Zenger, D.H., Dunham, J.B., Ethington, R.L. eds.: Concepts and Models of Dolomitization. Spec. Publ.-SEPM vol. 28, pp. 87–110.
- Land, L.S., 1985. The origin of massive dolomite: J. Geol. Educ. 33, 112–125.
- Longman, M., 1980, Carbonate diagenetic textures: AAPG Bulletin, v. 64, no. 4, p. 461-487.
- Lucia, F. J., 1961, Short Notes: Dedolomitization in the Tansill (Permian) Formation: Geological Society of America Bulletin, v. 72, July, p. 1107–1110.
- Mazzullo, S. J., 1980, Calcite pseudospar replacive of marine acicular aragonite, and implications for aragonite cement diagenesis: Journal of Sedimentary Petrography, v. 50, no. 2, p. 409-422.
- Mazzullo, S. J., 1999, Paleoenvironments, Cyclicity, and Diagenesis in the Outer Shelf Tansill Formation in the Carlsbad Embayment (Dark Canyon), Northern Guadalupe Mountains, New Mexico: SEPM Special Publications No. 65, p. 107–128.

- Mazzullo, S. J., and J. M. Cys, 1977, Submarine cements in Permian boundstones and reef-associated rocks, Guadalupe Mountains, West Texas and southeastern New Mexico: *in* Hileman, M. E., and S. J. Mazzullo, Upper Guadalupian facies, Permian Reef Complex, Guadalupe Mountains, New Mexico and West Texas, Field Conference Guidebook 77-16: Midland: Society of Economic Paleontologists and Mineralogists, Permian Basin Section, p. 151-200.
- Mazzullo, S. J., W. D. Bischoff, and C. L. Hendrick, 1989, Stacked island facies in Tansill outer-shelf platform, Dark Canyon, Guadalupe Mountains, New Mexico: SEPM, p. 287–293.
- Melim, L. A., and P. A. Scholle, 2002, Dolomitization of the Capitan Formation forereef facies (Permian, west Texas and New Mexico): seepage reflux revisited: *Sedimentology*, v. 49, no. 6, p. 1207–1227, doi:10.1046/j.1365-3091.2002.00492.x.
- Motts, W. S., 1972, Geology and Paleoenvironments of the Northern Segment, Capitan Shelf, New Mexico and West Texas: GSA Bulletin, doi:10.1130/0016-7606(1972)83.
- Motts, W. S., 1973, Structure, Sedimentation, and Paleoenvironments of Northern Capitan Reef Complex, New Mexico and West Texas: Abstract: AAPG, v. 57, no. 4, p. 796.
- Mruk, D. H., 1985, Cementation and dolomitization of the Capitan Limestone (Permian), McKittrick Canyon, West Texas: Unpublished M.S. Thesis, University of Colorado, Boulder, Colorado, 153 p.
- Mruk, D. H., 1989, Diagenesis of the Capitan Limestone, Upper Permian, Mckittrick Canyon, West Texas: SEPM, p. 387–406.
- Mutti, M. and Simo, J. A., 1994, Distribution, petrography, and geochemistry of early dolomite in cyclic shelf facies, Yates Formation (Guadalupian), Capitan Reef Complex, USA: *Spec.Publs Int. Ass. Sediment*, v. 21, p. 91-107.
- Newell, N. D., S. K. Rigby, A. G. Fischer, A. J. Whiteman, J. E. Hickox, and J. S. Bradley, 1953, The Permian Reef Complex of the Guadalupe Mountains region, Texas and New Mexico: San Francisco, Freeman, 236 p.
- O'Neil, J. R., 1987, Preservation of H, C, and O isotopic ratios in the low temperature environment: *in* Stable Isotope Geochemistry of Low Temperature Fluids, Kyser, T. K., ed., v. 13, p. 85-128.
- Patterson, R. J., and D. J. J. Kinsman, 1982, Formation of diagenetic dolomite in coastal sabkha along Arabian (Persian) Gulf: AAPG Bulletin, v. 66, no. 1, p. 28-43.

- Radke, Bruce M., and Robert L. Mathis, 1980, On the Formation and Occurrence of Saddle Dolomite: *Journal of Sedimentary Research*, v. 50, no. 4, p. 1149-1168.
- Ross, C. A., 1978, Late Pennsylvanian and Early Permian sedimentary rocks and tectonic setting of the Marathon Geosyncline: *in* Mazzullo, S. J., ed., *Tectonics and Paleozoic Facies of the Marathon Geosyncline, West Texas, Permian Basin Section*: SEPM, Publication 78-17, p. 89-93.
- Sarg, J. F., 1977, Sedimentology of the carbonate-evaporite facies transition of the Seven Rivers Formation (Guadalupian, Permian) in southeast New Mexico: *in* Upper Guadalupian Facies, Permian Reef Complex, Guadalupe Mountains, New Mexico and west Texas: *Midland Society of Economic Paleontologists and Mineralogists, Permian Basin Section, Publication*, 77-16, p. 451-478.
- Scholle, P.A., 1995, Carbon and sulfur isotope stratigraphy of the Permian and adjacent intervals: *in* *The Permian of Northern Pangea*, Vol. 1. Paleogeography, Paleoclimates, Stratigraphy, eds P.A. Scholle, T.M. Peryt and D.S. Ulmer-Scholle, p. 133–149.
- Scholle, P.A., 2002, An Introduction and Virtual Geologic Field Trip to the Permian Reef Complex, Guadalupe and Delaware Mountains, New Mexico-West Texas: <https://geoinfo.nmt.edu/staff/scholle/guadalupe.html>, (accessed Feb. 28, 2013).
- Scholle, P. A., R. H. Goldstein, and D. S. Ulmer-scholle, 2007, Classic Upper Paleozoic Reefs and Bioherms of West Texas and New Mexico: p. 1–171.
- Scholle, P. A., and D. S. Ulmer-Scholle, 2003, A Color Guide to the Petrography of Carbonate Rocks: Grains, Textures, Porosity, Diagenesis: AAPG Memoir 77.
- Scholle, P. A., D. S. Ulmer, and L. A. Melim, 1992, Late-stage calcites in the Permian Capitan Formation and its equivalents, Delaware Basin margin, west Texas and New Mexico: evidence for replacement of precursor evaporites: *Sedimentology*, v. 39, p. 207–234.
- Senowbari- Daryan, B. and J. K. Rigby, 1996, Brachiopod mounds not sponge reefs, Permian Capitan-Tansill Formations, Guadalupe Mountains, New Mexico: *Journal of Paleontology*, v. 70, p. 697-701.
- Sharp, Z., 2007, *Principles of Stable Isotope Geochemistry*, Upper Saddle River, Prentice Hall, 344 p.
- Shearman, D. J., J. Khouri, and S. Taha, 1961, On the replacement of dolomite by calcite in some mesozoic limestones from the French Jura: *Geol. London Assoc. Proc.*, v. 71, p. 1-12.

- Shinn, E. A., 1969, Submarine Lithification of Holocene carbonate sediments in the Persian Gulf: *Sedimentology*, v. 12, p. 109-144.
- Shinn, E. A., 1983, Tidal Flat Environment: *in* AAPG Memoir 33, Carbonate Depositional Environments Scholle, Peter A., Don G. Bebout, and Clyde H. Moore, eds. p. 173-310.
- Sibley, D. F. and Gregg, J. M., 1987, Classification of dolomite rock textures: *Journal of Sedimentary Petrography*, v. 57, p. 27-39.
- Tatarskiy, V. B., 1949, Distribution of rocks in which dolomite is replaced by calcite, *Akad, Nauk, SSSR, Dolkady*, v. 69 p. 849-851.
- Tinker, S. W., 1998, Shelf-To-Basin Facies Distributions and Sequence Stratigraphy of a Steep-Rimmed Carbonate Margin; Capitan Depositional System, McKittrick Canyon, New Mexico and Texas: *Journal of Sedimentary Research*, v. 68, no. 6, p. 1146-1174.
- Tyrrell, W., 1969, Criteria useful in interpreting environments of unlike but time-equivalent carbonate units (Tansill-Capitan-Lamar), Capitan Reef Complex, west Texas and New Mexico: *SEPM Special Publication*, no. 14, p. 80-97.
- Ulmer-Scholle, D. S., P. A. Scholle, and P. V Brady, 1993, Silicification of Evaporites in Permian (Guadalupian) Back-Reef Carbonates of the Delaware Basin, West Texas and New Mexico: *Journal of Sedimentary Research*, v. 63, no. 5, p. 955-965.
- van Lith, Y., C. Vasconcelos, R. Warthmann, J. C. F. Martins, and J. A. McKenzie, 2002, Bacterial sulfate reduction and salinity, two controls on dolomite precipitation in Lagoa Vermelha and Brejo do Espinho (Brazil): *Hydrobiologia*, v. 485, p. 35-49.
- Vasconcelos, C., and J. A. McKenzie, 1997, Microbial mediation of modern dolomite precipitation and diagenesis under anoxic conditions (Lagoa Vermelha, Rio De Janeiro, Brazil.): *Journal of Sedimentary Research*, v. 67, no. 3, p. 378-390.
- Veizer, J., Fritz, P., and B. Jones, 1986, Geochemistry of brachiopods: oxygen and carbon isotopic records of Paleozoic oceans: *Geochimica et Cosmochimica Acta*, v. 50, no. 8, p. 1679-1696.
- Von Morlot, A., 1847, Ueber Dolomit und seine keunstliche Darstellung aus Kalkstein, *Haidinger Naturwiss, Abhsndl.*, v. 1, p. 305-315. Warrak, M., 1974, The petrography and origin of dedolomitized, veined or brecciated carbonate rocks, the 'corneules', in the Frejus region, French Alps: *Jl Geol. Soc. Lond*, v. 130, p. 229-247.

- Warrak, M., 1974, The petrography and origin of dedolomitized, veined or brecciated carbonate rocks, the 'cornieules', in the Frejus region, French Alps: *Jl geol. Soc. Lond*, v. 130, p. 229-247.
- Warren, J., 2000, Dolomite: occurrence, evolution, and economically important associations: *Earth-Science Reviews*, v. 52, p. 1-81.
- Warthmann, R., Y. van Lith, C. Vasconcelos,, J. A. McKenzie, and A. M. Karpoff, 2000, Bacterially induced dolomite precipitation in anoxic culture experiments: *Geology*, v. 28, no. 12, p. 1091-1094.
- Weaver, C. E., 1975, Construction of limpid dolomite: *Geology*, v. 3, p. 407-420.
- Wilkinson, B. H., R. M. Owen, and A. R. Carroll, 1985, Submarine hydrothermal weathering, global eustacy, and carbonate polymorphism in Phanerozoic marine oolites: *Journal of Sedimentary Petrography*, v. 55, p. 171-183.
- Wood, R. A., 1999, Paleocology of the Capitan Reef: *SEPM*, no. 65, p. 129-137.
- Wood, R. A., J. A. D. Dickson, and George B. Kirkland, 1994, Turning the Capitan reef upside down; a new appraisal of the ecology of the Permian Capitan reef, Guadalupe Mountains, Texas and New Mexico: *Palaios*, v. 9, p. 422-427.
- Wood, R. A., J. A. D. Dickson, and George B. Kirkland, 1996, New Observations on the ecology of the Permian Capitan reef, Texas and New Mexico: *Paleontology*, v. 39, p. 733-762.
- Yurewicz, D. A., 1976, Sedimentology, paleocology, and diagenesis of the massive facies of the Lower and Middle Capitan Limestone (Permian), Guadalupe Mountains, New Mexico and Texas: Unpublished Ph. D. Dissertation, University of Wisconsin, Madison, 248 p.
- Yurewicz, D. A., 1977, The origin of the massive facies of the Lower and Middle Capitan Limestone (Permian), Guadalupe Mountains, New Mexico and west Texas: *in* Hileman, M. E., and S. J. Mazzullo, Upper Guadalupian facies, Permian Reef Complex, Guadalupe Mountains, New Mexico and West Texas, Field Conference Guidebook 77-16: Midland: SEPM, Permian Basin Section, p. 45-92.

APPENDIX A: Core Description

Both the Amoco No.1 and No. 2 cores from Dark Canyon in Carlsbad, New Mexico were briefly examined and described for this study. Amoco No.1 was drilled through the near backreef Tansill Formation and the upper part of the Capitan Reef Limestone. It consists mostly of skeletal packstones and grainstones. The abundant skeletal fragments, most of which are dolomitized, obscure the diagenetic textures.

Amoco No. 2, the focus of this study, was drilled farther backreef (Figure 1). The upper portion of this core is mainly made up of interbedded limestone and dolomite wackestones and packstones. Some of the bedded limestone, and all of the peloidal limestone, has been dolomitized (Figure 2). Calcitized botryoids of former aragonite are abundant. Porosity is mostly vuggy, and fenestral fabrics are abundant. Some of the limestone is dolomitized. It is dominantly wackestones with few skeletal fragments.

Dedolomite is present in Amoco No. 2 (Figure 3). It is not visible with the naked eye in the core. The dedolomite was discovered in a thin section made from this core. This will be discussed in later sections.

The contact between the Tansill and the Yates Formations is present at approximately 115 meters (380 ft) depth in the core. The top of the Yates Formation consists of very well sorted quartz siltstones interbedded with limestone, some of which is dolomitized.

Figure 2 is a simplified stratigraphic column of Amoco No. 2. This stratigraphic column is featured in the unpublished Amoco core report for this research core. Figure 4 is a much more detailed column constructed from observations of AmocoNo. 2 by both myself and the unpublished notes of Willis Tyrrell.



Figure A1: Amoco Core No. 2, 68-76 ft. This section of core displays most of the cements and major fabrics present in Amoco No. 2. Peloidal, dolomitized limestone, dolomitized limestone and botryoids, and calcitized botryoids.

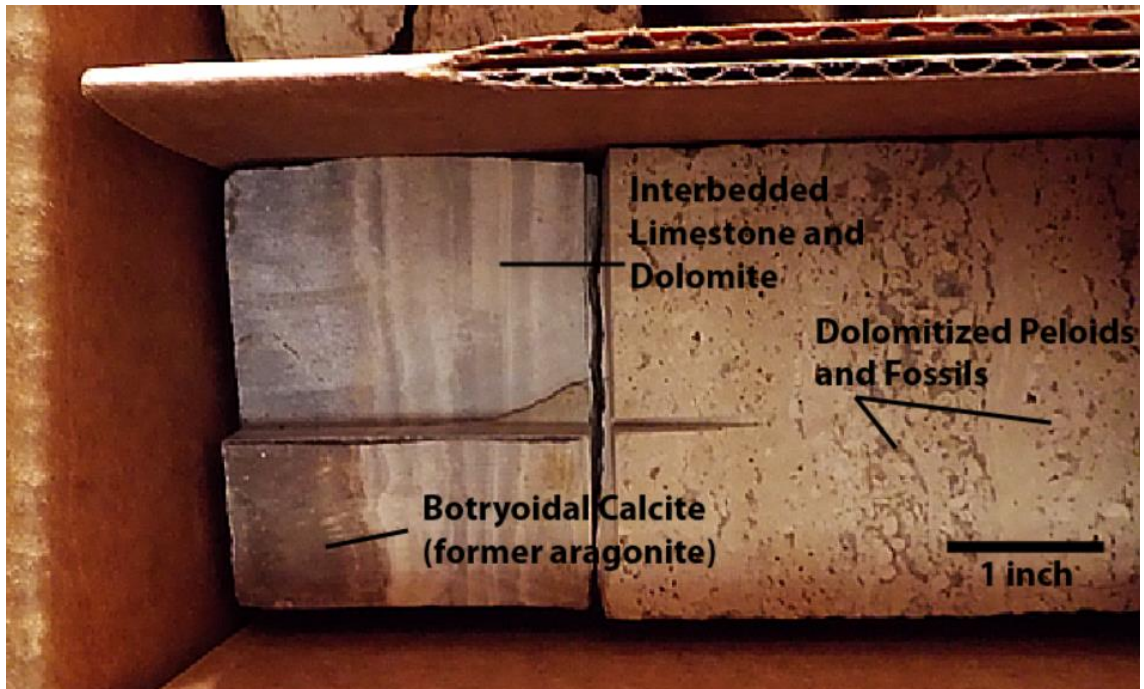


Figure A2: Amoco Core No. 2, 77 ft.

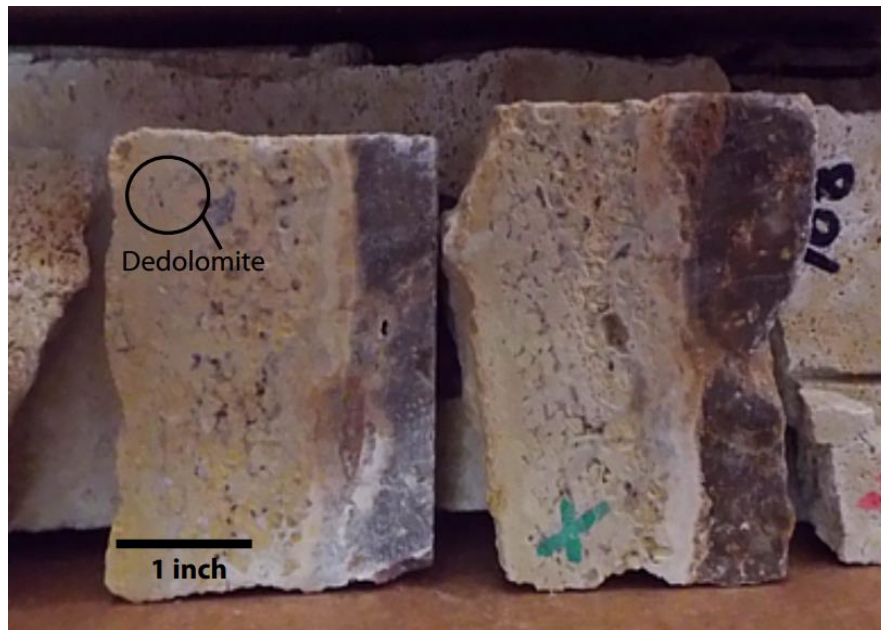


Figure A3: Amoco Core No. 2, 108 ft. The dedolomite is not visible with the naked eye; it was discovered in thin section and via microprobe analysis.

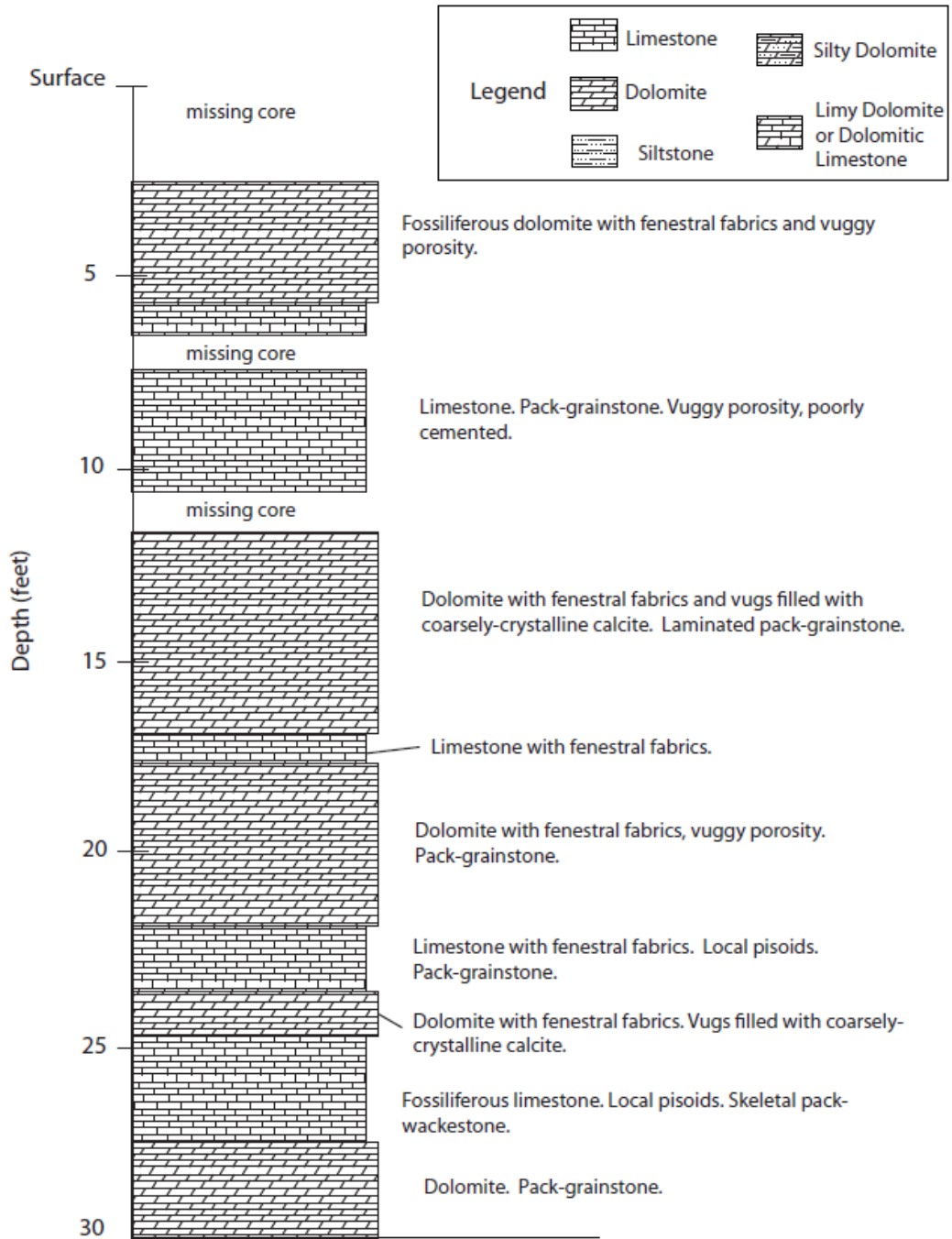


Figure A4: A cross section constructed from the Amoco No. 2 core.

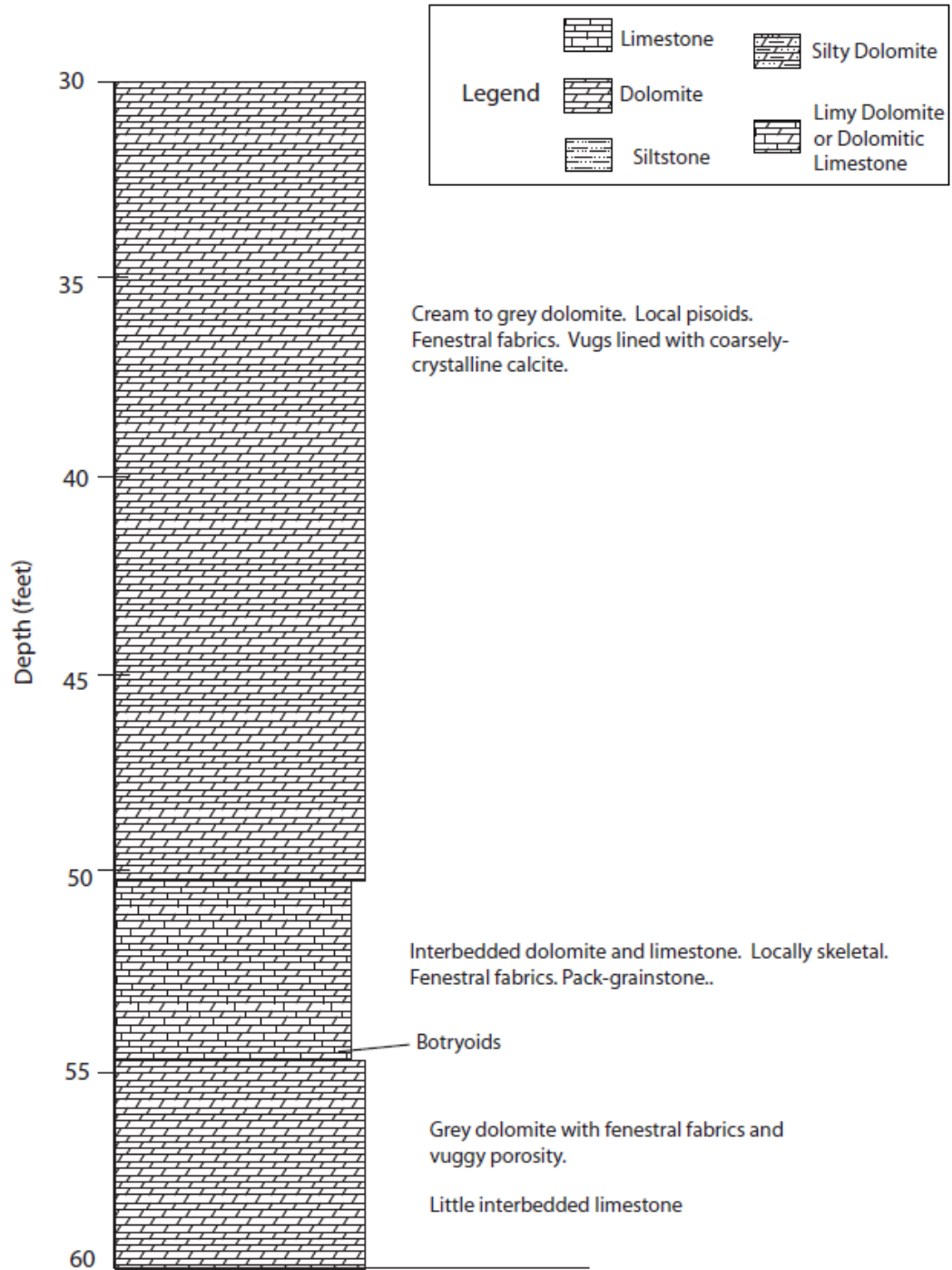


Figure A4- Continued

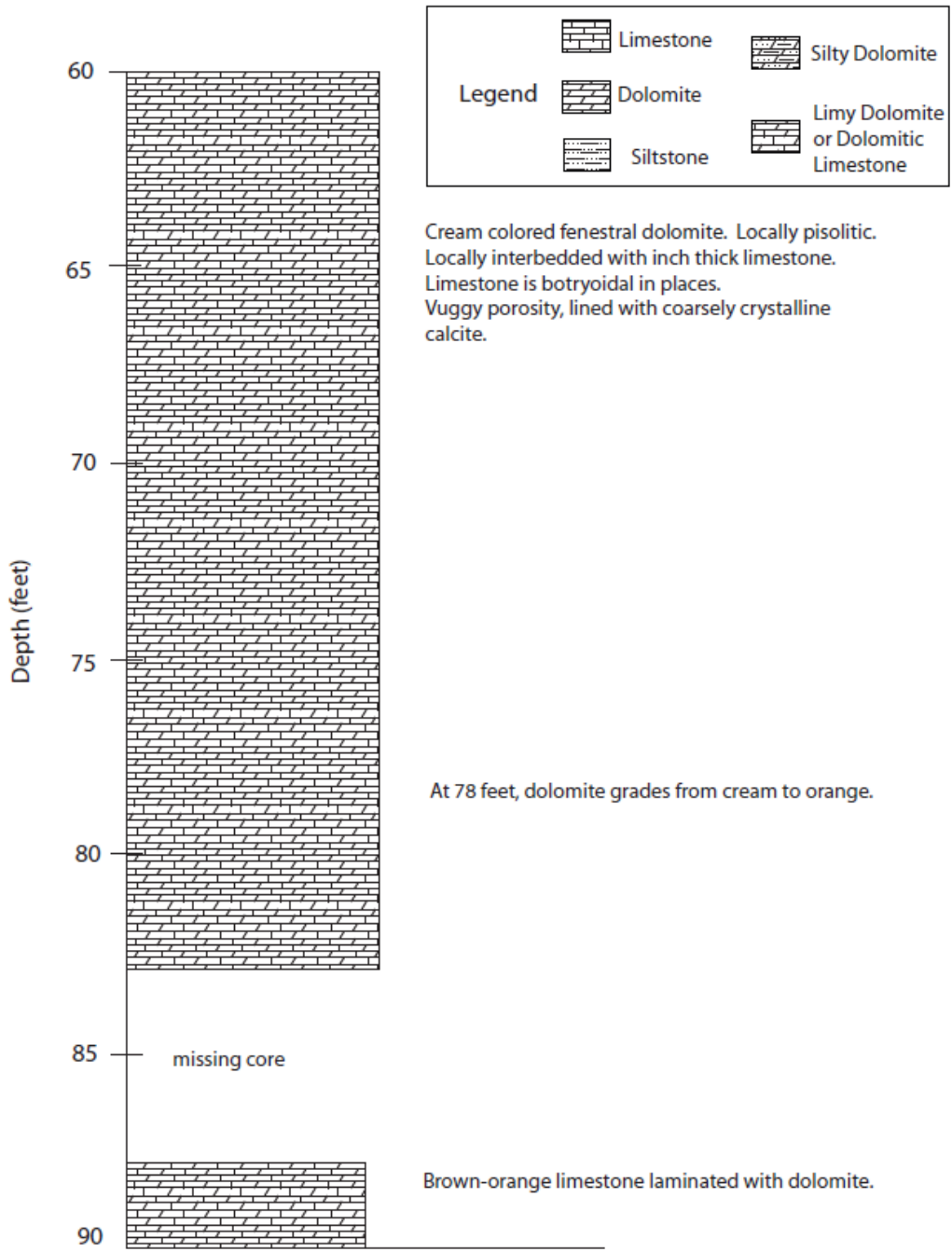


Figure A4- Continued

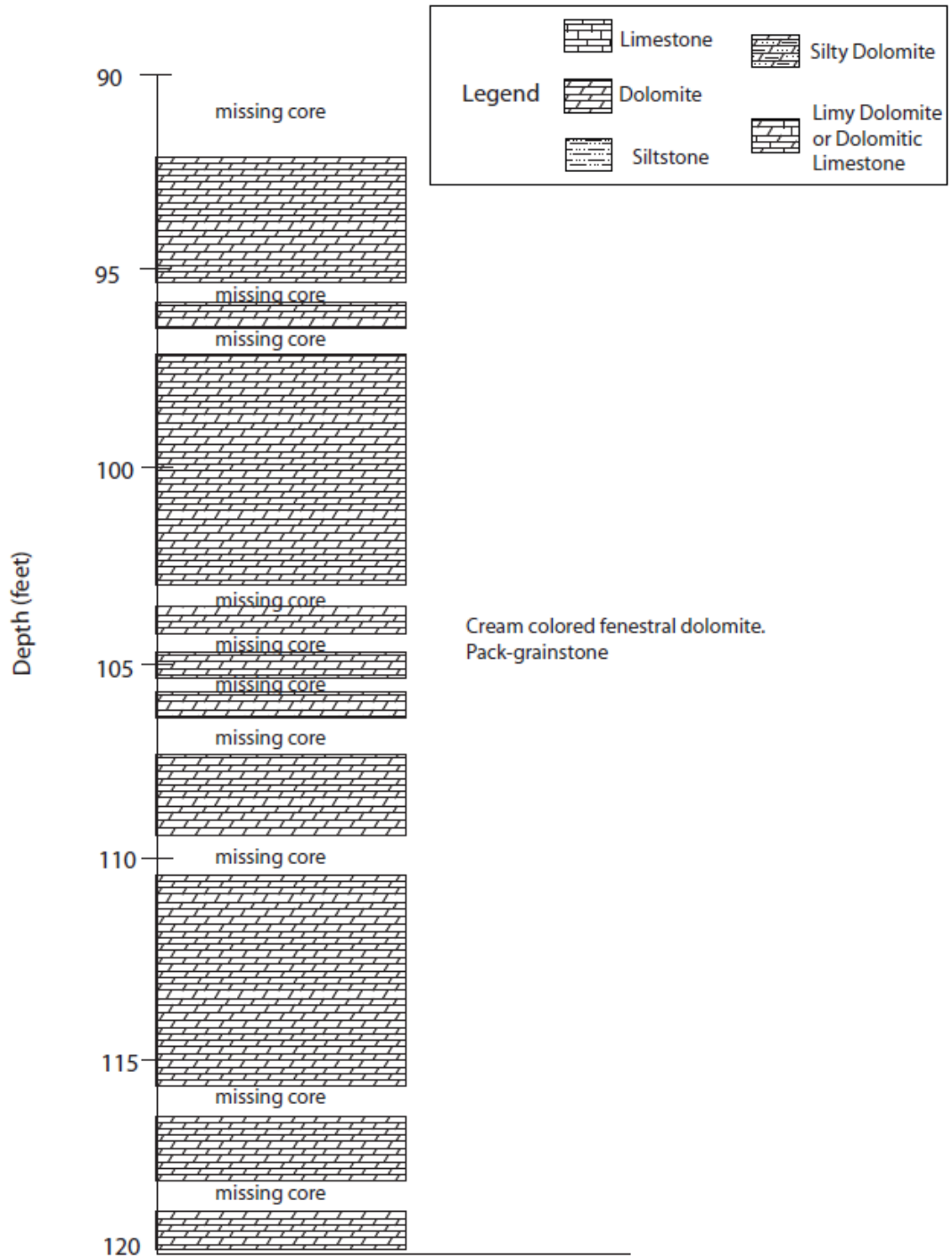


Figure A4- Continued

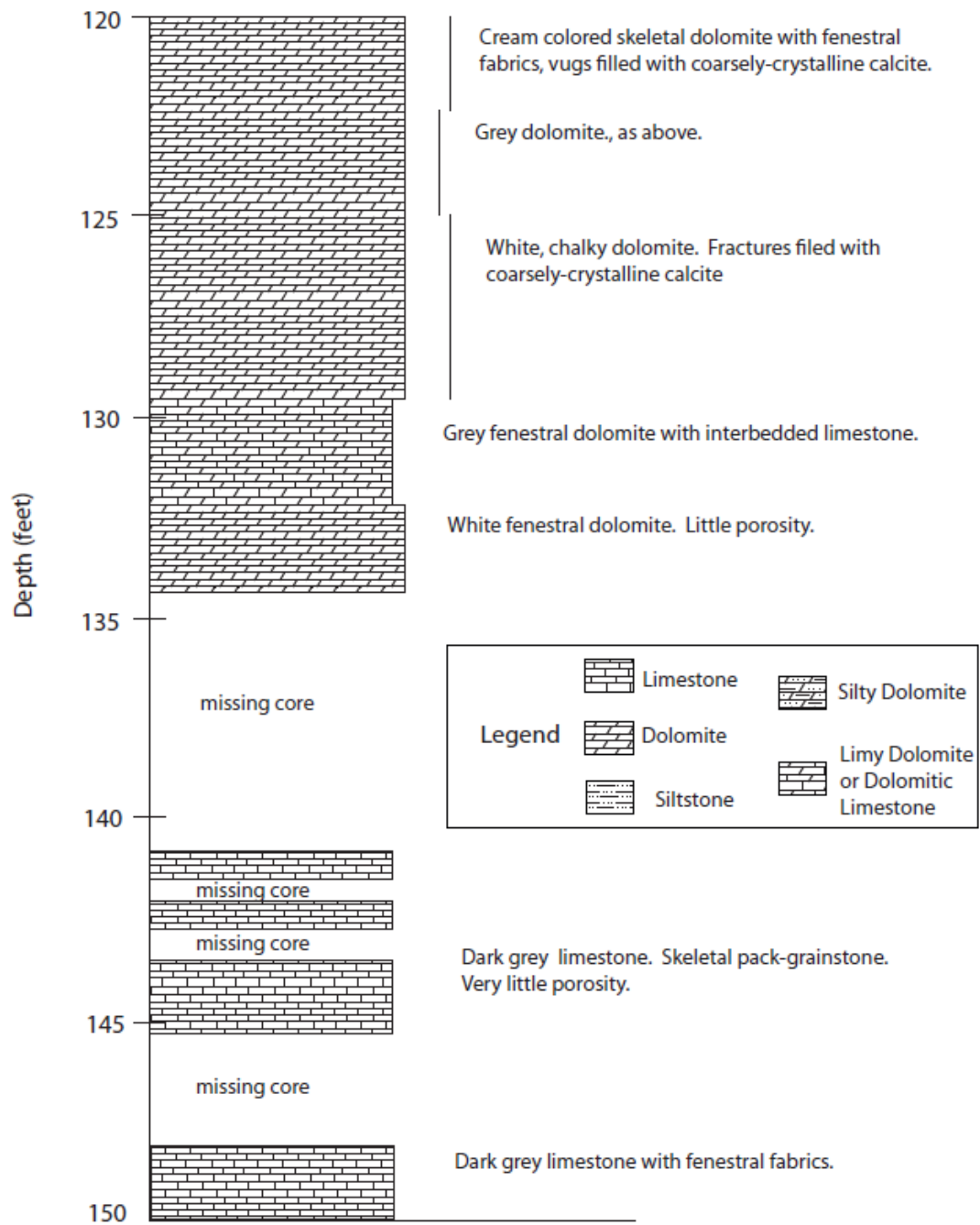


Figure A4- Continued

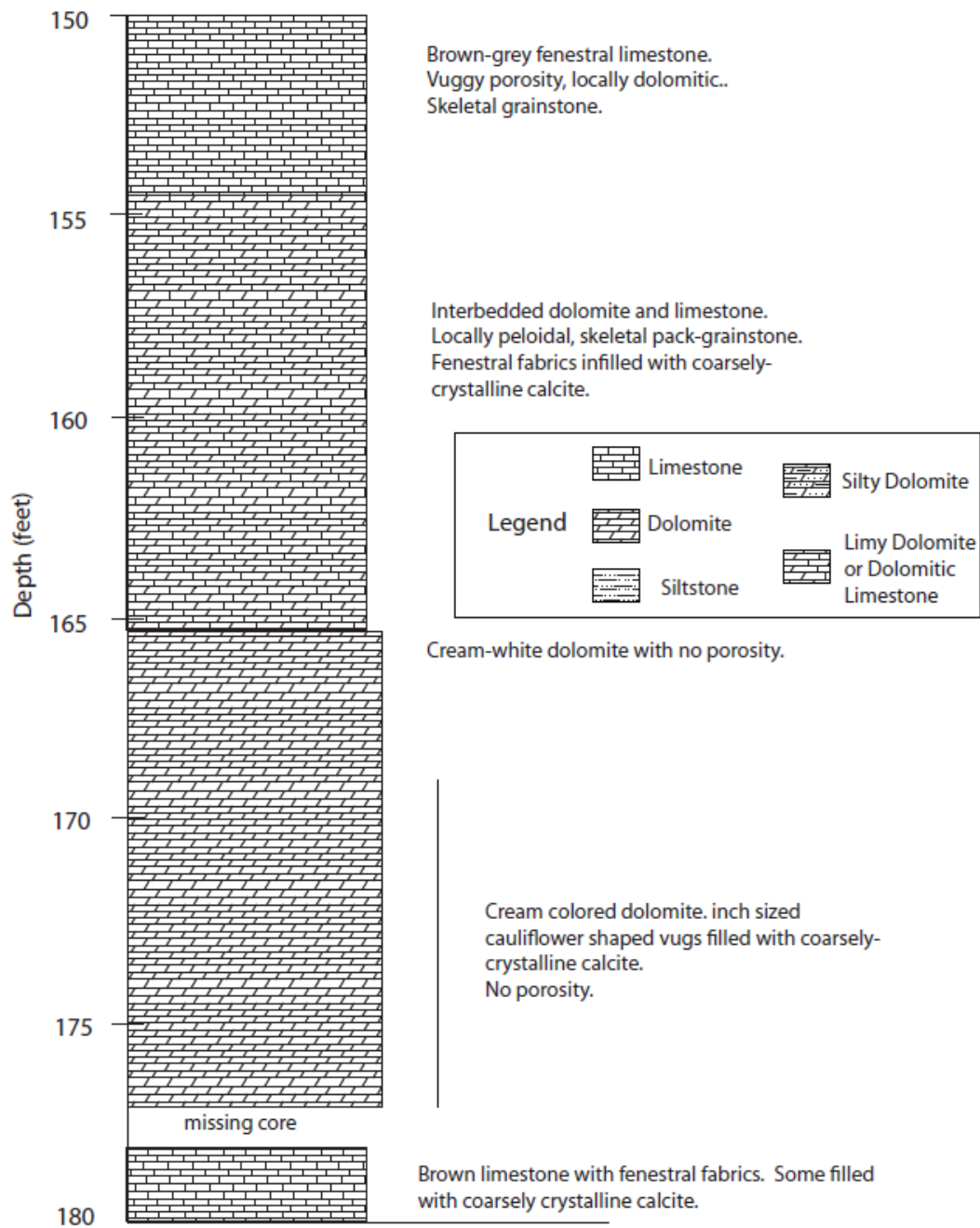


Figure A4- Continued

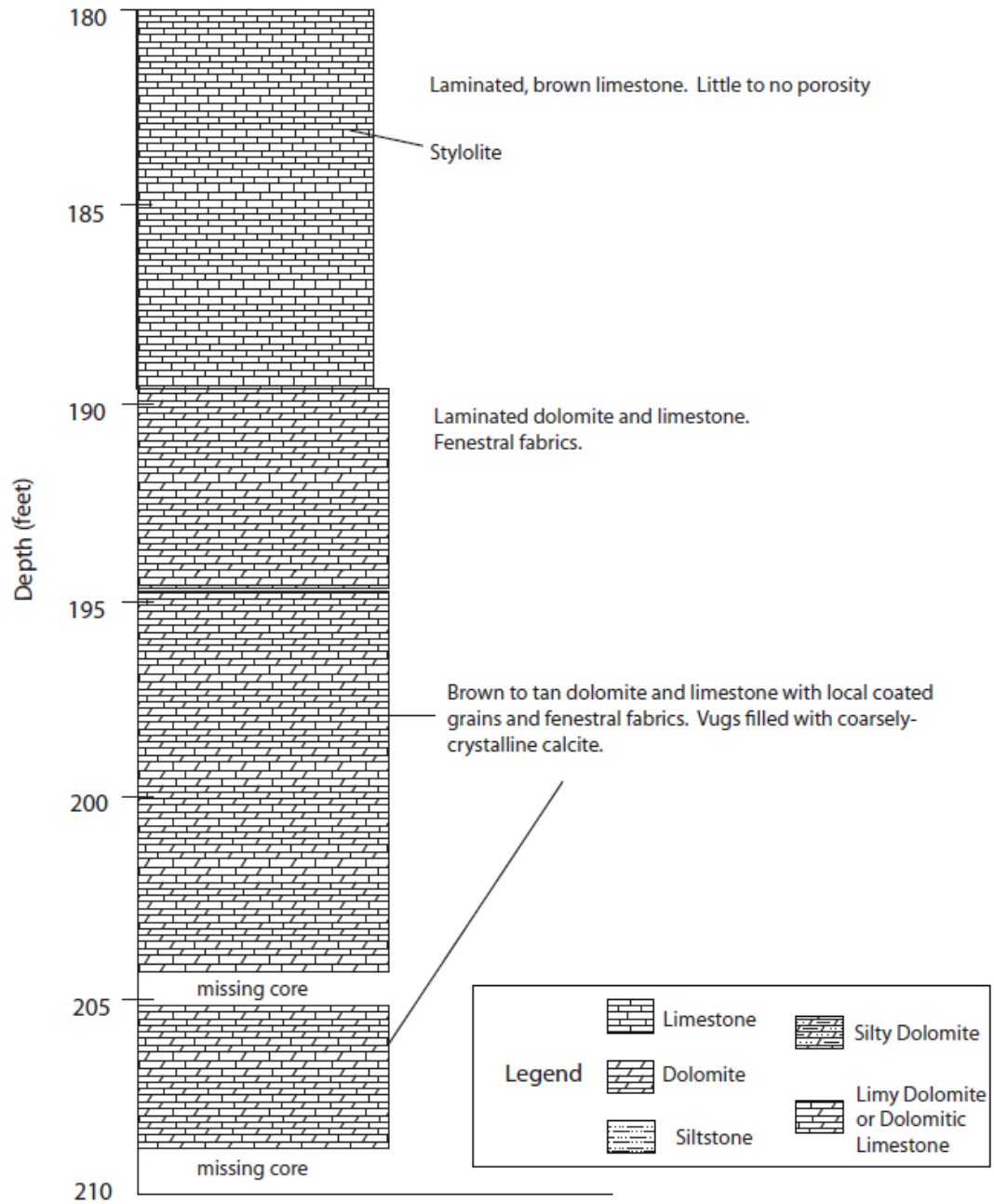


Figure A4- Continued

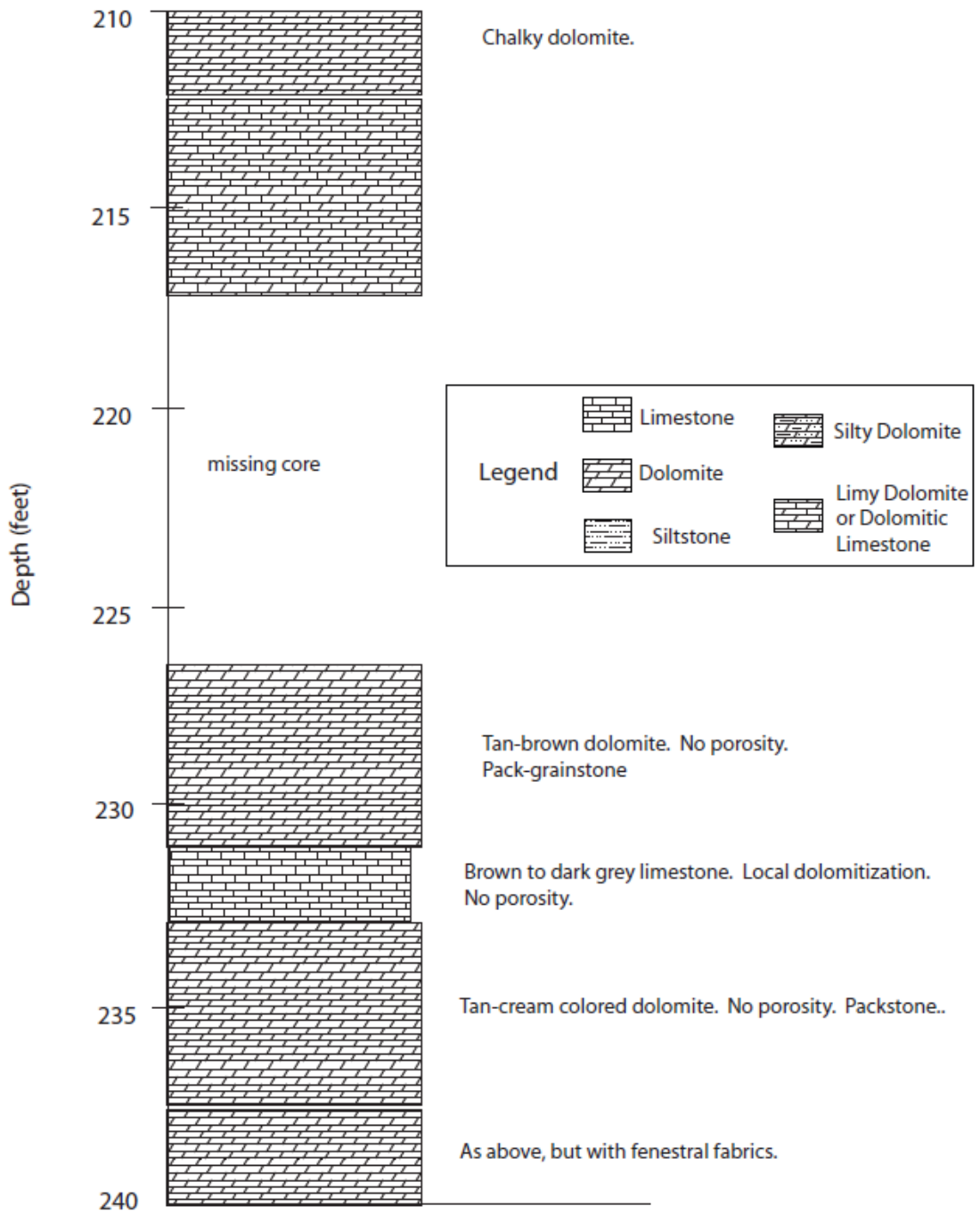


Figure A4- Continued

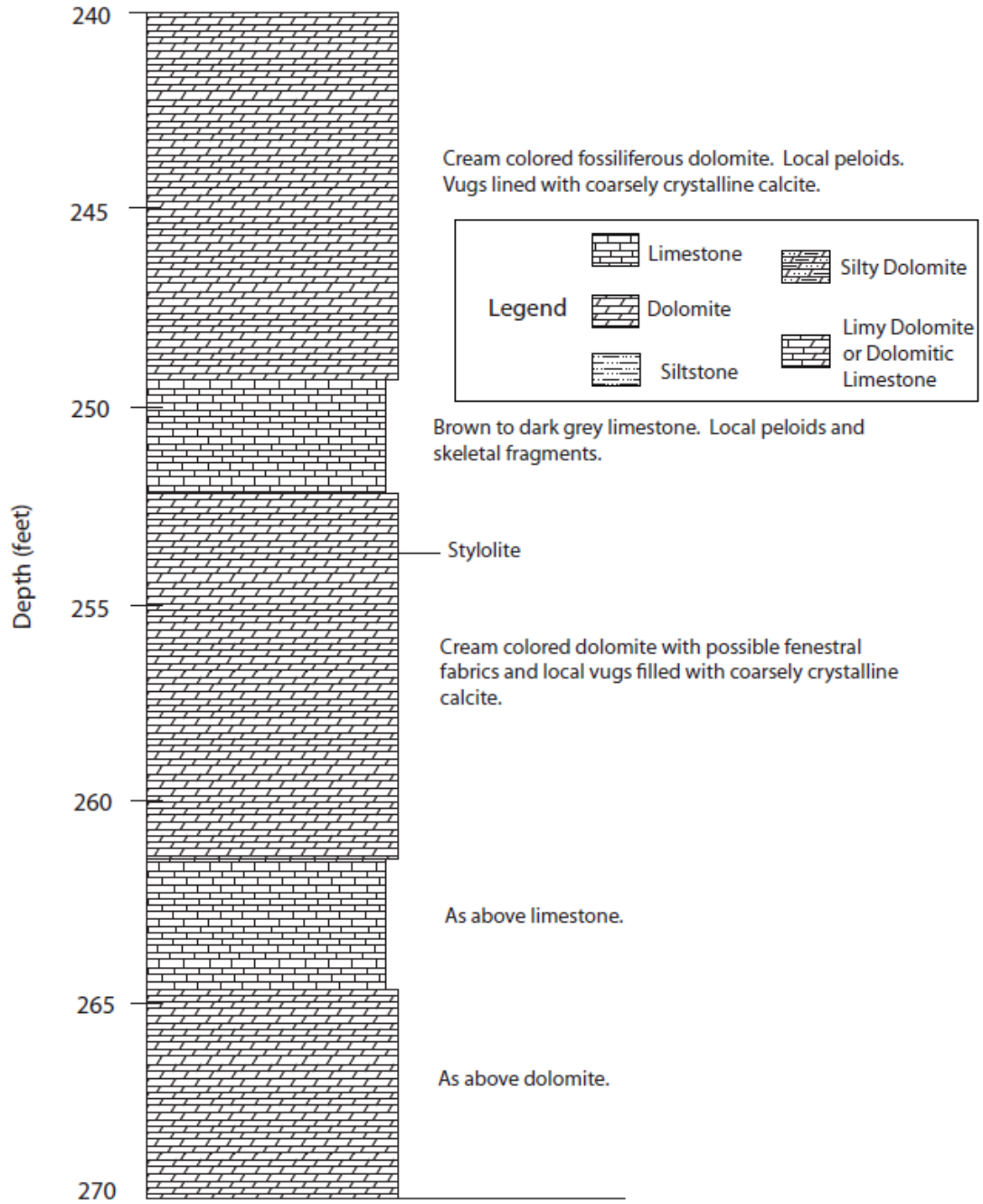


Figure A4- Continued

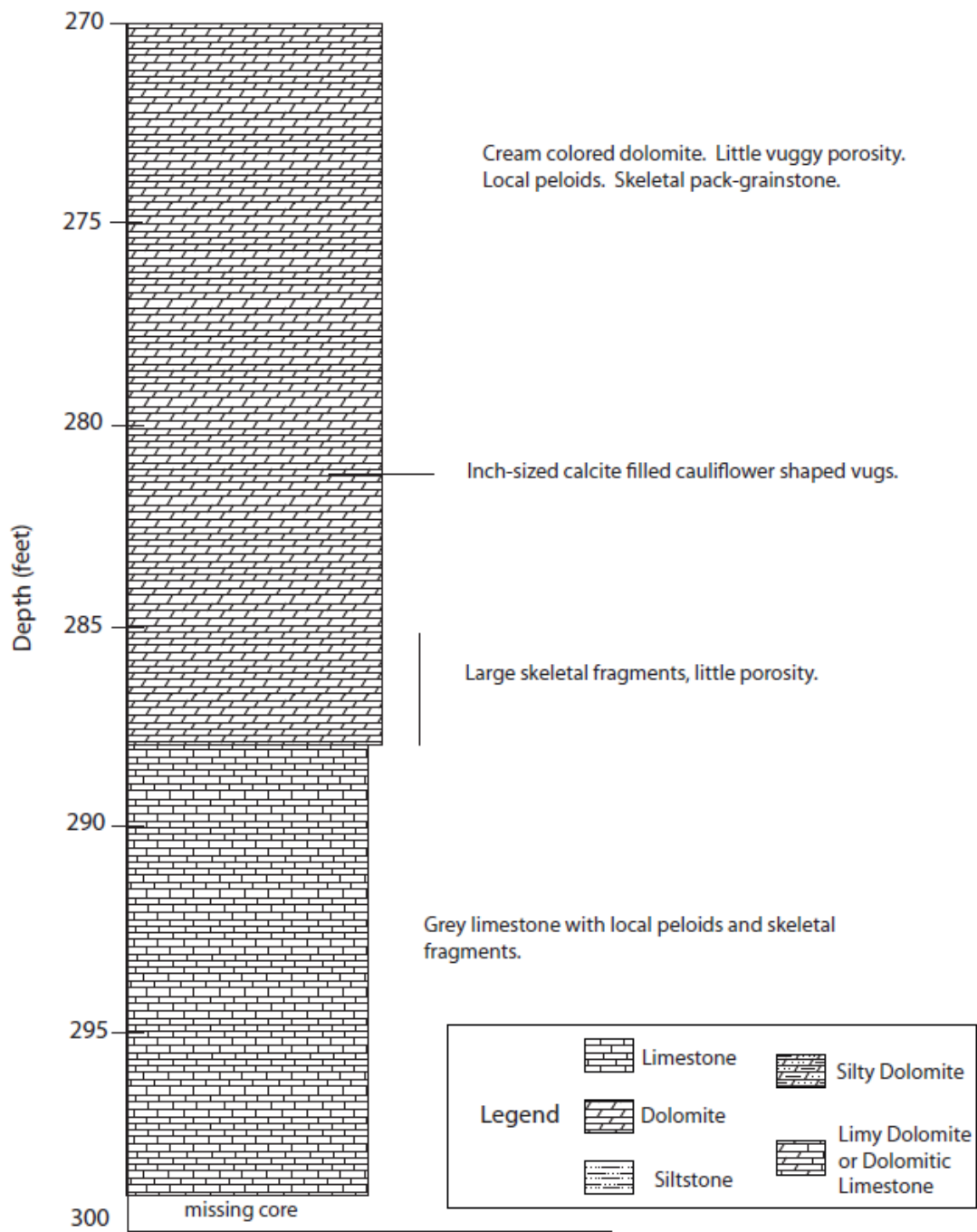


Figure A4- Continued

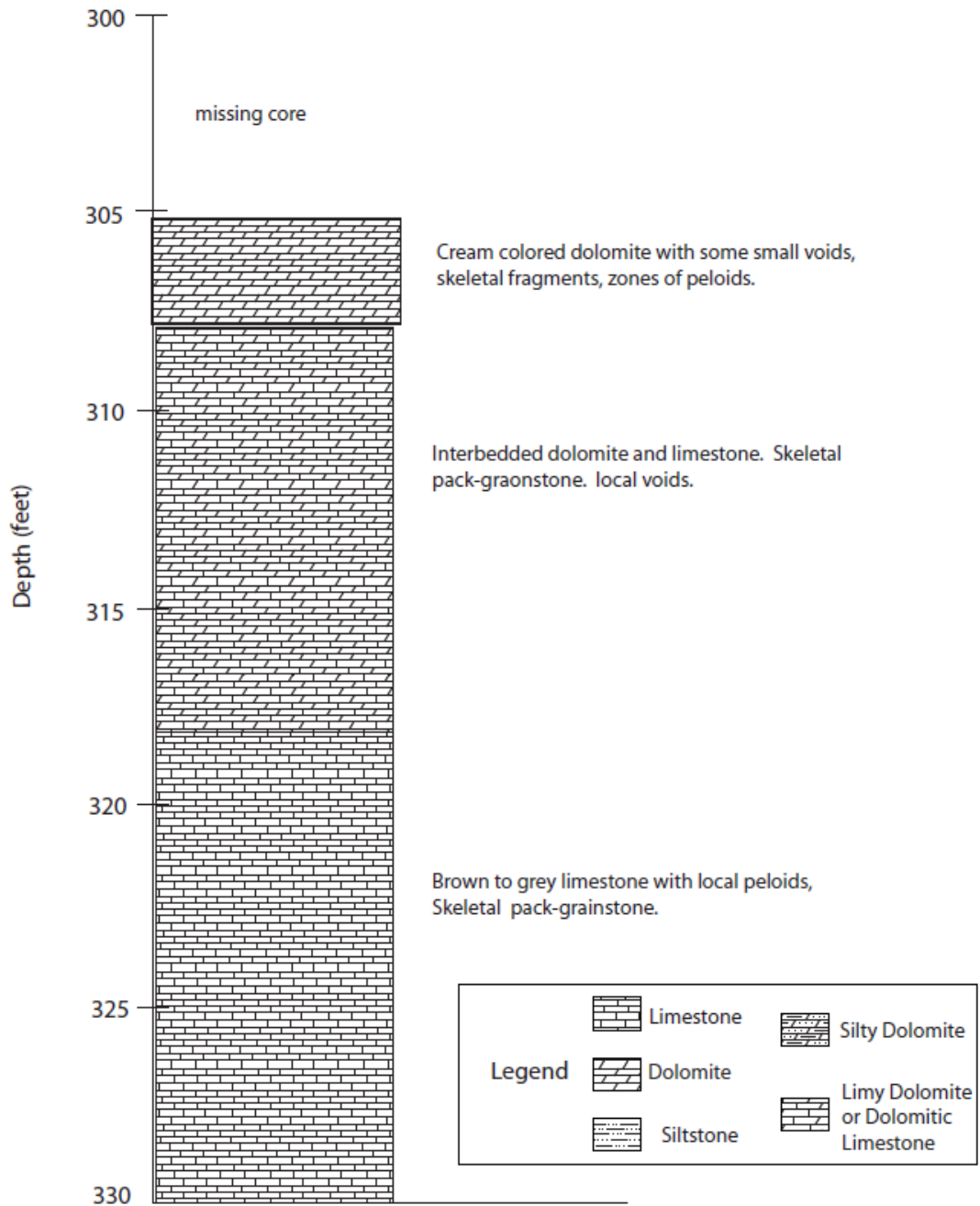


Figure A4- Continued

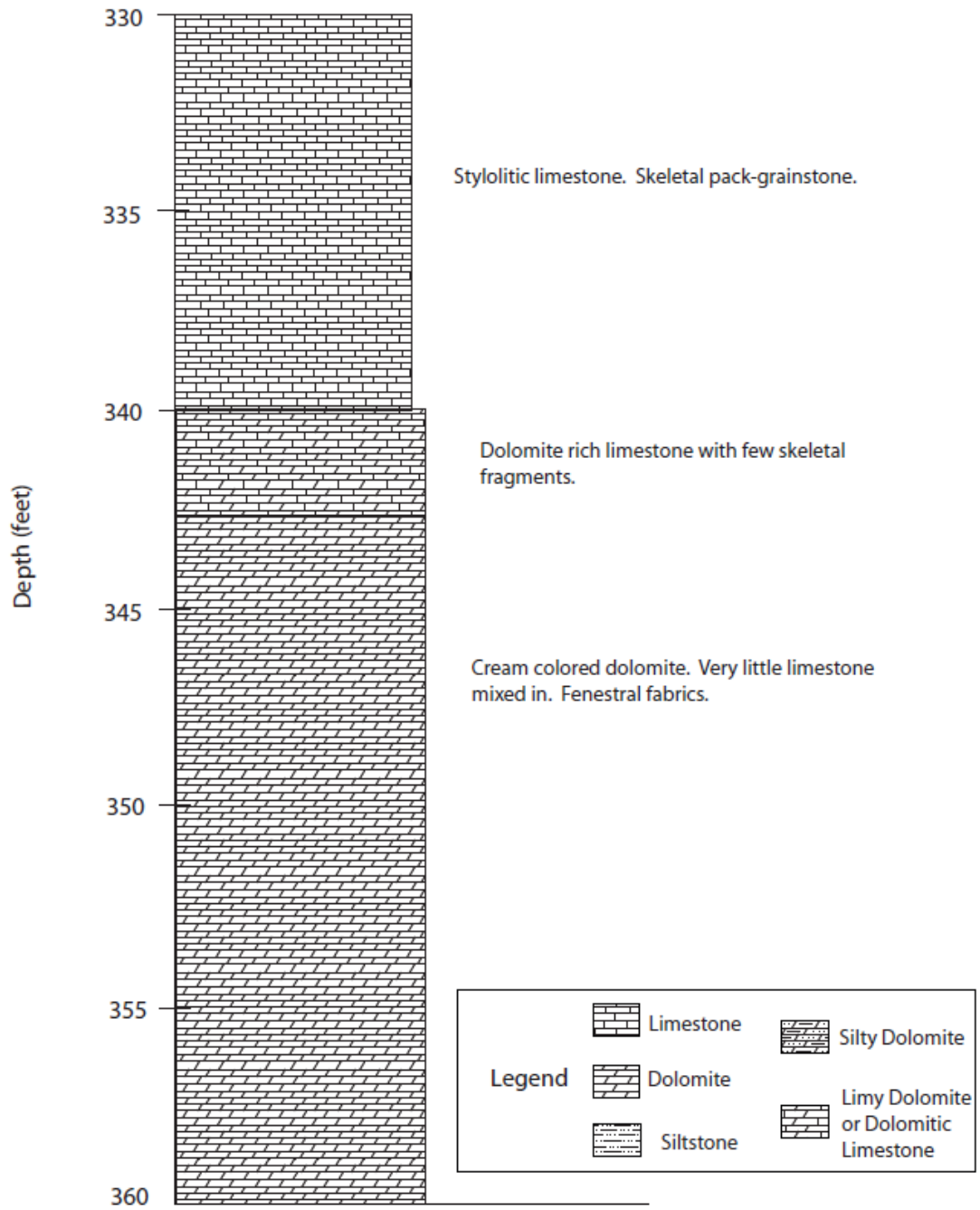


Figure A4- Continued

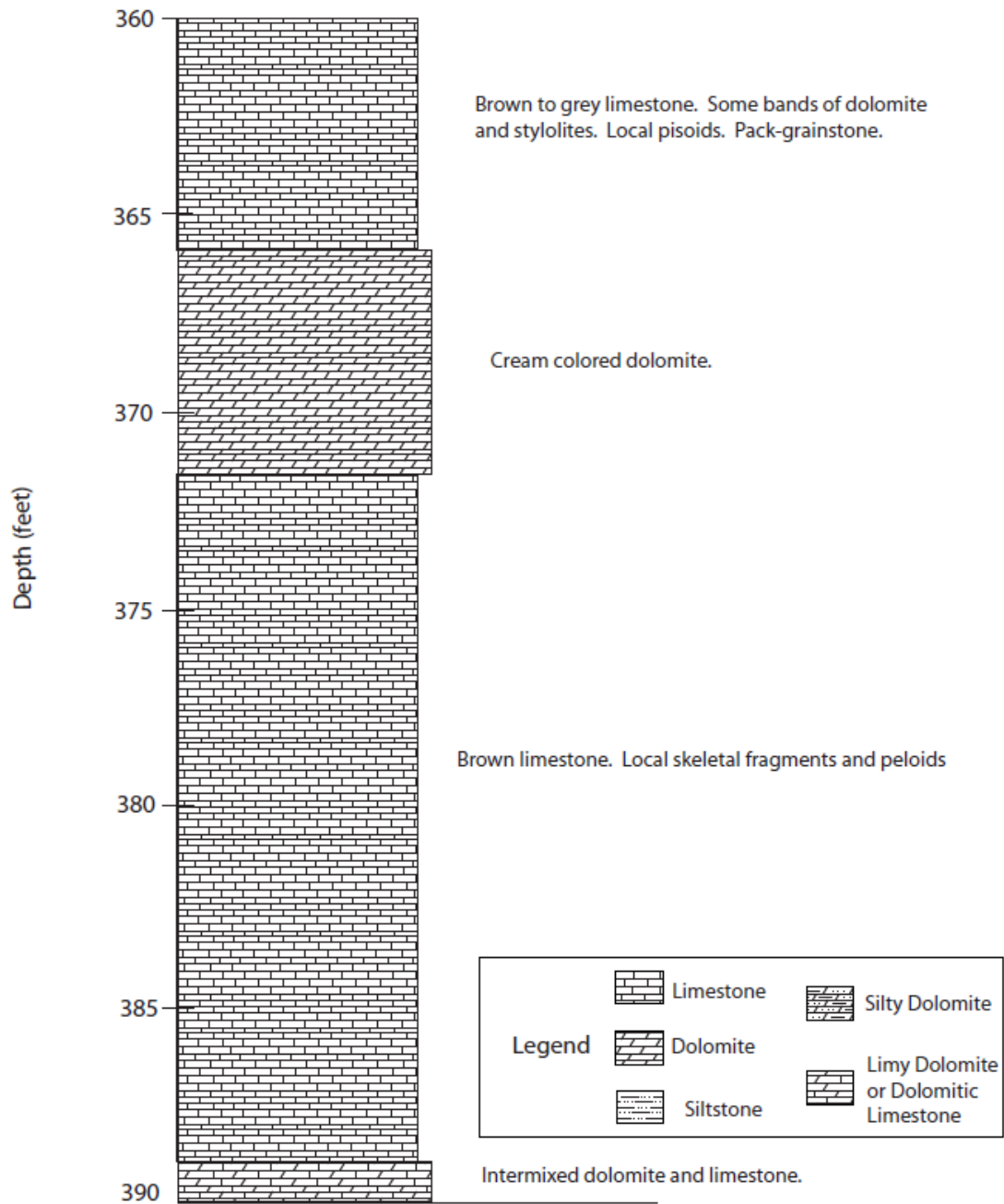


Figure A4- Continued

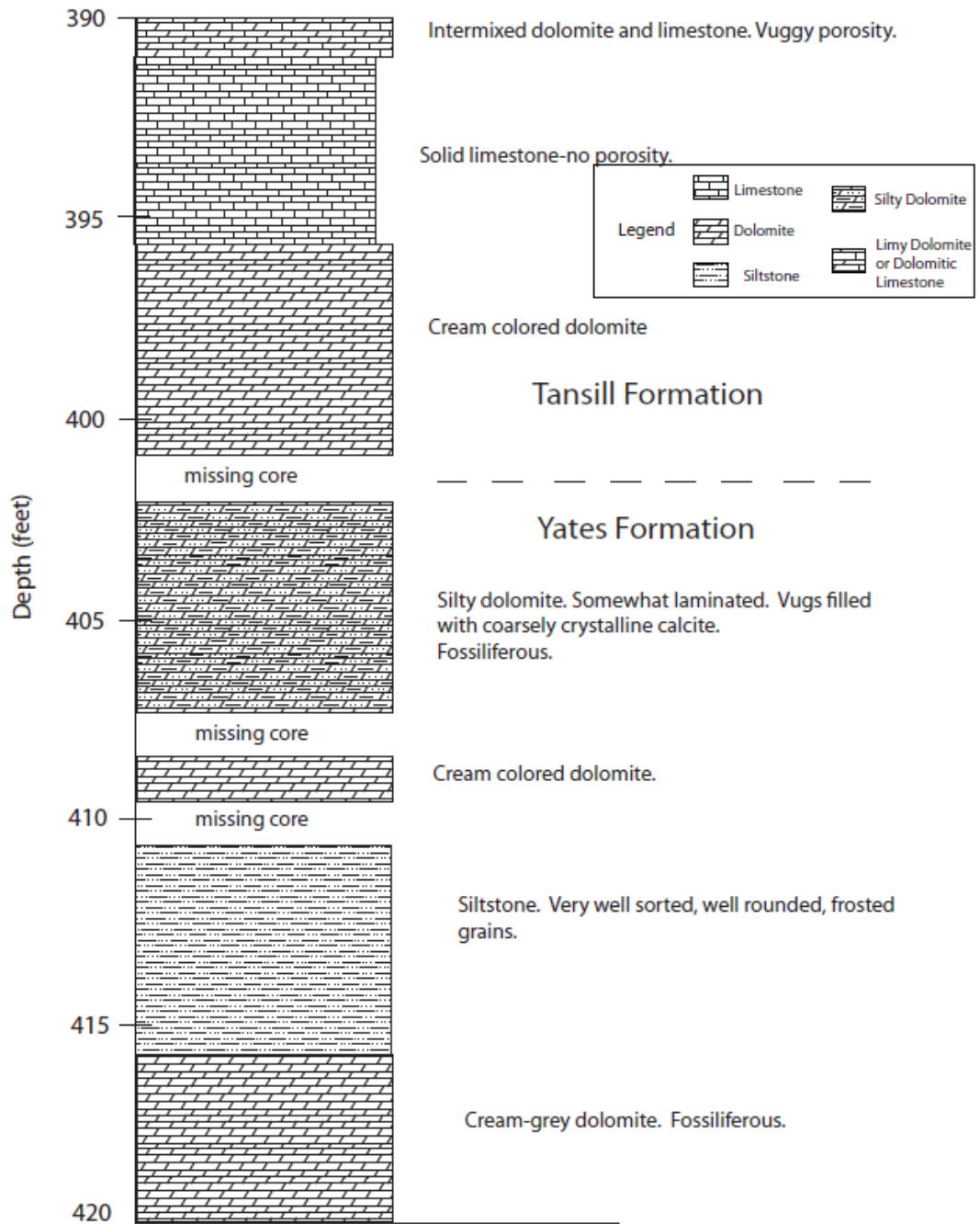


Figure A4- Continued

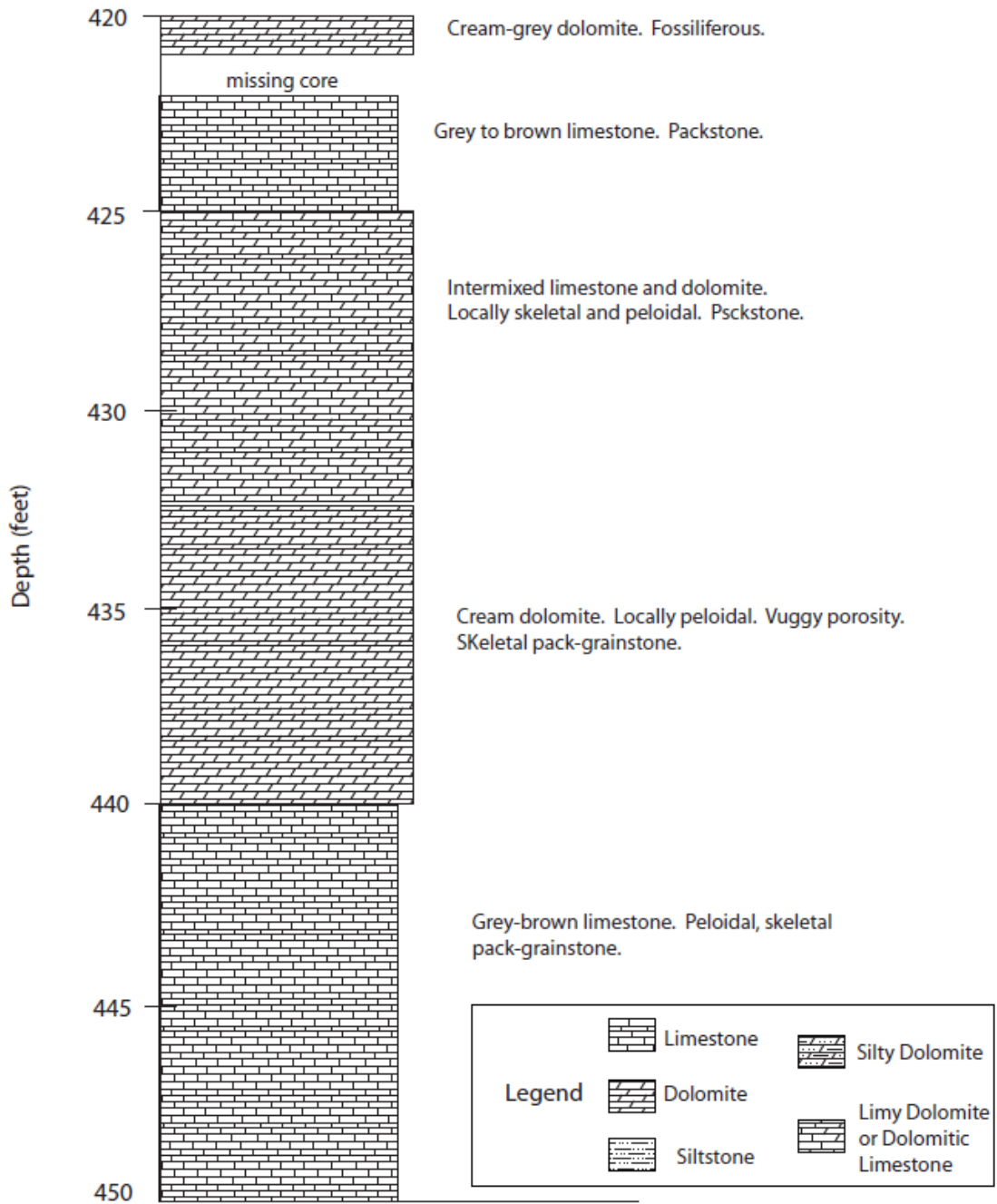


Figure A4- Continued

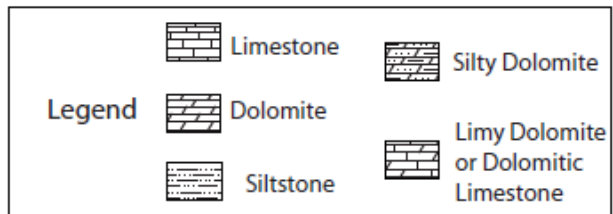
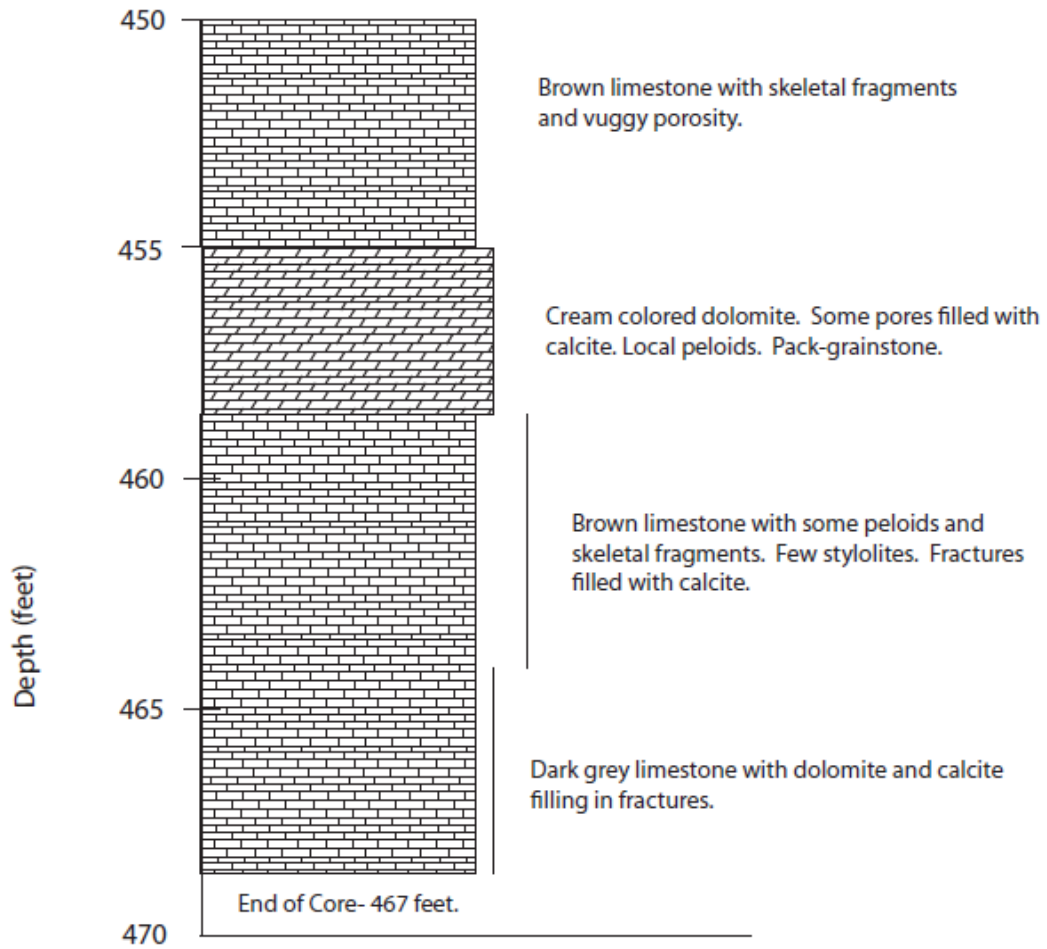


Figure A4- Continued

APPENDIX B: Raw Microprobe Data

Table B1: Raw microprobe data (Carb10 weight %) from Amoco No. 2, 76 ft.

Carb10 Wt% Oxide for DC2-76											
Sample	Species	CO2	SiO2	SO2	MgO	CaO	MnO	FeO	SrO	BaO	Na2O
DC-2-76-06	early dolomite	46.71	0.2	0.05	21.14	31.6	0	0.22	0.04	0.02	0.01
DC-2-76-07	early dolomite	46.98	0.16	0.02	21.11	31.35	0.02	0.3	0.03	0.02	0
DC-2-76-08	early dolomite	46.82	0.23	0.01	21.24	31.37	0	0.31	0.01	0	0
DC-2-76-09	early dolomite	46.83	0.1	0.04	21.23	31.54	0	0.17	0.02	0.04	0.02
DC-2-76-10	early dolomite	47.12	0.1	0.07	21.21	31.41	0	0.02	0.01	0	0.07
DC-2-76-25	early dolomite	47.07	0.04	0.03	21.34	31.24	0	0.21	0.04	0.04	0.01
DC-2-76-26	early dolomite	46.82	0.05	0.01	21.45	31.3	0.01	0.27	0.01	0.05	0.02
DC-2-76-27	early dolomite	47.16	0.04	0	21.21	31.34	0	0.22	0.02	0	0.01
DC-2-76-28	early dolomite	46.9	0.03	0.03	21.28	31.43	0.05	0.25	0.01	0	0.02

Table B2: Raw microprobe data (Carb20 weight %) for Amoco No. 2, 76 ft.104

Carb20 Wt% Oxide for DC2-76											
Sample	Species	CO2	SiO2	SO2	MgO	CaO	MnO	FeO	SrO	BaO	Na2O
CaCO3-01	Standard	42.05	0.06	0.00	0.00	57.75	0.11	0.01	0.01	0.00	0.00
CaCO3-02	Standard	42.58	0.04	0.00	0.01	57.12	0.13	0.03	0.02	0.07	0.01
CaCO3-03	Standard	41.86	0.05	0.01	0.00	57.92	0.08	0.00	0.06	0.00	0.01
FeCO3-01	Standard	37.03	0.09	0.02	0.15	0.00	3.00	59.70	0.00	0.00	0.00
FeCO3-02	Standard	36.8	0.07	0.00	0.14	0.02	3.02	59.86	0.01	0.06	0.01
FeCO3-03	Standard	36.78	0.08	0.01	0.14	0.03	3.06	59.88	0.00	0.02	0.01
MgCO3-01	Standard	46.97	0.03	0.00	22.20	30.56	0.03	0.12	0.04	0.04	0.01
MgCO3-02	Standard	46.82	0.03	0.00	22.26	30.73	0.03	0.05	0.03	0.05	0.01
MgCO3-03	Standard	46.95	0.04	0.00	22.18	30.70	0.01	0.09	0.03	0.00	0.00
DC-2-76-01	calcite	42.66	0.26	0.03	0.17	56.84	0.01	0.01	0.00	0.01	0.01
DC-2-76-02	late dolomite	46.49	0.25	0.00	21.30	31.64	0.00	0.22	0.00	0.07	0.02
DC-2-76-03	early dolomite	47.61	0.21	0.00	21.04	30.79	0.00	0.34	0.00	0.00	0.00
DC-2-76-04	early dolomite	47.33	0.28	0.01	20.97	31.02	0.04	0.33	0.01	0.00	0.01
DC-2-76-05	early dolomite	47.14	0.20	0.02	21.15	31.16	0.03	0.31	0.00	0.00	0.00
DC-2-76-11	calcite	42.34	0.15	0.07	0.44	56.81	0.03	0.00	0.01	0.04	0.09
DC-2-76-12	calcite	42.52	0.17	0.02	0.16	57.06	0.03	0.00	0.00	0.00	0.03
DC-2-76-13	calcite	43.94	0.17	0.04	0.19	55.64	0.00	0.01	0.00	0.00	0.00
DC-2-76-14	calcite	42.68	0.17	0.06	0.20	56.82	0.00	0.03	0.02	0.00	0.03
DC-2-76-15	late dolomite	46.77	0.15	0.02	21.14	31.60	0.01	0.26	0.01	0.04	0.00
DC-2-76-16	late dolomite	47.26	0.15	0.00	21.35	30.83	0.01	0.30	0.02	0.07	0.01
DC-2-76-17	late dolomite	47.26	0.15	0.00	21.25	30.91	0.02	0.36	0.00	0.03	0.00

Table B2- Continued.

DC-2-76-18	late dolomite	47.57	0.12	0.01	21.21	30.79	0.00	0.27	0.00	0.02	0.00
DC-2-76-19	calcite	43.46	0.08	0.03	0.21	56.19	0.00	0.03	0.00	0.00	0.00
DC-2-76-20	calcite	42.59	0.05	0.02	0.22	57.01	0.03	0.00	0.03	0.05	0.00
DC-2-76-21	calcite	43.08	0.06	0.04	0.13	56.53	0.03	0.04	0.04	0.05	0.00
DC-2-76-22	calcite	42.68	0.06	0.00	0.18	56.95	0.03	0.03	0.03	0.03	0.02
DC-2-76-23	late dolomite	46.8	0.04	0.00	21.21	31.55	0.03	0.32	0.02	0.02	0.01
DC-2-76-24	late dolomite	47.17	0.06	0.00	20.97	31.53	0.02	0.23	0.00	0.01	0.00
DC-2-76-29	calcite	42.82	0.27	0.04	0.17	56.65	0.02	0.01	0.02	0.00	0.01
DC-2-76-30	calcite	43.6	0.23	0.01	0.15	55.96	0.00	0.02	0.00	0.02	0.00
DC-2-76-31	calcite	42.73	0.22	0.04	0.14	56.77	0.00	0.06	0.03	0.00	0.02
DC-2-76-32	calcite	42.91	0.22	0.00	0.17	56.62	0.00	0.01	0.01	0.06	0.00
CaCO3-04	Standard	42.71	0.05	0.02	0.00	57.04	0.14	0.03	0.00	0.00	0.02
CaCO3-05	Standard	43.02	0.03	0.00	0.00	56.84	0.07	0.02	0.00	0.00	0.01
FeCO3-04	Standard	36.87	0.16	0.01	0.12	0.00	2.95	59.88	0.00	0.00	0.00
FeCO3-05	Standard	36.87	0.13	0.00	0.12	0.02	3.03	59.80	0.00	0.03	0.00
MgCO3-04	Standard	46.73	0.04	0.00	22.27	30.81	0.01	0.09	0.05	0.01	0.00
MgCO3-05	Standard	46.62	0.06	0.00	22.25	30.91	0.04	0.06	0.05	0.01	0.00

Table B3: Raw microprobe data (Carb20 weight %) for Amoco No. 2, 47 and 108 ft.

Carb20 Wt% Oxide for DC-2 47A and DC-2 108B											
Sample	Species	CO2	SiO2	SO2	MgO	CaO	MnO	FeO	SrO	BaO	Na2O
CaCO3-01	Standard	42.72	0.02	0.02	0.00	57.12	0.07	0.00	0.04	0.00	0.01
CaCO3-02	Standard	42.62	0.04	0.01	0.00	57.18	0.08	0.01	0.03	0.03	0.00
FeCO3-01	Standard	37.27	0.08	0.00	0.12	0.02	3.10	59.37	0.02	0.00	0.02
FeCO3-02	Standard	37.24	0.15	0.00	0.14	0.01	3.14	59.30	0.00	0.02	0.00
MgCO3-01	Standard	47.16	0.06	0.00	22.13	30.47	0.03	0.07	0.08	0.00	0.01
MgCO3-02	Standard	47.16	0.04	0.01	22.17	30.42	0.04	0.08	0.06	0.01	0.00
DC-2-47A-01	dedolomite	44.39	0.01	0.00	0.27	55.32	0.00	0.00	0.00	0.01	0.00
DC-2-47A-02	calcite	42.87	0.02	0.01	0.26	56.80	0.01	0.02	0.00	0.00	0.01
DC-2-47A-03	late dolomite	47.20	0.01	0.08	21.62	30.96	0.00	0.07	0.01	0.00	0.05
DC-2-47A-04	late dolomite	46.73	0.02	0.11	21.95	31.12	0.00	0.00	0.02	0.00	0.06
DC-2-47A-05	dedolomite	41.28	0.02	0.09	0.22	58.25	0.05	0.00	0.06	0.00	0.02
DC-2-47A-06	calcite	44.67	0.00	0.10	0.14	55.00	0.02	0.01	0.05	0.01	0.00
DC-2-47A-07	late dolomite	46.85	0.01	0.08	22.16	30.80	0.02	0.00	0.00	0.02	0.07
DC-2-47A-08	early dolomite	47.47	0.02	0.09	21.69	30.64	0.00	0.04	0.00	0.02	0.04
DC-2-47A-09	late dolomite	46.54	0.02	0.06	22.12	31.19	0.02	0.00	0.00	0.02	0.02
DC-2-47A-010	calcite	44.37	0.02	0.05	0.22	55.32	0.00	0.00	0.00	0.00	0.03
DC-2-47A-011	early dolomite	46.76	0.03	0.06	22.19	30.89	0.00	0.00	0.00	0.01	0.05
DC-2-47A-012	dedolomite	43.97	0.02	0.05	0.20	55.72	0.01	0.01	0.01	0.00	0.00
DC-2-47A-013	calcite	44.76	0.01	0.07	0.14	55.01	0.00	0.00	0.00	0.01	0.00
DC-2-108B-01	calcite	44.64	0.01	0.34	0.31	54.63	0.01	0.00	0.02	0.03	0.00
DC-2-108B-02	late dolomite	47.02	0.02	0.04	21.23	31.39	0.02	0.21	0.03	0.00	0.03

Table B3- Continued.

DC-2-108B-03	early dolomite	47.77	0.37	0.02	21.10	30.42	0.06	0.22	0.02	0.00	0.02
DC-2-108B-04	dedolomite	44.87	0.01	0.04	2.61	52.40	0.02	0.02	0.00	0.02	0.00
DC-2-108B-05	calcite	43.83	0.01	0.03	0.22	55.87	0.02	0.00	0.00	0.00	0.02
DC-2-108B-06	calcite	44.45	0.00	0.12	0.20	55.13	0.00	0.03	0.01	0.04	0.01
DC-2-108B-07	late dolomite	47.08	0.03	0.06	21.65	31.01	0.00	0.15	0.00	0.00	0.02
DC-2-108B-08	early dolomite	48.15	0.17	0.07	20.72	30.66	0.00	0.18	0.02	0.03	0.02
CaCO3-03	Standard	42.99	0.04	0.00	0.01	56.83	0.07	0.00	0.03	0.00	0.02
CaCO3-04	Standard	42.41	0.03	0.02	0.00	57.42	0.06	0.00	0.02	0.04	0.00
FeCO3-03	Standard	37.47	0.08	0.02	0.13	0.00	3.05	59.21	0.02	0.02	0.00
FeCO3-04	Standard	37.18	0.11	0.01	0.13	0.00	2.99	59.53	0.03	0.00	0.01
MgCO3-03	Standard	47.49	0.04	0.00	22.00	30.35	0.02	0.07	0.03	0.00	0.00
MgCO3-04	Standard	47.42	0.05	0.01	22.06	30.31	0.04	0.06	0.04	0.00	0.00